THE ROLE OF YES-ASSOCIATED PROTEIN (YAP) IN VERTEBRATE DEVELOPMENT

Stephen Timothy Gee

A dissertation submitted to the faculty of the University of North Carolina at Chapel Hill in partial fulfillment of the requirements for the degree of Doctor of Philosophy in the Department of Cell and Developmental Biology.

Chapel Hill
2010

Approved by:

Sharon L. Milgram, Ph.D.

Vytas A. Bankaitis, Ph.D.

Patrick J. Brennwald, Ph.D.

Sally A. Moody, Ph.D.

Abstract

Stephen Gee
The role of Yes-associated protein (YAP) in vertebrate development
(Under the direction of Sharon L. Milgram)

Yes-associated protein 65 (YAP) contains multiple protein-protein interaction domains and functions as both a transcriptional co-activator and as a scaffolding protein within the cytoplasm or nucleus. Given that YAP binds to so many proteins that are critical for proper embryonic development and that this factor functions as a transcriptional co-activator, YAP likely plays an important role during early embryonic development.

Given that YAP knockout mice struggled to progress normally through early development, in part because of nutritional deficiencies, we sought to better characterize a role for YAP during this time period by using embryos that develop externally: *Xenopus laevis* and *Danio rerio*. YAP morpholino (MO)-mediated loss-of-function resulted in a delay of mesoderm induction and severely impaired A-P axis elongation, phenotypes that were similar to $YAP^{-/-}$ mice. YAP gain-of-function experiments in *Xenopus laevis* expanded the progenitor populations in the neural plate and neural plate border zone, while concomitantly inhibiting differentiation markers for the neural crest, preplacodal ectoderm, hatching gland, epidermis, and somitic muscle.

Regulation of gene expression is critically important in development and improper regulation of gene expression can lead to a variety of developmental defects, such as loss of

conceptus, birth defects, and cancer. I found that *yap* expression is controlled by a TATA-less promoter, which includes a GC box where Sp1 binds and regulates *yap* transcription. I also found that *adrenomedullin*, a multifunctional peptide hormone known to act as a vasodilator, angiogenic factor, regulator of placental development, and tumor growth promoter, is a newly identified, putative target of YAP.

These studies demonstrate that YAP is involved in the process of cell differentiation and the lack or overabundance of YAP protein disrupts the developmental time line of vertebrates with grievous consequences. Understanding the mechanistic details of these effects involve delineating the transcriptional control of YAP and its target genes. In the future, elucidating the linkage between YAP, the nuclear architecture, and transcriptional regulation will bolster our understanding of cell differentiation.

Acknowledgements

During a graduate student's pursuit to graduation, they receive many forms of advice, both personal and professional, from a multitude of people with varied backgrounds. I would like to use this space to acknowledge those for whom without whom this document would have been completed. I am eternally grateful and indebted to those scientists before me, who persisted, sacrificed, and persued their less traveled investigations even when others thought the ideas imprudent.

My parents, Roger and Nita Gee, provided a loving, supportive family in which to learn and grow. Without their continued love and support, this work would not exist. I am also grateful to the positive mentors who encouraged me throughout my early education, including my Seventh Grade Biology Teacher, Gail Sumwalt, my Advanced Placement High School Biology Teacher, Paula Alderfer, my High School Band Director, Benny Ferguson, and my High School Cross Country and Track coach, Bob Jenkins.

There are many people to thank for their contributions to this work, but I would like to start by thanking Sharon L. Milgram for giving me the opportunity to complete this work in her lab, for her invaluable advice and guidance, and for her continued positive reenforcement. This work could not have been completed without the support, mentoring, patience, and scientific guidance of Sally A. Moody. I thank Jeremy Teed and Robin Shah for their persistant hard work in collecting portions of the described work, which contributed to their UNC Honor's Theses. I also thank the varied contributions, both personal and

scientific, of the following: Elizabeth M. Morin-Kensicki, Frank L. Conlon, Vytas A. Bankaitis, Patrick J. Brennwald, Kenneth L. Kramer, Michael Howell, Anthony P. Barnes, Caleb A. Hodson, William R. Thelin, Chris Showell, Daniel D. Brown, Augustin G. Caballero, Brian Boone, Gaby Haddock, Blake Carrington, Bo Yan, Karen M. Neilson, David Phillibert, and Lindsey Buckingham. I thank my wife, Dawn Kashelle Lockman, and my daughter, Kailey Arden Gee for their love, encouragement, and continued support.

Finally, I would like to dedicate this dissertation to those important to me, whom were unable to see the completion of this work: Ruth Stroud Gee (grandmother), Mary Sue Crump (grandmother), and Vonnie Roberts (grandfather-in-law).

Table of Contents

List of Tables

List of Figures

List of Abbreviations

ADM	Adrenomedullin
BAF155	Barrier-to-autoantigen factor 155
BMP	Bone morphogenetic protein
Brg1	Brahma related gene 1
BSA	Bovine serum albumin
Calcrl	Calcitonin receptor-like receptor
Cbfa1	Core binding factor-1
cDNA	Complementary deoxyribonucleic acid
CFTR	Cystic fibrosis transmembrane conductance reglator
ChIP	Chromatin immunoprecipitation
CTD	Phosphorylated C-terminal domain of RNA polymerase II
DMEM	Dulbecco's modified eagle medium
DNA	Deoxyribonucleic acid
EBP50	Ezrin/radixin/moesin (ERM)-binding phosphoprotein of 50kDa
EGF	Epidermal growth factor
EMSA	Electrophoretic mobility shift assay
ERM	Ezin/radixin/moesin
ESC	Embryonic stem cell
FBS	Fetal bovine serum
GST	Glutathione-S-transferase
GFP	Green fluorescence protein
HA	Hemagglutinin tag

HATs	Histone acetyltransferases
HG	Hatching gland
hnRNP U	Heterogeneous nuclear ribonuclear protein U
hpf	Hours post-fertilization
IgG	Immunoglobulin G
IRdye	Infrared dye
LATS	Large tumor suppressor
LPA	Lysophosphatidic acid
MITF	Microphthalmia-associated transcription factor
MBS	Modified Barth's Saline
MEF	Mouse embryonic fibroblast
MO	Morpholino
NCP	Neural crest progenitors
NHERF	Na(+)/H(+) exchanger regulatory factor
p53BP-2	p53-binding protein-2
Pax3	Paired box 3
PC	Polycystin
PBS	Phosphate buffered saline
PDZ	Postsynaptic density 95/Discs-large/Zonula occludens-1
PECAM1	Platelet endothelial cell adhesion molecule 1
PKD	Polycystic kidney disease
PPARγ	Peroxisome proliferator-activated receptor-γ
PVDF	Polyvinylidene fluoride

qPCR	Quantitative polymerase chain reaction
RIPA	Radioimmunoprecipitation assay buffer
RNA	Ribonucleic acid
RT-PCR	Reverse transcription-polymerase chain reaction
SH3	Src homology domain
Sp1	Specificity protein 1
SV40	Simian virus 40
TAZ	Transcriptional co-activator with a PDZ-binding motif
TBS	TEAD binding site
TBST	Tris-buffered saline with Tween 20
Tbx-5	T-box transcription factor-5
TEAD	Tea domain proteins
TEF	Transcription enhancer factors
TEM	Transmission electron microscopy
TGF-β	Transforming growth factor-beta
TTF-1	Thyroid transcription factor-1
WISH	Whole mount *in situ* hybridization
WWTR1	WW domain containing transcription regulator 1
YAP	Yes-associated protein 65

List of Symbols

α	Alpha
β	Beta
γ	Gamma
Ψ	Psi

Chapter I – Background

The goal of my work is to better understand the role of YAP in vertebrate development. In this chapter, I provide background information regarding the initial identification of YAP, the *in vitro* identification of proteins shown to bind to the protein-protein interaction domains present in YAP, and the consequences of deleting either YAP or its interacting proteins from the mouse. In addition, I provide background information regarding the YAP paralog, transcriptional co-activator with a PDZ-binding motif (TAZ), and briefly compare and contrast them.

Yes-associated protein (YAP)

c-Yes is a member of the Src family of tyrosine kinases. To investigate potential signaling targets and/or signaling regulators of c-Yes, Marius Sudol developed a polyclonal antibody to the Src homology domain (SH3) of c-Yes, which allowed for the generation of polyclonal anti-idiotypic antibodies, which were used for the isolation of proteins binding to the c-Yes SH3 domain (Sudol, 1994). A 65 kDa protein was precipitated from [^{35}S]methionine labeled chicken embryo fibroblasts using these anti-idiotypic antibodies. Because high levels of c-Yes protein were present in the chick cerebellum and these anti-idiotypic antibodies recognized the 65 kDa band, mRNA was isolated from the cerebella of 2-week-old chicks and used for the creation of cDNA library in lambda gt11 phage. Screening this chick cerebellar cDNA library with the anti-idiotypic sera allowed for the identification of the first sequence data for Yes-associated protein 65 (YAP).

Although YAP's initial identification was based on its ability to bind to members of the Src tyrosine kinase family via its SH3 binding motif, it quickly became one of the founding members of a newly identified protein motif family, the WW domain containing

family. Upon database searches of a hinge region present between the spectrin repeats in Dystrophin, the product of the Duchenne muscular dystrophy locus, it was found that other genes such as Nedd-4, a ubiquitin ligase, Pin1, a proyl isomerase, Fe65, an adaptor protein with possible functions in regulating transcription, chromatin modification, cell growth, apoptosis, and axonogenesis, and YAP, an adaptor protein and transcriptional co-activator all contained a conserved stretch of amino acids that had two tryptophans spaced 20-22 amino acids apart. For this reason, this amino acid stretch was defined as the WW domain, which contains β-strands situated around four conserved aromatic amino acids and is 38 amino acids in length (Bork *et al.*, 1994). The WW domain allows the binding of proteins containing a PPxY motif (Macias *et al.*, 1996) and the known YAP interactors are summarized below (Figure 1).

In one report, YAP was pulled out of a cDNA expression library using a fusion protein of Smad7, an established inhibitor of transforming growth factor-β (TGF-β) signaling (Ferrigno *et al.*, 2002). To confirm binding, myc-Smad6 or myc-Smad7 were co-over-expressed with a 6xHis-YAP in Cos cells, but pulldowns showed that only myc-Smad7 interacted with YAP. However, deletion of the PPxY motif from Smad7 only reduced its binding capacity to YAP instead of eliminating its interaction entirely. To test the functionality of the interaction, a keratinocyte cell line was co-transfected with Smad7 and/or YAP and a Smad responsive luciferase vector, (CAGA)9-Lux, or its mutant form, in the presence or absence of TGF-β. While Smad7, expectantly, inhibited luciferase activity in the presence of TGF-β, the addition of YAP potentiated Smad7's inhibition. The proposed mechanism of action for this inhibition was that YAP helps to inhibit TGF-β signaling by stabilizing the interaction of Smad7 with the activated receptor, TGF-β receptor I, and thus

Figure 1. Protein-protein interaction domains of YAP. Frog and zebrafish YAP possess the following functional and protein-protein interaction domains: a TEAD-binding site (purple), a LATS phosphorylation site (orange), two WW domains (red) that allow for PPxY binding, a Src Homology 3 (SH3)-binding domain (green), a coiled-coil region (blue), a transactivation domain (underline), and a PDZ-binding motif (pink). hnRNP U (yellow) binding has only been experimentally tested with human YAP, but related sites are found in the fish and frog proteins. This diagram also illustrates the relative location of *Xenopus laevis* (x) and *Danio rerio* (z) morpholino (MO)-binding sites.

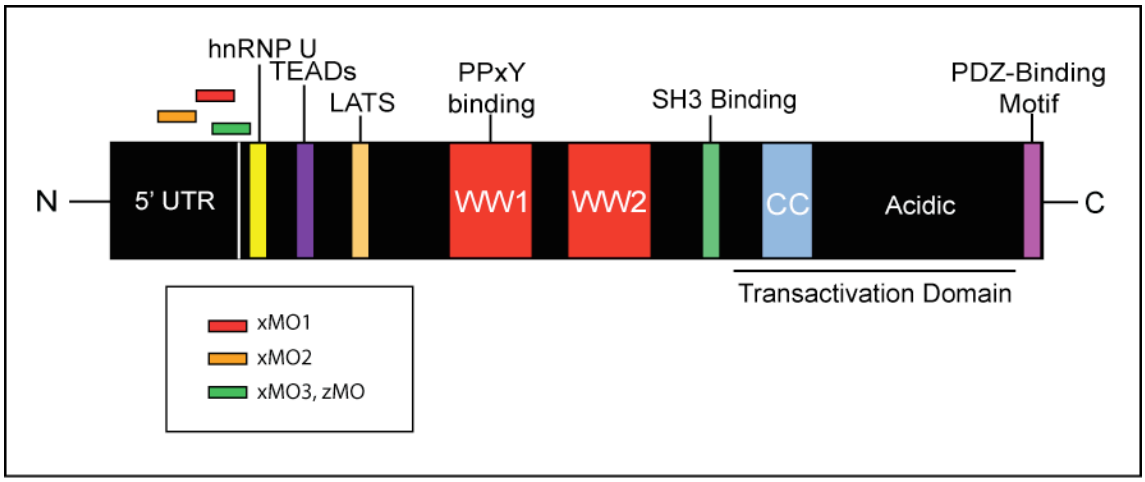
hnRNP U
TEADs
LATS
PPxY
binding
SH3 Binding
PDZ-Binding
Motif
N
5' UTR
WW1
WW2
CC
Acidic
C
Transactivation Domain
xMO1
xMO2
xMO3, zMO

prevents receptor associated Smad (Smads1-3, and Smad5) phosphorylation. It should be noted that Smad7 is also capable of binding to the WW-domain containing ubiquitin ligases, Smurf1 and Smurf2, and recruiting them to activated TGF-β receptor I, which results in proteasomal degradation of the receptor (Chong *et al.*, 2006, Kavsak *et al.*, 2000). More recently, YAP and Smurf1 were shown to bind to Smad1/5 via their WW domains in the presence of bone morphogenetic protein (BMP) (Alarcon *et al.*, 2009). Thus, YAP may play a role in modulating TGF-β and BMP signaling, both of which are involved in mesoderm induction and anterior-posterior (AP) axis formation.

ErbB-4, a receptor tyrosine kinase, is activated by members of the EGF (betacellulin, epiregulin, and HG-EGF) and the Neuregulin (neuregulin 1-4) families via homo- or hetero-dimerization with ErbB-2. ErbB-4 binds YAP upon cleavage of its cytoplasmic tail and the two proteins translocate to the nucleus to activate ErbB-4 target genes. ErbB-4 knockout mice die by embryonic day 10.5 due to the lack of cardiac trabeculation, which is similar to mice lacking ErbB-2 and neuregulin-1 (Gassmann *et al.*, 1995). In addition, mice lacking ErbB-4 exhibited a phenotype not seen in ErbB-2 and neuregulin-1 knockout mice, which was a defect in axon guidance in the central nervous system. Therefore, YAP could be involved in regulating cardiac muscle differentiation and axon guidance in the central nervous system.

p53-binding protein-2 (p53BP-2) was identified as binding to the first WW domain of YAP using a yeast two hybrid system. p53BP-2 contains a PPxY motif, four ankyrin repeats and one SH3 domain (Espanel *et al.*, 2001). p53BP-2 binds to the DNA binding domain of p53 via its ankyrin repeats and SH3 domain, but not to common p53 mutants, which are associated with cancer (Gorina *et al.*, 1996, Iwabuchi *et al.*, 1994). Although the binding of

p53BP-2 and YAP could occur using GST-pulldowns as well as yeast and mammalian two-hybrid assays, co-immunoprecipitations using antibodies to the proteins failed, despite immunoprecipitating their intended protein (Espanel *et al.*, 2001). Further experiments showed that p53BP-2 could also interact with the SH3 domain of YAP in addition to its WW domain; however, a lack of co-IP of the two proteins makes the plausible interaction of the proteins transient at best.

The WW domain of YAP was determined to bind to p73α via GST-pulldowns as well as co-immunoprecipitations from cells overexpressing tagged versions of each protein and endogenously (Strano *et al.*, 2001). In addition, other p53 family members were found to bind to YAP, which included p73β, and p63α, whereas p73γ and p53 did not. Functionally, co-overexpression of YAP and p73α was capable of increasing the transcriptional activity of p73α, as evidenced by increased luciferase activity from Mdm2 and Bax reporter plasmids. In addition, an increase in the Bax protein was observed when YAP and p73α were co-overexpressed. Point mutations in the p73α PPxY motif disrupted binding in GST-pulldowns and the activity of the Bax reporter plasmid confirmed the validity of the interaction.

We found that endogenous YAP bound to the second PDZ domain of Na(+)/H(+) exchanger regulatory factor 1/ezrin/radixin/moesin (ERM)-binding phosphoprotein of 50 kDa (NHERF1/EBP50) and localized to the apical membrane of polarized epithelial cells, thus linking apical membrane bound proteins to the actin cytoskeleton via the interaction between NHERF1 and ezrin (Mohler *et al.*, 1999).

YAP also contains a domain that interacts with the Tea domain (TEAD) proteins, also known as transcription enhancer factors (TEFs). TEADs are a family of transcription factors that contain the TEA domain DNA binding domain and are expressed ubiquitously.

However, some TEADs are expressed at higher levels at certain times during development, which suggests that each of them may possess unique functions under certain developmental contexts (Vassilev *et al.*, 2001). From a variety of TEAD knockout mice, we now know that when some are absent, certain organs are more susceptible than others. Yet there is functional redundancy among the TEAD family members because when two TEADs are missing from the developing mouse, their developmental deficits are much more severe than their single knockout counterparts (Chen, Z. *et al.*, 1994, Sawada *et al.*, 2008).

YAP's interaction with TEAD-2 was identified using an unbiased approach to co-purify TEAD-2 binding proteins with a tagged TEAD-2 protein using affinity chromatography and under otherwise naïve conditions. While YAP was initially found to bind to TEAD-2, it was also capable of binding to all four mouse TEAD homologs. Using GST pulldowns, YAP was found to bind to the carboxy-terminus of mTEAD-2 (amino acids 224-445), whereas TEAD-2 was found to bind to a defined amino terminus region of mYAP (amino acids 77-96). To test the functional ability of the TEAD-2/YAP interaction, a TEAD-dependent promoter (pGT4Tluc) was used to co-transfect NIH-3T3 cells (endogenous YAP present) and EL4 cells (no endogenous YAP present) with increasing concentrations of TEAD-2 and with or without YAP. Results from these experiments showed that by increasing TEAD-2 concentrations, the measured TEAD-2 transcriptional activity decreased, which suggested that excess TEAD-2 competed with TEAD-2/YAP complexes for binding to the promoter. In the T-lymphocyte cell line, EL4, which was verified to not express TEAD or YAP, the addition of YAP alone was incapable of increasing TEAD-dependent promoter activity, yet when increasing amounts of TEAD-2 were added to this cell line the promoter activity steadily rose. However, when this same promoter activity was tested in NIH-3T3

mouse fibroblasts, which endogenously express TEAD-2 and YAP, increasing levels of YAP squelched this promoter activity. In agreement with YAP binding to all four mTEADs homologs, TEAD/YAP co-transfections with the TEAD responsive reporter confirmed that YAP can use any TEAD to activate the reporter plasmid, and when the TEAD binding site is deleted the promoter activity is lost.

In an unbiased screen for binding partners to the proline rich amino terminus of hYAP (1-57), it was found that hnRNP U bound to this region of YAP (Howell *et al.*, 2004). By radiolabeling cells with [^{32}P]orthophosphate, performing hot and cold GST pulldowns with purified GST, GST-hYAP(1-57), GST-hYAP WW1 (162-217), and subsequent mass spectrometry analyses, hnRNP U was shown to bind to the proline rich amino terminus of hYAP. In addition, YAP and hnRNP U were capable of interacting only within the nuclear fraction even though both proteins can be found in the nuclear and cytoplasmic domains, suggesting that their association is regulated. The ascribed function of hnRNP U is varied and includes possibly regulating pre-RNA processing, mRNA transport, translation, and/or stability, transcriptional regulation via its interactions with RNP particles, whereby it can associate with histone acetylases (HATs), p300, and chromosomal attachment regions. The details however are still being worked out. What is known is that hnRNP U can be divided into three main interacting protein pieces. The amino terminus of hnRNP U interacts with DNA, the middle interacts with the phosphorylated C terminal domain (CTD) of RNA polymerase II, and the carboxy terminus interacts with nuclear actin and mRNA. Interestingly, hnRNP U can also associate with the E3 ubiquitin ligase, Skp1, Cul1, Roc1/Rbx/Hrt1 ($SCF^{\beta\text{-}TrCP}$) (Davis *et al.*, 2002). Given that YAP can bind to so many different kinds of proteins, it is expected to be involved in a plethora of cell biological

processes; however, to best delineate YAP function *in vivo*, an understanding of the similarties and differences between its vertebrate paralog must be considered.

Transcriptional co-activator with a PDZ-binding motif (TAZ)

Transcriptional co-activator with a PDZ-binding motif (TAZ), also known as WW domain containing transcription regulator 1 (WWTR1), is a YAP paralog that is only present in vertebrates. Comparing and contrasting the similarities and differences between these paralogs is important for delinating the functional significance of each in developmental contexts. TAZ was identified using radio-labeled translated cDNA pools to identify proteins that bound to 14-3-3 (Kanai *et al.*, 2000). The mouse form of TAZ is forty-five percent identical at the amino acid level to mouse YAP.

YAP and TAZ are similarly expressed in the heart, lung, liver, and kidney of mice by Northern blot analysis; however, analyses using RT-PCR suggest that YAP and TAZ are more broadly expressed (Kanai *et al.*, 2000). TAZ is similar to YAP in that it contains a phosphorylation site that permits the binding of 14-3-3 in the N-terminal region of the protein, a TEAD binding region, a single WW domain in the middle, and a PDZ interaction motif at the C-terminus. However, YAP differs from TAZ in that it contains a second WW domain, an SH3 binding motif as well as a proline-rich N-terminus. The binding of 14-3-3 to mTAZ requires the phosphorylation of serine eighty-nine; however, that binding reduces its transcriptional activity by sequestering it away from the nucleus and holding it in the cytoplasm. Surprisingly, it was found that deletion of the PDZ-binding motif at the extreme C-terminal region of TAZ eliminated TAZ-mediated transcriptional co-activation. Because we previously showed that YAP bound to NHERF1, Kanai *et al.* used direct binding assays

to test the binding of YAP and TAZ to NHERF1 and NHERF2 (Kanai *et al.*, 2000, Mohler *et al.*, 1999). YAP was capable of binding to both, but TAZ seemed to selectively bind to NHERF2. TAZ and NHERF2 did not, however, co-localize within the cell's punctate nuclear bodies, suggesting there must be other nuclear PDZ containing proteins responsible for regulating its transcriptional co-activation.

Similarly to YAP, TAZ is often shown to associate with other proteins through one of its protein-protein interaction domains. In contrast, the two paralogs are sometimes unable to bind to the same proteins, suggesting functional specificity of the paralogs whereby one is unable to compensant for the function of the other. One study illustrated an interaction with the N-terminus of thyroid transcription factor-1 (TTF-1), also known as Nkx2.1, via its WW domain (Park, K. S. *et al.*, 2004). TTF-1 is important for regulating and activating genes, such as surfactant proteins A, B, and C in the lung and thyroglobulin, thyroperoxidase and sodium-iodide symporter in the thyroid. TTF-1 null mice lacked thyroid and pituitary glands, while also exhibiting defects in the lung and ventral forebrain. Overexpression of TTF-1 in alveolar type II cells in the lungs of transgenic mice resulted in emphysema, epithelial cell hyperplasia, and inflammation. In the presence of TAZ, the efficacy of TTF-1's transcriptional activity on the SP-C promoter was increased when co-transfected into both MLE-15, a large T antigen immortalized mouse lung epithelial cell line, and HeLa cells (Park, K. S. *et al.*, 2004).

TAZ may bind Runx2, also known as core binding factor 1 (Cbfa1), via its WW domain and the PY motif of Runx2 (Cui *et al.*, 2003, Zaidi *et al.*, 2004). Runx2 belongs to the Runt family of transcription factors and controls the expression of osteoblast specific genes, such as osteocalcin. Runx2 is critical for proper bone development. Runx2 null mice

lack differentiated osteoblasts and their progenitors (Komori *et al.*, 1997, Otto *et al.*, 1997) and this can be partially rescued by transgenic overexpression (Takeda *et al.*, 2001). Cui *et al.* presented evidence for a functional interaction between TAZ and Runx2, which resulted in the upregulation of osteocalcin promoter activity (Cui *et al.*, 2003). Although Zaidi *et al.* also showed the TAZ/Runx2 interaction, the interaction repressed osteocalcin promoter activity in their studies (Zaidi *et al.*, 2004). Further support for the TAZ/Runx2 interaction regulating bone development was shown in TAZ morphant zebrafish, whereby bone development was reduced as evidenced by the lack of skeletal ossification (Hong *et al.*, 2005). More importantly in this report, TAZ was demonstrated to be at the crossroads of mesenchymal stem cell differentiation into either osteoblasts (bone) or adipocytes (fat). BMP-2 is a known inducer of osteoblast differentiation and was shown to induce TAZ mRNA and protein. The interaction of Runx2 with TAZ promoted bone formation via upregulation of the osteocalcin promoter, while inhibiting the transcriptional activity of the peroxisome proliferator-activated receptor γ (PPARγ), a ligand-activated transcription factor involved in adipocyte differentiation.

The proposal that TAZ is involved in cardiac and limb development came form the observation that it could directly bind to the T-box transcription factor, Tbx5, and activate Tbx5-dependent transcription (Murakami *et al.*, 2005). In addition, TAZ was shown to physically associate with the histone acetyltransferases (HATs), p300 and PCAF, and thus may activate Tbx5-dependent transcription by some unknown mechanism via binding to these HATs. Interestingly, YAP could also stimulate Tbx5-dependent transcription, but could not directly associate with Tbx5. However, TAZ and YAP can form heterodimers with one another via their coiled-coil domains. TAZ was capable of forming a homodimer with

itself, while YAP was not. Mutational analysis indicated that TAZ could interact with Tbx5 via multiple domains, including the C-terminus of TAZ. Finally, TAZ was incapable of binding to Tbx5 truncations that are associated with Holt-Oram syndrome, which is a disease associated with cardiac and upper limb abnormalities.

Using a yeast two-hybrid screen with full-length Pax3 as bait, it was found that TAZ could bind to Pax3 via the WW domain of TAZ and a C-terminal PY motif in Pax3 (Murakami *et al.*, 2006). However, the PY motif was non-essential for the coactivation of a Pax3 target gene, microphthalmia-associated transcription factor (MITF), but the C-terminal region of Pax3 was essential, suggesting other protein interactions may be involved in Pax3/TAZ-mediated transcriptional activation. In Chapter II, I will demonstrate that YAP is a regulator of Pax3 transcription.

Like YAP, TAZ interacts with intracellular effectors of TGF-β signaling. TAZ can bind to the Smad2/3 complex (Varelas *et al.*, 2008), which can mediate activation of the TGF-β/Activin/Nodal receptors (Moustakas *et al.*, 2009). TAZ interacted more strongly with the receptor activated Smad2/3/4 complex than with activated Smad1 (Varelas *et al.*, 2008), which resulted in the recruitment of the TAZ/Smad2/3/4 complex to the TGF-β response elements in the promoter of Smad7.

Loss of TAZ in human embryonic stem cells (hESCs) resulted in the loss of Oct4 and Nanog, both pluripotency markers, and pluripotency is controlled via Smad2/3 signaling in hESCs. Interestingly, knockdown of TAZ in mouse embryonic stem cells (mESC) did not affect Oct or Nanog levels or their pluriopotent state, which correlates with the fact that pluripotenty in mESCs is controlled by Smad1/5/8. Finally, in the absence of TAZ, activated

Smad2/3/4 complexes do not accumulate in the nucleus and thus do not activate target genes (Hong *et al.*, 2005, Varelas *et al.*, 2008).

Do YAP and TAZ share developmental functions?

The YAP paralog, TAZ (WWTR1), is expressed throughout development. Mice null for TAZ survived until birth, although 35-50% did not survive past the age of weaning (Hossain *et al.*, 2007). TAZ null mice were smaller in stature, exhibited lower body weights, and died earlier (10-12 months) than wild type or heterozygous animals. Although severe defects in bone development were reported in TAZ-morphant zebrafish, only minor skeletal defects were observed in TAZ null mice. More persistent were the presence of enlarged, anemic kidneys, which were filled with cysts, primarily of glomerular origin. The formation of these cysts began as early at E15.5, while cyst number and size increased with age.

In a report by a separate group, half of the expected number of TAZ null mice was recovered at birth, indicating partial embryonic lethality (Tian *et al.*, 2007). Surviving TAZ null mice were smaller and inactive compared to wild type and heterozygous littermates, yet production of bone and fat was relatively normal. Similar to the previous report, the surviving TAZ null mice developed severe polycystic kidney disease (PKD), also of cortical origin, but with the additional phenotype of severe pulmonary disease. Since 85% and 15% of human autosomal dominant polycystic kidney disease are due to mutations in PKD1 (PC1) and PKD2 (PC2), respectively, the levels of the associated mouse genes, *pc1* and *pc2*, respectively, were examined. Although similar protein levels of PC1 were observed in wild type and TAZ null animals, approximately two fold increased levels of PC2 were found in the kidneys of TAZ null mice. Interestingly, the levels of *pc2* transcripts were actually

reduced, suggesting that TAZ did not directly regulate the transcription of *pc2*, but instead controlled a poststranscriptional mechanism for regulating the levels of PC2 protein. Similarly, PC2 protein levels were increased in TAZ morphant zebrafish, which also developed "large bilateral cystic dilations in the pronephric tubules." Further investigation into TAZ's role in regulating PC2 protein levels revealed that TAZ interacts with PC2 via its coiled-coil domain and possesses a phosphodegron motif, which is phosphorylated by an unknown kinase, recognized by β-Trcp, and allows for TAZ's incorporation into the $SCF^{\beta\text{-}TrCP}$ ubiquitin ligase complex whereby PC2 is targeted for degradation. Thus, without TAZ, PC2 is not brought into the ubiquitin ligase complex and not targeted for degradation. Another interesting observation from this study was that mutation of TAZ's phosphodegron motif or siRNA mediated reduction of β-Trcp resulted in augmented TAZ protein levels, suggesting that TAZ may also be directly targeted for ubiquitin-mediated degradation. It is interesting to note here that hnRNP U, which binds to YAP and not TAZ, can bind to $SCF^{\beta\text{-}TrCP}$ ubiquitin ligase, suggesting an even more complex role for YAP's regulation of cellular components (Davis *et al.*, 2002, Howell *et al.*, 2004).

Much less is known about the role of YAP in developmental processes. By RT-PCR analysis, *myap* mRNA was detected as early as embryonic day 3.5 and was maintained throughout embryonic development (Morin-Kensicki *et al.*, 2006). *In situ* hybridization analyses revealed that *yap* mRNA expression was ubiquitous, but dynamic throughout development. *yap* mRNA was present in the extraembryonic ectoderm, epiblast, and nascent mesoderm at E6.5 (the beginning of mouse gastrulation), abundant in the extraembryonic mesoderm and ectoderm and lower in visceral and definitive ectoderm at E7.5. By E8.5,

when the chorion and allantois fuse, *yap* remained ubiquitous, but was more strongly expressed at the distal tip of the allantois.

Using homologous recombination, we targeted the *yap* allele with a targeting construct intended to disrupt transcription at the *yap* locus. Once embryonic stem cells were electroporated, selected, and screened for the integration event, mice carrying the allele were established via blastocyst embryonic stem (ES) cell injection. Germ line transmission from chimeric mice was confirmed by the heterozygosity of the targeted allele. These heterozygotes showed no obvious malformations and were then crossed to one another to produce genetically altered offspring at the expected Mendelian ratios for the targeted YAP allele. No YAP-null offspring were recovered postnatally, while less than 1% were recovered after E10.5; however, the nearly expected 23% of YAP-null embryos were recovered between E6.5-9.5. Therefore, we concluded that mice lacking YAP rarely survived past E9.5. This is in stark contrast to TAZ-null mice, indicating that these two closely related proteins have different developmental roles.

YAP-null embryos demonstrated developmental malformations beginning at E7.5. YAP-null mice appeared smaller in stature compared to wild type E7.5 mice and exhibited constriction at the embryonic-extraembryonic boundary or a profound separation between the hypoblast and the epiblast; however, most of the embryos at this stage did possess a properly formed amnion and chorion. By E8.5, the YAP-null embryos' body axes were shorter and wider, the anterior epithelium was improperly folded, the allantois failed to fuse with the chorion, and there was evidence of caudal dysgenesis. E9.5 embryos showed defective ventral closure, a failure to make its emblematic turn, a disorganized anterior neurepithelium, a swollen allantois, and a ruffled yolk sac. Detailed analyses of hematoxylin and eosin

stained sections showed a disorganized embryonic mesoderm and confirmed separation of the embryonic-extraembryonic border in E7.5 embryos, while E8.5 embryos showed excessive folding of the anterior neurectoderm and a thinner epiblast-like epithelium overlying the mesoderm along the streak region, compared to wild type embryos. Although E8.5 embryos showed the presence of a node, anterior somites, primitive heart tissue, allantois, and yolk sac mesodermal cells, the blood islands within the yolk sac were atypical, suggesting potential defects in the yolk sac vascular system. Using immunostaining for Platelet endothelial cell adhesion molecule-1 (PECAM1), which is a marker for endothelial cells, and whole mount *in situ* hybridization (WISH) for *alpha globin*, a marker for erythrocyte precursors (erythroblasts), we showed that although both endothelial cells and erythroblasts were specified in the yolk sac, the primitive vascular plexus was disorganized. To determine whether anterioposterior patterning was disrupted in the YAP-null mice, two markers, *fgf8* and *hesx1*, were used for WISH. Normally, *fibroblast growth factor-8* (*fgf8*) is expressed at the anterior neurectoderm, midbrain-hindbrain boundary, branchial arches, and tail bud, whereas *hesx1* marks the most anterior portion of the neurepithelium. Several restricted bands of *fgf8* staining and anterior staining for *hesx1* was observed in YAP-null mice. These results indicate that although the embryos are morphologically atypical, anterior and posterior patterning was maintained. Because the body axis of YAP-null embryos were shorter, yet broader than wild type embryos, WISH staining for *brachyury* was performed. Although *brachyury* expression was present in the streak, tailbud, and midline, it was unusually wide and discontinuous.

Given these findings, we postulated that YAP could affect axis elongation through alterations in the following: proliferation, apoptosis, morphogenetic movements during

gastrulation, or gene expression changes. Results from proliferation and apoptotic assays did not discern appreciative differences between null and wild type embryos. The last two possible mechanisms are addressed in Chapter II.

YAP-null mice are more severely affected during early development than are TAZ-null mice. In fact, *taz* mRNA levels are normal in YAP-null embryos, indicating that it can not fully compensate for loss of YAP. However, since $YAP^{-/-}$ and $TAZ^{-/-}$ double mutant mice die before the morula stage (16-32 cell stage), the presence of TAZ in YAP-null mice does partially compensate for the early function of YAP (Nishioka *et al.*, 2009). Thus, although YAP and TAZ share many structural features they are likely to have different developmental roles. In hindsight, this may not be so surprising given that the vertebrate YAP homolog is more closely related to that of the invertebrate homolog than is TAZ and thus may have retained the necessary functions established in earlier evolution before the duplication event that resulted in the presence of YAP and TAZ within vertebrates. Thus, we began a series of studies to elucidate the developmental function of YAP.

Comparison of YAP-null mice to protein interacting-null mice

To begin to uncover the developmental function of YAP, we asked whether mouse lines that were null for proteins known to interact with YAP shared any developmental phenotypes with $YAP^{-/-}$ mice. In this section, I briefly describe some of the phenotypes associated with the knockout mice of YAP's interacting partners.

While deletion of the Src family tyrosine kinase, Yes, resulted in mice that appeared viable and fertile with no apparent adverse phenotype (Stein *et al.*, 1994), Src-null mice die within weeks of birth (Soriano *et al.*, 1991). They also develop osteopetrosis and fail to

properly remodel bone due to defects in osteoclast function (Lowe *et al.*, 1993, Soriano *et al.*, 1991). Mice lacking Fyn die around birth and exhibited postnatal defects, such as defective T-cell activation (Stein *et al.*, 1992). Interestingly, the number of perinatal deaths increases in mice with compound mutations, illustrating the functional redundancy of the Src family tyrosine kinase (SFK) family members (Stein *et al.*, 1994). Triple (Src, Fyn, and Yes) mutant mice were recovered at the expected frequency of one in sixteen at E9.5, but these embryos were one-half the size of wild type embryos, had not undergone turning, and were beginning to be resorbed (Klinghoffer *et al.*, 1999). They also exhibited a wavy neural tube, defective chorioallantoic fusion, and yolk sacs that were properly vascularized, illustrating that mice lacking Src/Fyn/Yes had phenotypes similar to those seen in YAP-null mice.

Deletion of the MH2 domain within Smad7 caused the majority of the homozygous mutant mice to die *in utero* due to multiple defects in cardiovascular development, while any surviving mutant mice exhibited impaired cardiac functions and severe arrhythmia (Chen, Q. *et al.*, 2009). Deletion of exon 1 of Smad7 resulted in mice that were viable, yet smaller on an outbred mouse CD-1 strain (Li, R. *et al.*, 2006). Furthermore, B cells from these Smad7 mutant mice showed increased TGF-β signaling as evidenced by increased phosphorylated Smad2. None of these defects are similar to YAP-null embryos.

ErbB-4-null mice fail to differentiate the heart into trabeculae, which leads to reduced blood flow and death at E10.5 (Gassmann *et al.*, 1995). This phenotype is shared by embryos lacking ErbB-2 and neuregulin-1 (Lee, K. F. *et al.*, 1995, Meyer *et al.*, 1995). ErbB-4-null mice also exhibit failures in innervation of the hindbrain, while ErbB-2-null mice exhibited defects in the development of cranial neural-crest-derived sensory ganglia and motor nerves resulting from a failure to produce and ensheath the nerves with myelin (Gassmann *et al.*,

1995, Lee, K. F. *et al.*, 1995, Park, S. K. *et al.*, 2001). YAP-null mice are lethal prior to these developmental events.

No p53-binding protein-2 (p53BP-2) homozygous mutant mice were recovered as early as E6.5, illustrating that p53BP-2 is essential for early mouse development (Kampa *et al.*, 2009). Heterozygous p53BP-2 mice appeared to develop normally; however, they were more susceptible to the development of spontaneous tumors as they aged. The creation of a different p53BP-2 mutant mouse revealed that fewer (6.4%) than the expected 25% homozygous mutant mice were recovered at birth and that the ones that were not recovered survived until E18.5 with defects in the heart and central nervous system (Vives *et al.*, 2006). These heterozygous p53BP-2 mutant mice also developed normally and exhibited a higher frequency in the formation of spontaneous tumors. YAP-null mice share a similar early lethality.

Mice lacking all isoforms of p73 exhibit hippocampal dysgenesis, hydrocephalus, chronic infections and inflammation, as well as abnormalities in pheromone sensory pathways (Yang *et al.*, 2000). Mice lacking p63 are born alive but exhibit complete loss of or truncation of their limbs, defective differentiation of the apical ectodermal ridge, and defective stratification and differentiation of the skin (Mills *et al.*, 1999, Yang *et al.*, 1999). In addition, hair follicles, teeth, and mammary glands are absent in p63 homozygous mutant mice due to defective epidermal-mesenchymal interactions. Based on the phenotypes of these p63 homozygous mutant mice, it was concluded that p63 is essential for the proper maintenance of epidermal progenitors. These phenotypes all occur later than the YAP-null phenotypes, but as I will demonstrate in Chapter II, we also have evidence that YAP maintains certain ectodermal progenitors.

NHERF1/EBP50 mutant male mice developed normally except for exhibiting increased urinary excretion of phosphate due to the mislocalization of the sodium-phosphate co-transporter type IIa to internal sites within the renal proximal tubule cells compared with its normal apical localization (Shenolikar *et al.*, 2002). NHERF1 mutant female mice weighed 30-50% less than their wild type littermates, died 30-35 days after birth, and exhibited reduced bone density, muscle weakness and in some cases hydrocephaly. It should also be noted that "attempts to generate an isogenic strain of NHERF1$^{-/-}$ mutant mice in the F129/Svj strain yielded few, small litters (two to three animals)" (Shenolikar *et al.*, 2002). In contrast, another NHERF1$^{-/-}$ mutant mouse generated by a different group did not see the dramatic phenotypes seen in their females, yet they did admit that some females were weaker and eventually died earlier (Morales *et al.*, 2004). However, this group did confirm the phosphate wasting phenotype and expanded the phenotype to include a reduction of ezrin–radixin–moesin (ERM) proteins in the epithelial cells of the small intestines and the cortical brush border membranes of the kidney. Again, the phenotypes associated with these null-mice all occur later than the primary defects seen in YAP-null embryos.

YAP is capable of binding to all four mammalian TEAD transcription factors. Both YAP and the TEADs are broadly expressed during development, while their expression levels are dynamic throughout development. Homozygous TEAD1 mutant mice die by E11.5 with heart defects due to improper cardiac muscle growth, not its differentiation (Chen, Z. *et al.*, 1994). Homozygous TEAD2 mutant mice exhibited no discernable phenotype from wild type littermates (Sawada *et al.*, 2008). However, TEAD1 and TEAD2 double mutant mice exhibited general growth retardation, displacement of the paraxial and lateral plate mesoderm, defective notochord development, and defective yolk sac vasculogenesis. The

defective notochord development in TEAD1 and TEAD2 double mutant mice is likely due to their regulation of a FoxA2 enhancer in the notochord (Sawada *et al.*, 2005). TEAD4 mutant mice died during the stages of pre-implantation without forming a blastocoele, failed to differentiate trophoblast giant cells, and ICM specific genes were expressed in all blastomeres, indicating that TEAD4 is essential for trophectoderm specification (Nishioka *et al.*, 2008, Yagi *et al.*, 2007). Although no data on TEAD3 mutant mice yet exists in the literature, personal communication with H. Sasaki suggests that TEAD3$^{-/-}$ mice appear normal and fertile (Sawada *et al.*, 2008). Alternatively, published data suggests that TEAD3 could be essential for the formation of the placenta and differentiation of cardiomyocytes (Brunskill *et al.*, 2001, Jiang, S. W. *et al.*, 1999, Maeda *et al.*, 2002, Peng *et al.*, 2004).

Mice carrying a hypomorphic mutation in hnRNP U resulted in postimplantation lethality (Roshon *et al.*, 2005). While E3.5-E6.5 homozygous mutant mice appeared no different from their wild type and heterozygous littermates, by E7.5 hnRNP U homozygous mutant mice appeared similar to those of wild type E6.5 mice. By E8.5, wild type mice had begun to undergo organogenesis and the neural folds, primitive heart, and somities were present, while homozygous hnRNP U mutant mice appeared not to have progressed further in development, but exhibited an expansion of the extraembryonic tissue. In fact, homozygous hnRNP U mutant mice possessed an enlarged allantois, which was likely due to the failure of the chorion to fuse with the allantois.

In this section, I briefly described some of the phenotypes associated with the knockout mice of YAP's interacting partners; however, only Src/Fyn/Yes, p53SP-2, p73, TEAD, and hnRNP U mutant mice exhibited phenotypes even closely resembling those of YAP-null embryos. Therefore, in order to best understand YAP's role in early vertebrate

development, it was imperative that I perform a series of knockdown and gain-of-function experiments in animal models more amenable to early developmental invesitgations.

Chapter II – YAP expands neural progenitors and regulates *pax3* expression in the neural plate border zone

Introduction

Yes-associated protein 65 (YAP) contains multiple protein-protein interaction domains and functions as both a transcriptional co-activator and as a scaffolding protein. YAP was first identified and named based on its association with the Src-family tyrosine kinase and proto-oncogene, c-Yes (Sudol, 1994). YAP is a founding member of the WW domain-containing protein family (Bork *et al.*, 1994, Sudol *et al.*, 1995). The WW domain allows the binding of proteins containing a PPxY motif (Macias *et al.*, 1996). Proteins shown to bind to YAP via its two WW domains include: p53 family members (p73α, p73β, p63 (Strano *et al.*, 2001); Smad7 (Ferrigno *et al.*, 2002); Runx2 (Yagi *et al.*, 1999); and ErbB-4 (Komuro *et al.*, 2003, Omerovic *et al.*, 2004).

In addition to the two WW domains, YAP also contains other protein-protein interaction domains (Figure 1). Proteins that interact at the N-terminus of YAP include hnRNP U, a nuclear ribonucleoprotein shown to be important for RNA polymerase II transcription (Howell *et al.*, 2004, Kukalev *et al.*, 2005), the TEA domain-containing transcription factor (TEAD/TEF) family (Vassilev *et al.*, 2001), and the Large tumor suppressor (LATS). The phosphorylation event involving LATS allows for the binding of 14-3-3, which leads to the subsequent sequestration of YAP to the cytoplasm (Zhao *et al.*, 2007). At its C-terminus, YAP contains a postsynaptic density 95, discs large, and zonula occludens-1 (PDZ)-binding motif that allows for binding to PDZ domain-containing proteins.

Our initial interest in YAP came from the finding that YAP bound to the second PDZ domain of Na(+)/H(+) exchanger regulator factor 1/ezrin/radixin/moesin (ERM)-binding phosphoprotein of 50 kDa (NHERF1/EBP50) and co-localized to the apical membrane of polarized airway epithelia along with Cystic fibrosis ransmembrane conductance regulator

(CFTR) and c-Yes (Mohler *et al.*, 1999). To determine the *in vivo* importance of this scaffolding complex, we used homologous recombination to remove YAP from the mouse and found that few embryos survived past embryonic day 8.5 (E8.5), a much earlier time point than would be expected for an associated lung development phenotype (Morin-Kensicki *et al.*, 2006). Detailed analyses of these mice illustrated that they suffered from defects in yolk sac vasculogenesis, chorioallantoic fusion, and anterior-posterior (A-P) axis elongation.

Given that YAP knockout mice struggled to progress normally through early development, in part because of nutritional deficiencies, we sought to better characterize a role for YAP during this time period by using embryos that develop externally: *Xenopus laevis* and *Danio rerio*. YAP morpholino (MO)-mediated loss-of-function resulted in a delay of mesoderm induction and severely impaired A-P axis elongation, phenotypes that were similar to $YAP^{-/-}$ mice. YAP gain-of-function experiments in *Xenopus laevis* expanded the progenitors of the neural plate and neural plate border zone, while concomitantly inhibiting expression of later markers of tissues derived from the neural plate border zone (neural crest, preplacodal ectoderm (PPE), hatching gland), as well as epidermis, and somitic muscle. Through loss- and gain-of-function experiments and endogenous chromatin immunoprecipitations (ChIP) for YAP, we show that YAP directly regulates *pax3* expression via association with TEAD1 (N-TEF) and ultimately localizes to a highly conserved, previously undescribed, TEAD-binding site within the 5' regulatory region of *pax3*. Finally, structure/function analyses revealed that the PDZ-binding motif of YAP contributes to the inhibition of epidermal and somitic muscle differentiation, but a complete, intact YAP

protein is required for expansion of the neural plate and neural plate border zone progenitor pools.

Materials and Methods

Animal use and ethics statement

All experimental procedures described in this study followed the U.S. Public Health Service Policy of Humane Care and Use of Laboratory Animals and were approved by the Institutional Animal Care and Use Committee at the National Institutes of Health (NHLBI Animal Study Protocol: #H-0063), University of North Carolina at Chapel Hill (IACUC ID: 10-277.0), and the George Washington University (GWU Animal Study Protocol: #A-3205).

xYAP and morpholinos

A *Xenopus laevis* full-length cDNA clone (XL211h05) of *yes-associated protein 65* (*xyap*) was obtained from the National Institute for Basic Biology **(**Japan) and sequenced in both directions (GenBank Accession #FJ979828). Three morpholinos, MO1 (GGA GGT GGG AGC TAG GAC AGC GG), MO2 (GGA GAG GAC GCG GTA GGA GAC TGT G), and MO3 (GGG CTC CAT GGC TGC GGG GAG GTG G), were designed to the 5'UTR of *xyap* for translational blocking (Figure 1; GeneTools). Two splice blocking and putative early translational truncation MOs, exon 1 (GTA GAG GAG CAT ATA CCT GCC GTG A) and exon 2 (CCT GCA AAG AAC AAG TGG GAC AAT A) (GeneTools) were designed across exon/intron boundaries. *In vitro* translation reactions were performed using the TnT Quick Coupled Transcription/Translation System (Promega), according to the manufacturer's protocol. Each MO (80 ng) was injected into *in vitro* fertilized one-cell *Xenopus laevis*

embryos according to established methods (Sive *et al.*, 2000). To observe phenotypes associated with lower MO concentrations (0, 1.25, 2.5, 5, 10, 20, and 40 ng total), a cocktail of all three (MO1, MO2, and MO3) translational blocking MOs was injected into *in vitro*-fertilized one-cell sibling embryos.

xYAP RT-PCR

Using *Xenopus tropicalis* genomic scaffolds containing *xyap*, exon-intron boundaries were determined with Spidey (http://www.ncbi.nlm.nih.gov/spidey/) by aligning the scaffolds with the *xyap* mRNA. The Primer3 program was used to generate a pair of primers (Forward: GAG CCC TCA GAC TGG AGT GTT G, Reverse: TCA TGC TCA ATC CGC TTT CAG T) between exon 6 and exon 8 for use in reverse transcriptase-polymerase chain (RT-PCR) reactions. Twenty *Xenopus laevis* embryos were collected for each of the following developmental stages (Nieuwkoop *et al.*, 1994): unfertilized egg, 2, 3, 6, 7, 9, 10, 11, 12, 16-17, 19-21, 21-23, 23-25, 26-28, 29-30, 36-38, 40 and stored in RNAlater (Ambion) at -20°C. Embryos were removed from the RNAlater (Ambion) and homogenized in 1 mL of Trizol reagent (Invitrogen) and RNA was isolated according to the manufacturer's specifications. Prior to precipitation, glycogen was added to the aqueous phase as a co-precipitant. After drying, the RNA pellet was resuspended in 50 µl of nuclease-free water and quantified by its absorbance at 260 nm, while its purity was based on the ratio of A_{260}/A_{280}.

3 µg of RNA from each *Xenopus laevis* stage was treated with DNase I (Promega) according to the manufacturer's specifications and heat inactivated at 65°C for 10 minutes. These samples were split in half with half being used to synthesize cDNA and the other half

used for a no reverse transcriptase control. Reverse transcription was performed using random hexamer priming and Superscript II reverse transcriptase (Invitrogen) according to the manufacturer's specifications. 1 μl of each reverse transcribed cDNA template, no-reverse transcriptase control, and no template control was added to a 50 μl PCR reaction cocktail, denatured at 94°C for 2 minutes, and cycled 32 times as follows: 94°C for 30 sec, 55°C for 30 sec, and 72°C for 1 min. 15 μl of each PCR reaction was electrophoresed on a 2% agarose gel and the resulting 305 base pair products were visualized using ethidium bromide and ultraviolet light. As a loading control, a primer set (Forward: GGG ATA ACA TTC AGG GTA TC, Reverse: CAT GGC GGT AAC TGT CCT) for *Xenopus laevis* histone H4 was used for PCR amplification from the reverse transcribed cDNA template and 100 ng of *xyap* plasmid DNA was used as a positive control.

Genomic DNA was isolated from thirty stage 29 *Xenopus laevis* embryos stored in RNAlater at -20°C using the protocol for isolating genomic DNA from Ambion. The resulting pellet was resuspended in 200 ul of nuclease free water, quantified by measuring A_{260}, and treated with RNase-T1 (Sigma). Amplification of the *Xenopus laevis* genomic product was performed using the Expand Long Template PCR System (Roche) according to the manufacturer's protocol.

Cloning methods and constructs

For use in all of our gain-of-function analyses, we initially cloned an HA tag (ATG TAC CCA TAC GAT GTT CCA GAT TAC GCT) into the *Xho*I and *Eco*RV sites of the pSP64TXB vector so that proper expression could be detected by western blot analysis. *xyap* and *xtead1* were subcloned in frame with the HA tag into the *Eco*RV and *Not*I sites of the

pSP64TXB-HA vector. A set of xYAP mutant constructs, which included a constitutively active form of xYAP (cActive xYAP) with a mutated LATS phosphorylation site (S98A), a deletion (aa 61-81) of the TEAD-binding site (xYAPΔTBS), a deletion (aa 78-161, aa 199-236) of the WW domains (xYAPΔWW), a deletion (aa 1-90) of the entire N-terminus (xYAPΔN), and a deletion (aa 455-459) of the PDZ-binding motif at the C-terminus (xYAPΔC), were also subcloned into the pSP64TXB-HA vector at the *Eco*RV and *Not*I sites.

Gain-of-function analyses

For initial gain-of-function analyses, the animal poles of one-cell *Xenopus laevis* embryos were injected with 2 ng of *in vitro*-transcribed *ha-xyap* mRNA (mMessage Machine, Ambion). For additional gain-of-function analyses, two-cell *Xenopus laevis* embryos were co-injected with 1 ng of *in vitro*-transcribed *ha-xyap* or *ha-xyap* mutant mRNAs and 100 pg of *in vitro*-transcribed *nls-β-galactosidase* mRNA into the lateral, animal pole of one of the two blastomeres. Similarly, 100 pg of the *in vitro*-transcribed *ha-xtead1* (*xn-tef1*) (Naye *et al.*, 2007) or 100 pg of *ha-xyap* mRNAs, were injected alone or in combination.

Western blots

Embryos were injected at the 1-cell stage with a cocktail of the three (MO1, MO2, and MO3) translational blocking xYAP MOs (40 ng or 80 ng total) or the standard control MO (40 ng or 80 ng). These sibling embryos were allowed to develop until control embryos reached stage 15. Whole embryo lysates were snap frozen in a dry ice/ethanol bath and lysed in RIPA buffer (50 mM Tris, pH 8.0, 150 mM NaCl, 1% NP-40, 0.5% sodium deoxycholate,

0.1% SDS) containing a protease inhibitor cocktail (Roche). Subsequently, Freon (1,1,2-trichlorotrifluoroethane, Sigma-Aldrich) was used to remove the yolk from the samples, which were then boiled for 5 min and stored at -80°C. Total protein concentrations were quantified using the BCA Protein Assay Kit (Pierce), according to the manufacturer's protocol. Equal amounts of protein were loaded onto a 10% SDS-PAGE gel, separated by electrophoresis, transferred to a PVDF membrane, and probed for xYAP using an affinity purified rabbit anti-YAP antibody (1:1000), which was generated against human YAP (274-454) (Howell *et al.*, 2004). The blots were then probed with a secondary HRP conjugated anti-rabbit IgG antibody (1:10,000) (Jackson ImmunoResearch). The blots were incubated in stripping buffer (62.5 mM Tris, 2% SDS, 0.1 M β-mercaptoethanol, pH 6.7) and re-probed for elongation factor-2 (EF-2) using a goat anti-EF-2 antibody (1:500) (Santa Cruz) and a secondary HRP-conjugated anti-goat IgG antibody (1:4000) (Jackson ImmunoResearch).

zYAP and embryo manipulations

A *Danio rerio* full-length cDNA IMAGE clone 7066008 of *yes-associated protein 65* (*zyap*) **(**NM_001115121) was obtained from Open Biosystems. A zYAP MO (5' CTC TTC TTT CTA TCC AAC TGA AAC C 3') was designed to the 5' UTR of *zyap* (Figure 1, GeneTools). *In vitro* translation reactions were performed using the TnT Quick Coupled Transcription/Translation System (Promega), according to the manufacturer's protocol.

1-cell embryos were injected with 16 ng of the zYAP MO, a standard control MO (GeneTools), or 300 or 600 pg of *in vitro*-transcribed *ha-zyap* mRNA. Once embryos reached the 1000-2000-cell stage, their chorion membranes were removed and embryos were placed on a custom fitted imaging mold (kindly supplied by Dr. Sean Megason) (Megason, 2009)

for time-lapse videography. Embryos were subsequently allowed to progress to the prim-11 stage and fixed.

qPCR

Xenopus laevis embryos were injected with 80 ng of the translational blocking xYAP MO cocktail or a control MO at the 1-cell stage. When sibling control embryos reached stage 11, total RNA was isolated using the Trizol reagent (Invitrogen), according to the manufacturer's protocol. RNA was quantified using a RiboGreen RNA quantitation kit (Invitrogen), according to the manufacturer's instructions. Total RNA (2 μg) was reverse transcribed using Vilo cDNA synthesis (Invitrogen), according to the manufacturer's protocol. Then, qPCR was performed on a 7900HT 380-well block Real-Time PCR system (Applied Biosystems) using Maxima SYBR green qPCR master mix (Fermentas) on serial dilutions of the RT product to ensure the efficiency of amplification with each primer set was within 10% of one another. A relative quantification study was performed using 5 μL of a 1:100 dilution of the RT product, which was amplified using gene-specific primers: *brachyury* (Forward: 5' TCT CTT TCA CAT GCT GTG CC 3', Reverse: 5' GTG CCG TGA CAT CAT ACT GG 3'); *goosecoid* (Forward: 5' CAC ACA AAG TCG CAG AGT CTC 3', Reverse: 5' GGA GAG CAG AAG TTG GGG CCA 3'); *wnt8* (Forward: 5' TAT CTG GAA GTT GCA GCA TAC A 3', Reverse: 5' GCA GGC ACT CTC GTC CCT CTG T 3'); *nodal-related 3* (*nr3*) (Forward: 5' CGA GTG CAA GAA GGT GGA CA 3', Reverse: 5' ATC TTC ATG GGG ACA CAG GA 3'); *siamois* (Forward: 5' AAG ATA ACT GGC ATT CCT GAG C 3', Reverse: 5' GGT AGG GCT GTG TAT TTG AAG G 3'); *sox17α* (Forward: 5' GCA AGA TGC TTG GCA AGT CG 3', Reverse: 5' GCT GAA GTT CTC TAG ACA CA

3'); *sox11* (Forward: 5' GGC TCT GGA TGA GAG TGA CC 3', Reverse: 5' TGA TGA AGG GGA TTT TCT CG 3'); *h4* (Forward: 5' GGG ATA ACA TTC AGG GTA TC 3', Reverse: 5' CAT GGC GGT AAC TGT CTT C 3')

In situ hybridization and β-galactosidase staining

Xenopus laevis embryos were fixed in MEMFA, stained for expression of a NLS-β-galactosidase lineage tracer, and processed for whole mount *in situ* hybridization according to standard protocols (Harland, 1991, Sive *et al.*, 2000). Anti-sense DIG-labeled RNA probes were synthesized from the following plasmids: *chordin* (*Eco*RI, T7) (Sasai, Y. *et al.*, 1994), *eomesodermin* (*Xho*I, T7) (Ryan *et al.*, 1996), *brachyury* (*Cla*I, T7) (Smith *et al.*, 1991), *vent2* (*Eco*RI, T7) (Ladher *et al.*, 1996), *not* (*Hind*III, T7) (von Dassow *et al.*, 1993), *sox2* (*Hind*III, T7) (Lu *et al.*, 2004), *neuroD* (*Xho*I, T3) (Lee, J. E. *et al.*, 1995), *n-tubulin* (*Bam*HI, T3) (Chitnis *et al.*, 1995), $p27^{Xic1}$ (*Bam*HI, T7) (Hardcastle *et al.*, 2000), *sox11* (*Sal*I, T3) (Hiraoka *et al.*, 1997), *six1* (*Not*I, T7) (Pandur *et al.*, 2000), *notch* (*Cla*I, Sp6) (Coffman, C. R. *et al.*, 1993), *hes1* (*Sal*I, T7) (Open Biosystems, BC070988), *zic1* (*Eco*RI, T3) (Mizuseki *et al.*, 1998), *foxD3* (*Bam*HI, T3) (Sasai, N. *et al.*, 2001), and *pax3* (*Sal*I, T7) (Lu *et al.*, 2004). A full-length probe for *myoD* was PCR amplified from a *Xenopus laevis* (stage 19-26) cDNA library, which was kindly provided by Dr. Aaron Zorn, using the following primers: forward (GGA CTA GTA TGG AGC TGT TGC CCC CAC CAC TG) and reverse (CGG AAT TCC TAT AAG ACG TGA TAG ATG GTG CTG), and subcloned into the pBluescript SK(-) vector at the *Spe*I and *Eco*RI sites. This *myoD* probe was then synthesized as described above (*Spe*I, T7).

Chromatin Immunoprecipitation (ChIP)

ChIP assays were performed with the ChIP-IT Express kit (Active Motif) with some modifications. Three hundred stage 14-16 *Xenopus laevis* embryos were incubated, with gentle rolling, in 10 ml of 1% formaldehyde/0.1X modified Barth's solution (MBS) for 30 minutes at room temperature to crosslink genomic DNA and protein complexes. Crosslinking was stopped by incubating the embryos in 125 mM glycine/0.1X MBS with gentle rolling. Following two washes in 0.1X MBS, the embryos were snap-frozen and stored at -80°C. Chromatin was sheared with a Misonix 3000 cup horn by repeating 6 cycles of 30sec: 1sec pulse, 0.5 sec off at a power of 5. Samples rested on ice for 1 minute between each cycle. Shearing efficiency was determined by resolving a reverse-crosslinked, precipitated sample of chromatin on a 1% agarose gel. This sample was quantified using a Nanodrop, and 12.5 or 25 μg of chromatin was subsequently immunoprecipitated for 4 hours with 2 mg of affinity-purified YAP antibody or rabbit IgG (Genscript) in the presence of 0.25mg/ml BSA and 0.1 mg/ml herring sperm DNA. Beads were washed once with ChIP buffer 1 (Active Motif) and twice with ChIP buffer 2 (Active Motif) prior to elution and proteinase K treatment. Five percent of the eluate was used to amplify the *pax3* promoter TEAD-binding site region using the following *xpax3*-specific primers: forward (GCC TGA CAA TGG CAC CTT AT) and reverse (AGG CGC ACT TGT GTG ATT C). For subcloning this region, a proofreading DNA polymerase (cloned *Pfu* DNA polymerase, Stratagene) was used to PCR amplify the product from the isolated YAP co-immunoprecipitated *Xenopus laevis* genomic DNA. This PCR product was then gel-purified from a 1% agarose gel. Alanines were then added back to the ends using a non-proofreading DNA polymerase (Jumpstart Taq polymerase, Sigma-

Aldrich). The products were then ligated into the pCRII-TOPO vector (Invitrogen) and sequenced.

Luciferase Assays

The 5'-flanking transcriptional regulatory region for *pax3* was amplified by PCR from *Xenopus laevis* genomic DNA using forward (5' GCC TGA CAA TGG CAC CTT AT 3') and reverse primers (TCC TGC CTC GGA GGT AAC TAG TG) and subcloned into the *Kpn*I and *Eco*RV sites of the pGL4.10 luciferase vector (Promega). A three-base mutation of the putative xTEAD1-binding site within this 5'-flanking region was performed using a forward primer (CTG GCC ACT GCT ATA AGG TAC TTT CAA CAA ATG C) and a reverse primer (GCA TTT GTT GAA AGT ACC TTA TAG CAG TGG CCA G) and the Quikchange II Site-Directed Mutagenesis Kit (Stratagene). *In vitro*-fertilized *Xenopus laevis* embryos were co-injected with a β-galactosidase (β-gal) reporter under the control of the *actin* promoter in combination with the pGL4.10, pGL4.10-*pax3*, or pGL4.10-*pax3*-Mut with or without the addition of 100 ng of *xtead1* and *xyap*. Each sample (n) consisted of fifteen, pooled, stage 14-16, embryos, which were collected, lysed in 150 µL Glo Lysis Buffer (Promega), and snap-frozen in an ethanol-dry ice bath. Upon thawing, an equal volume of Freon (1,1,2-trichlorotrifluoroethane, Sigma) was added to each sample, spun at 13000 x g for 15 minutes at 4°C, and transferred to a new tube. Luciferase activity was measured by combining 50 µL of embryo lystates with 50 µL of the Steady-Glo luciferase assay substrate (Promega). Samples were then gently rotated for 5 minutes at room temperature, and the activity was detected with a Victor luminometer (PerkinElmer). β-gal activity was measured using 10 µL of the embryo lysate in 67 µL of sodium phosphate buffer (0.1 M, pH 7.5), 1 µL

of 100X Mg^{2+} solution (0.1 M $MgCl_2$, 4.5 M β-mercaptoethanol), and 22 µL of 1X ONPG (Sigma) in sodium phosphate buffer (Sambrook and Russell, 2001). The reaction was carried out in a 37°C incubator for 1 hour and stopped by the addition of 167 µL of 1 M sodium carbonate. β-gal activity was determined by measuring the level of the hydrolysis product of 1X ONPG at a wavelength of 405 nm (Victor microplate reader, PerkinElmer). The luciferase activity was normalized according to the β-gal activity by taking the ratio of luciferase activity to β-gal expression in the embryos.

Similarly, 100 pg of TOPflash (Clontech), a Wnt luciferase reporter containing TCF-binding sites or FOPflash (Clontech), a luciferase reporter with these TCF sites mutated, were co-injected with 100 pg of a β-gal reporter, alone or in the presence of 1 ng RNA encoding for HA-xYAP or HA-xYAP ΔC-term into *in vitro*-fertilized 1-cell *Xenopus laevis* embryos. Sample collection, preparation, and analyses were performed as described above.

Results

We previously showed that $YAP^{-/-}$ mice were embryonic lethal and exhibited severe developmental abnormalities that included defects in yolk sac vasculogenesis, chorioallantoic fusion, and A-P axis elongation (Morin-Kensicki *et al.*, 2006). Given that these defects could be due to nutritional deficiencies, we sought to better characterize a role for YAP during early development by using *Xenopus laevis* and *Danio rerio*, animal models for which the nutritional needs of the embryos are self-contained. In addition, these embryos permit easy knockdown of targeted protein expression via injection of gene-specific MOs and efficient gain-of-function assessment via mRNA injections.

YAP is required for progression through gastrulation.

The full-length *Xenopus laevis yap* (*xyap*) EST encodes a protein that is 78% identical to mouse YAP and contains all the described protein-protein interaction domains, as well as the transcriptional activation domain (Figure 1). Isolation of *Xenopus laevis* genomic DNA and subsequent PCR validated that our RT-PCR primer design amplified a PCR product across exon-intron boundaries (Figure 2). RT-PCR and western blot analyses revealed that *xyap* mRNA and protein are maternally expressed in an unfertilized egg and persists throughout *Xenopus laevis* tadpole stages (Figure 3), which is consistent with results from mouse and *Xenopus tropicalis* (Morin-Kensicki *et al.*, 2006, Nejigane *et al.*, 2011, Sawada *et al.*, 2005). Four xYAP MOs were designed around the translational start site (Figure 1) and the efficacies of three of them (MO1, MO2, and MO3) were confirmed *in vitro* (Figure 4). An antibody directed against the C-terminus (274-454) of human YAP (hYAP) detected a band at the appropriate size from cold *in vitro*-translated xYAP product and stage 15 whole embryo lysates (Figure 5). We used this hYAP antibody to test the efficacy of our xYAP MOs *in vivo*. Lysates from stage 15 MO-injected embryos showed efficient knockdown of endogenous xYAP expression to undetectable levels (Figure 6).

In vitro-fertilized sibling *Xenopus laevis* embryos that were injected with 80 ng of any one of these xYAP MOs at the 1-cell stage failed to complete epiboly and close the blastopore (MO1, n=200, 100%; MO2, n=185, 100%; MO3, n=191, 100%), while uninjected (n=349) and control MO-injected (n=231) embryos progressed through gastrulation unexpurgated (Figure 7). Furthermore, these xYAP MO-injected embryos arrested at the open-blastopore stages. The same effect was observed using 40 ng (n=725, 100%) and 80 ng (n=352, 100%) of an equimolar cocktail of all three translation-blocking MOs injected into

Figure 2: Validity of xYAP RT-PCR primer design. The proper design of the xYAP RT primers was confirmed by amplification of a larger, 2200 base pair, PCR product from isolated *Xenopus laevis* genomic DNA compared to the amplification of a 305 base pair PCR product from a xYAP cDNA.

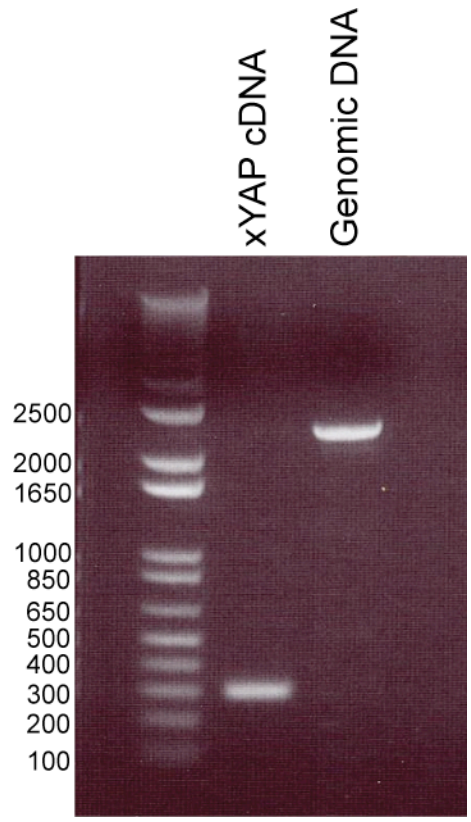
xYAP cDNA
Genomic DNA
2500
2000
1650
1000
850
650
500
400
300
200
100

Figure 3: mRNA and protein expression of xYAP during *Xenopus laevis* development. RT-PCR analyses showed that *xyap* RNA was maternally expressed in an unfertilized egg and early cleavage (stage 3), decreases slightly between late cleavage (stage 6) and the mid-blastula transition (stage 9), but was then expressed abundantly through subsequent stages of *Xenopus laevis* development through feeding tadpole (stage 40). The (+) indicates lanes that included reverse transcriptase in the RT-PCR reaction, while the (-) indicates lanes that lacked the reverse transcriptase in the RT-PCR reaction. Western blot analysis showed that xYAP protein was maternally present at cleavage stages (stages 2-7), was detectable at the onset of epiboly and gastrulation (stages 9-10), and increased dramatically from mid-gastrula (stage 11) onwards. The (+) represents the positive control lane, which contains a cold *in vitro* translated xYAP product.

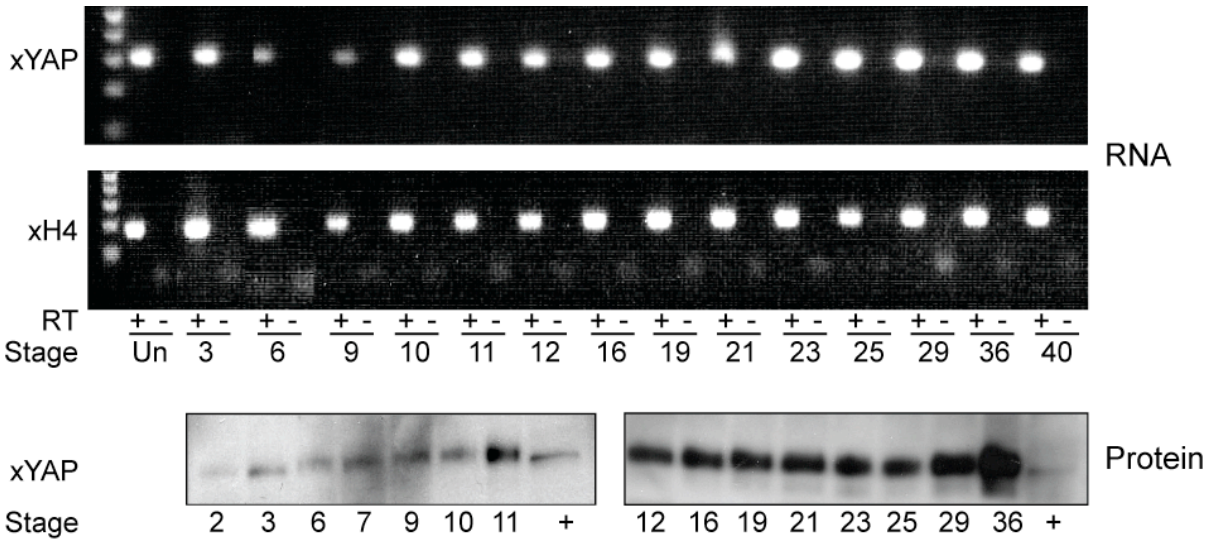
xYAP
xH4
RNA
RT
+ - + - + - + - + - + - + - + - + - + - + - + - + - + -
Stage
Un 3 6 9 10 11 12 16 19 21 23 25 29 36 40
xYAP
Protein
Stage
2 3 6 7 9 10 11 +
12 16 19 21 23 25 29 36 +

Figure 4: Efficacy of xYAP-MOs *in vitro*. *xyap* mRNA was *in vitro* translated with or without the presence of four MOs designed to target the 5' UTR of *xyap*. All *in vitro* translations were performed in the presence of [^{35}S]methionine and proteins were visualized by phosphoimage analysis. MO1, MO2, and MO3 efficiently knocked down xYAP protein expression *in vitro*, whereas a fourth (-) did not.

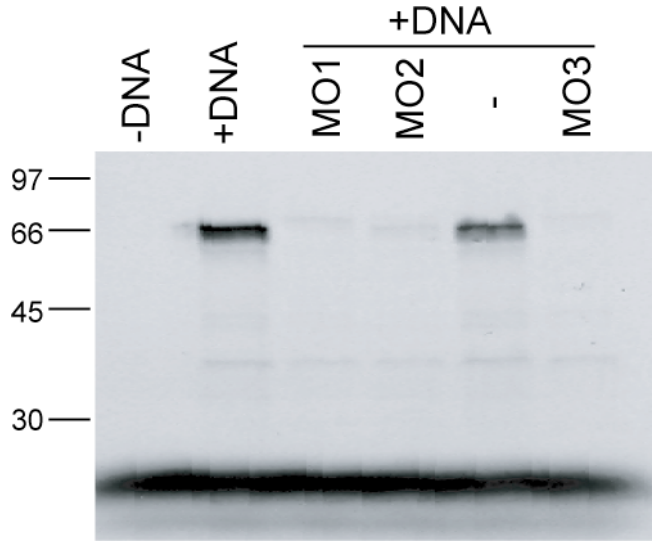
+DNA
-DNA
+DNA
MO1
MO2
-
MO3
97
66
45
30

Figure 5: hYAP antibody recognized *Xenopus laevis* YAP. A rabbit polyclonal antibody, generated against the C-terminus of human YAP, specifically recognized *in vitro* translated xYAP (+DNA), but not the mock translated control (-DNA). Similarly, the antibody recognized a single protein in stage 15 *Xenopus laevis* whole embryo lysates.

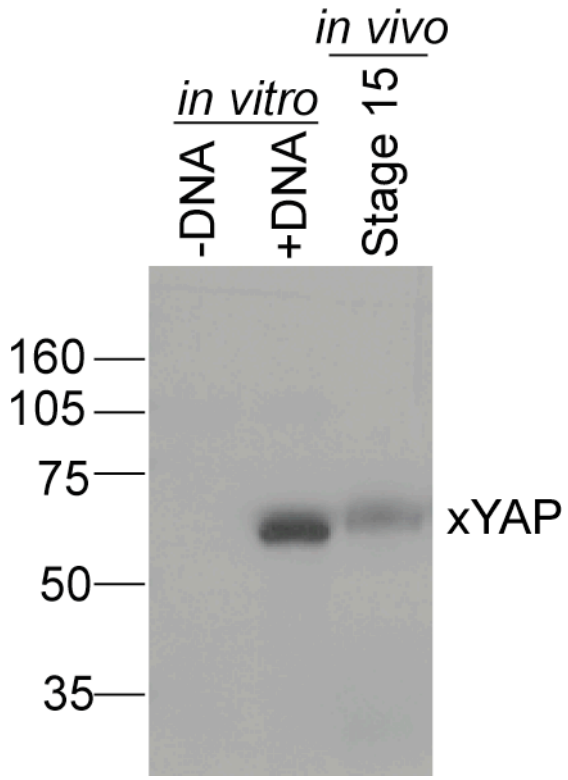
in vivo
in vitro
-DNA
+DNA
Stage 15
160
105
75
50
35
xYAP

Figure 6: Efficacy of xYAP-MOs *in vivo*. Injection of an equimolar cocktail of xYAP MO1, MO2, and MO3 at two concentrations (40 ng and 80 ng) resulted in efficient knockdown of endogenous xYAP protein in stage 15 embryos as measured by western blot analysis. EF-2 expression from the same blot served as the loading control.

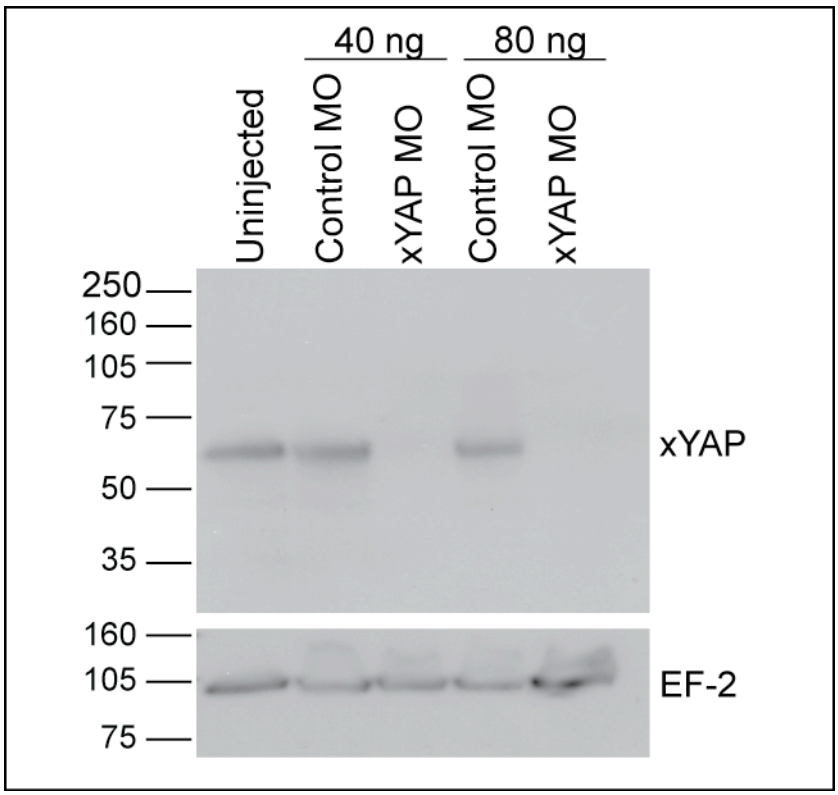
40 ng
80 ng
Uninjected
Control MO
xYAP MO
Control MO
xYAP MO
250
160
105
75
50
35
xYAP
160
105
75
EF-2

Figure 7: Phenotype resulting from the individual xYAP MOs. Uninjected (UN) and control MO injected (cMO) embryos have closed blastopores (arrows) at the end of gastrulation. Sibling embryos injected with one of the three different xYAP MOs (80 ng; see Figure 1 for binding sites) resulted in failure to close the blastopore (arrows) at the same developmental time.

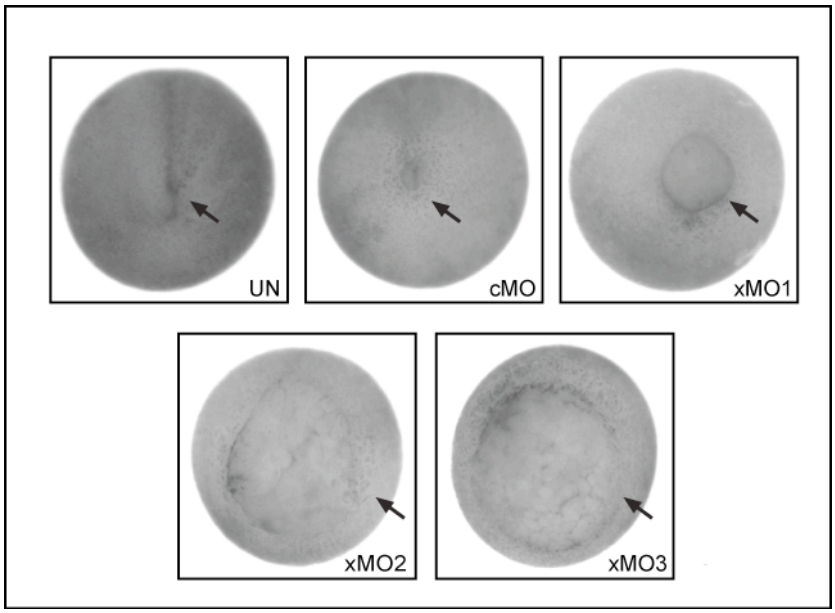
UN
cMO
xMO1
xMO2
xMO3

1-cell embryos (Figure 8), into one blastomere of 2-cell embryos (Figure 9), or with xYAP splice MOs targeted to exon 1 (n=328, 76%) and exon 2 (n=131, 77%) (not shown). The phenotype associated with the xYAP splice MOs likely was not as robust because they were less efficient at knocking down endogenous protein expression (Figure 10). Together, these results demonstrate the specificity of the xYAP MOs.

Reducing the concentration of the xYAP MO cocktail allowed blastopore closure, but resulted in dose dependent A-P axis elongation defects (Figure 11). Embryos injected with 1.25 ng (n=113) or 2.5 ng (n=142) of the xYAP translation blocking MO cocktail appeared unaffected, whereas embryos injected with 5-20 ng (5 ng, n=152; 10 ng, n=155; 20 ng, n=163) of this cocktail did not progress through gastrulation as rapidly as their control siblings, which resulted in shortened body axes (Figure 11).

Although the defective blastopore closure phenotype was reproducible using three different translational blocking xYAP MOs individually or in combination as well as two different splice blocking xYAP MOs, the phenotype was not rescued by co-injecting 2 ng of frog (*xyap*), mouse (*myap*), or human (*hyap*) mRNAs (not shown), even though they all were properly translated in *Xenopus laevis* embryos (Figure 12C). This result suggested that xYAP gain-of-function may also have an adverse effect on developmental progression, as reported for other scaffolding proteins (Lee, H. S. *et al.*, 2008). Interestingly, 0.25, 0.5, 1, and 2 ng of *xyap* mRNA injected into 1-cell embryos did not cause observable blastopore closure defects or observable morphological alterations until the tadpole stage (Figure 12B). In fact, all three mRNAs produced similar morphological alterations in the elongation of the A-P axis (Figure 12B), suggesting conservation of function. Therefore, we tested whether knockdown of YAP in another animal model, using similar methods, would produce a similar phenotype.

Figure 8: Phenotype resulting from a cocktail of the three xYAP MOs. *In vivo* knockdown of xYAP by injection of 40 ng of an equimolar the xYAP MO cocktail (green) into 1-cell *Xenopus laevis* embryos prevented the blastopore (arrow) from closing. Injections with an equal concentration of a control MO (red) allowed blastopore closure and had no other discernable effect on embryo development.

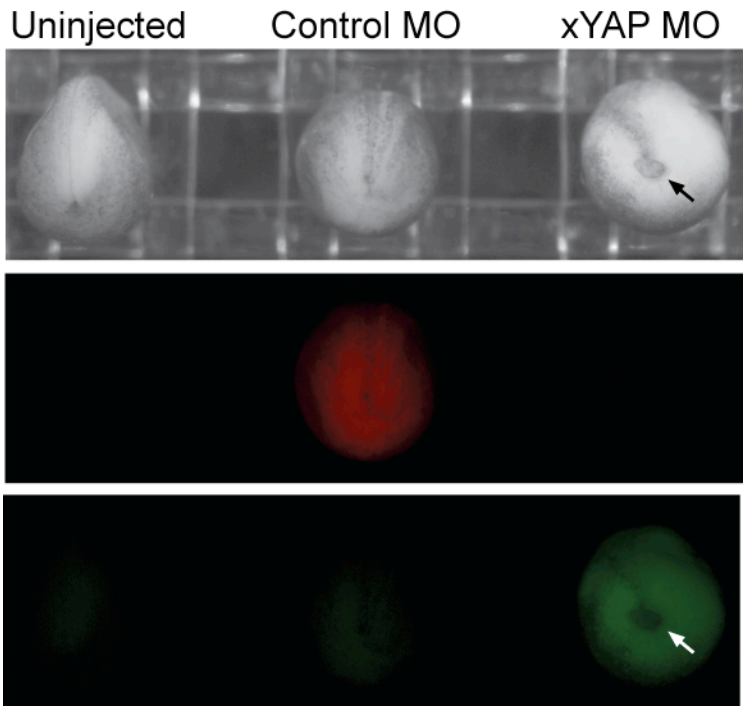
Uninjected
Control MO
xYAP MO

Figure 9: Phenotype resulting from injecting the xYAP MO cocktail into one cell of the 2-cell embryo. *In vivo* knockdown of xYAP by injection of 40 ng of the xYAP MO cocktail (green) into one blastomere of the 2-cell *Xenopus laevis* embryo prevented the blastopore (arrow) from closing. Injections with an equal concentration of a control MO (red) allowed blastopore closure and had no other discernable effect on embryo development.

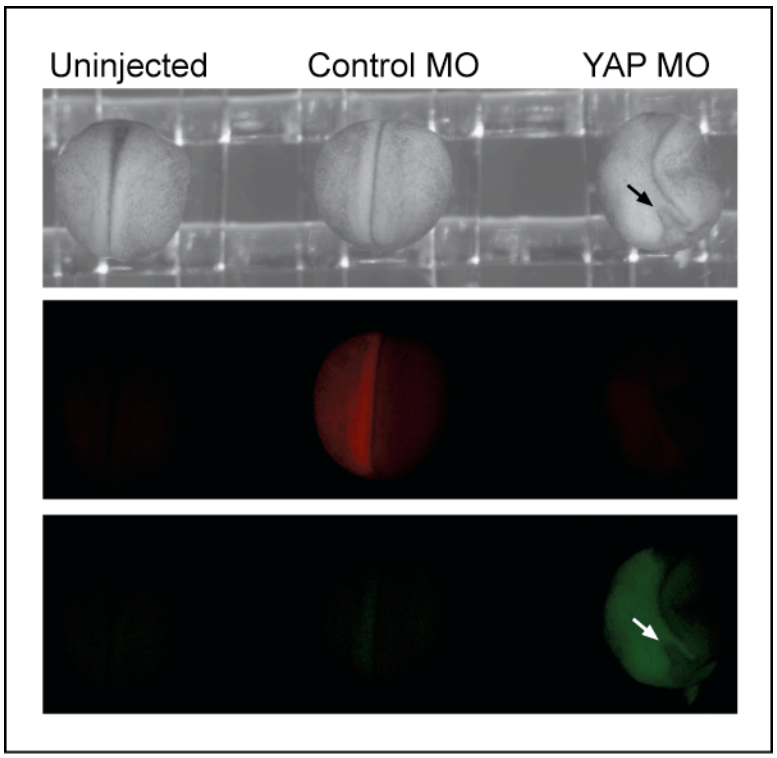
Uninjected
Control MO
YAP MO

Figure 10: Efficacy of xYAP splice blocking MOs. Two different concentrations (40 ng and 80 ng) of xYAP splice blocking MOs (xYAP Exon 1 MO and xYAP Exon 2 MO) reduced endogenous xYAP protein compared to control MO injected embryos. However, they were less efficient than the MOs targeted to the translational start site (Figures 4 and 6).

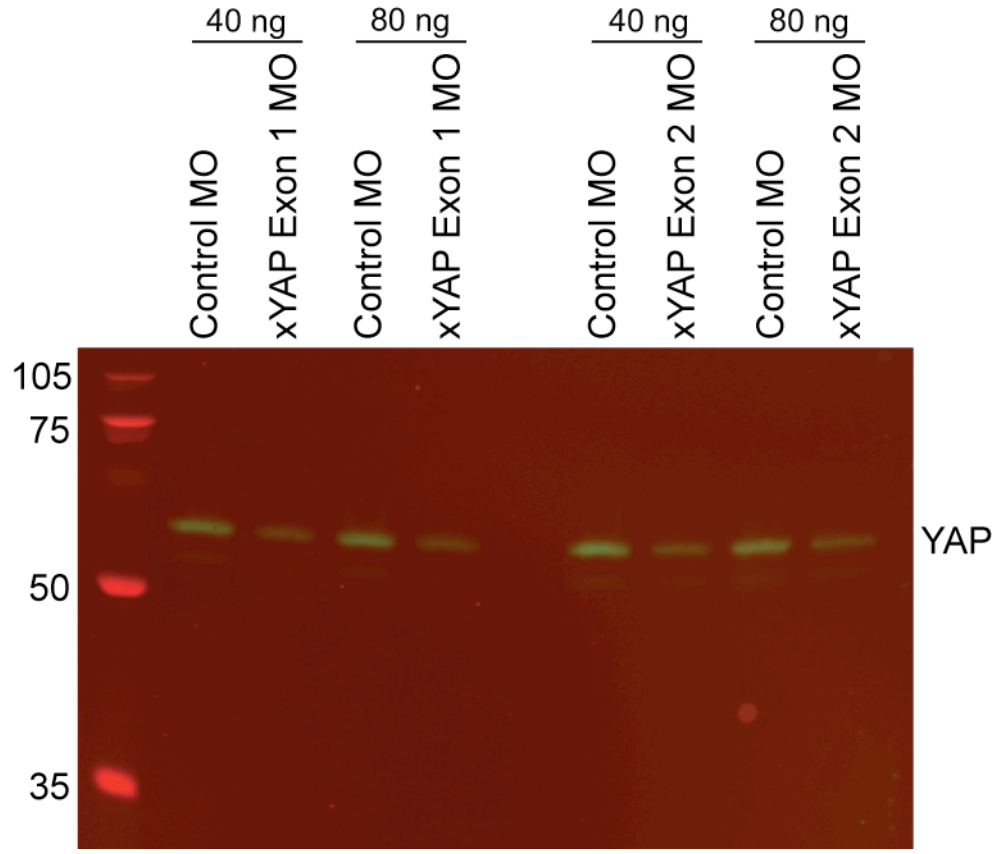
40 ng
80 ng
40 ng
80 ng
Control MO
xYAP Exon 1 MO
Control MO
xYAP Exon 1 MO
Control MO
xYAP Exon 2 MO
Control MO
xYAP Exon 2 MO
105
75
50
35
YAP

Figure 11: Phenotype resulting from titration of xYAP MO concentrations. Reducing the concentration (1.25, 2.5, 5, 10, and 20 ng) of the xYAP MO cocktail (left side) allowed blastopore closure, but resulted in dose-dependent A-P axis shortening. Embryos are siblings collected at the same developmental time.

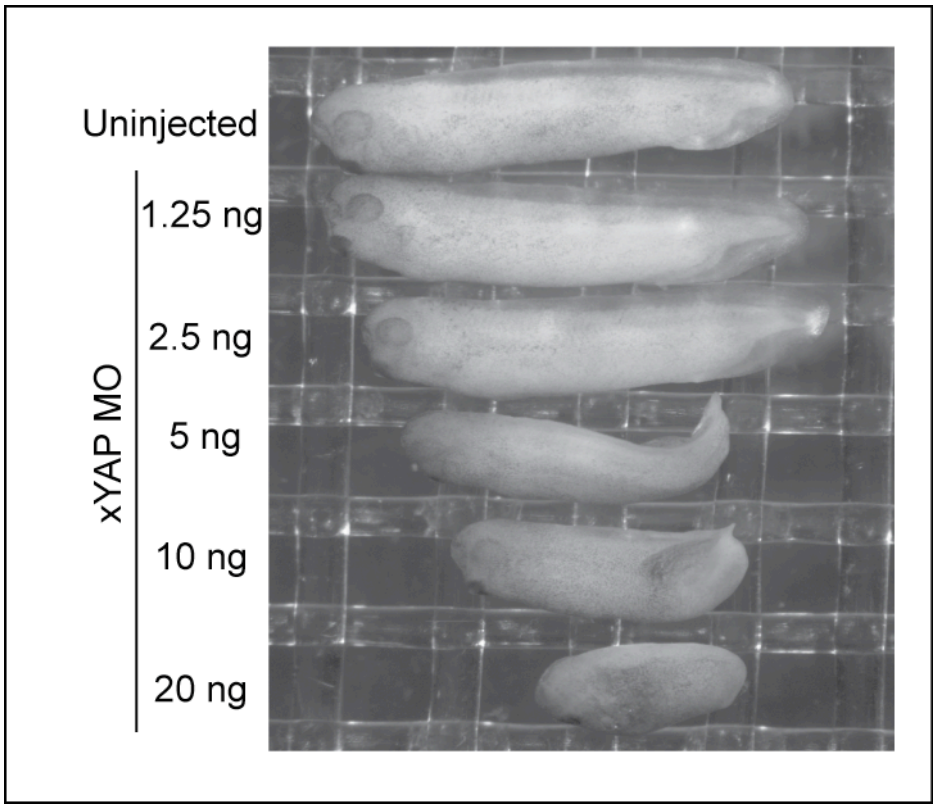
Uninjected
xYAP MO
1.25 ng
2.5 ng
5 ng
10 ng
20 ng

Figure 12: xYAP, mYAP, and hYAP gain-of-function in *Xenopus laevis*. (A) Western blot showing proper expression of increasing concentrations of HA-xYAP in stage 15 whole *Xenopus laevis* embryo lysates. (B) Frog (x), mouse (m), and human (h) YAP gain-of-function in *Xenopus laevis* embryos all showed similar axial phenotypes. (C) Using antibodies against the HA tag (left) and YAP (right), western blots of stage 15 whole *Xenopus laevis* embryo lysates illustrated proper overexpression of xYAP, mYAP, and hYAP.

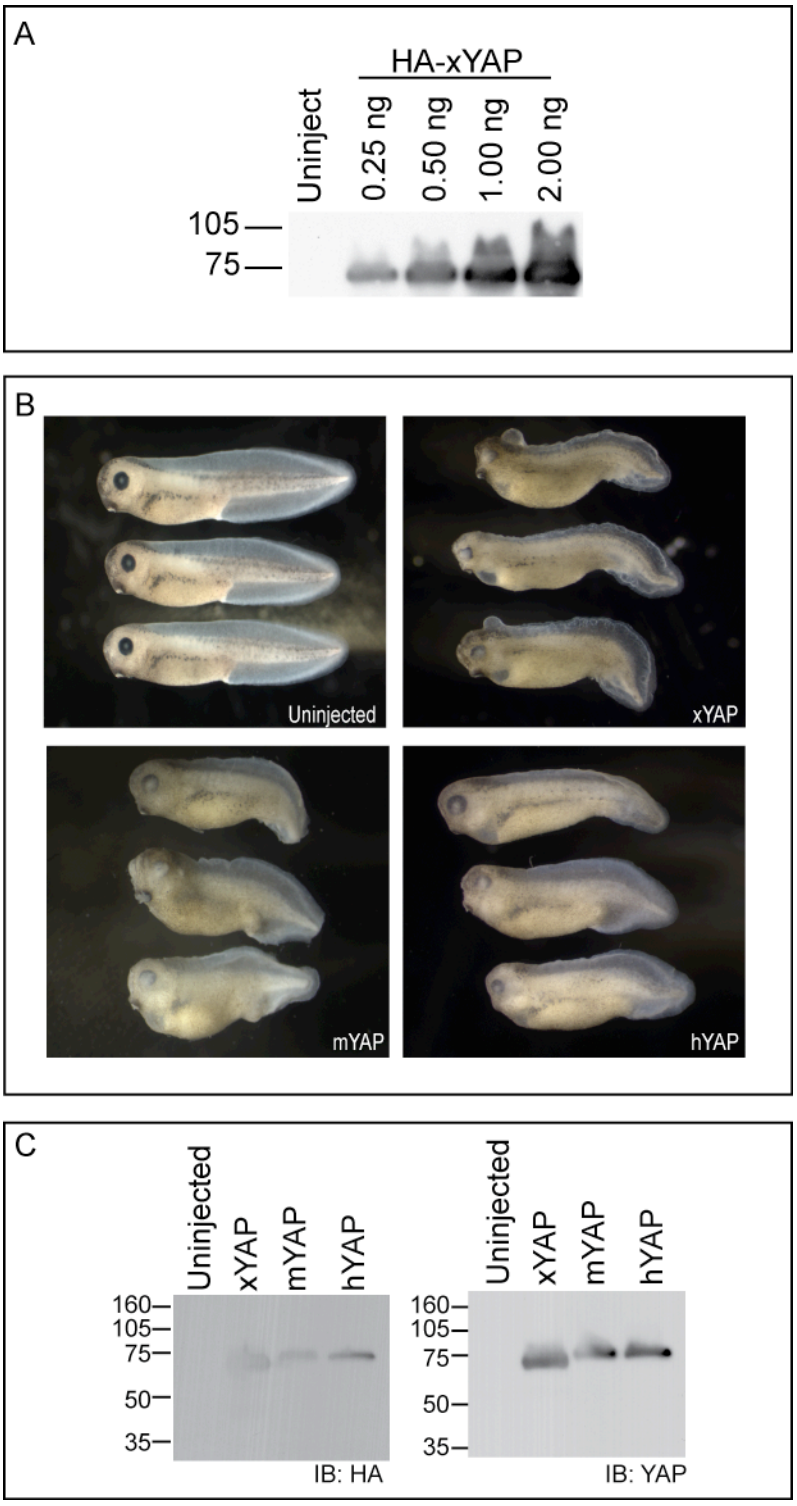
A
HA-xYAP
Uninject
0.25 ng
0.50 ng
1.00 ng
2.00 ng
105
75
B
Uninjected
xYAP
mYAP
hYAP
C
Uninjected
xYAP
mYAP
hYAP
160
105
75
50
35
IB: HA
IB: YAP

Injection of 16 ng of a zYAP MO into fertilized 1-cell zebrafish embryos resulted in delayed epiboly (Figure 13). Time-lapse videography showed that, in the absence of zYAP, developmental progression was perturbed beginning at 50% epiboly (5.25 hours post-fertilization, hpf) compared to uninjected and control MO-injected embryos (Figure 14, n=15 per each group). Although we used a high concentration of the zYAP MO to determine the start of the YAP MO-mediated developmental delay, our results are consistent with another group that used lower MO concentrations to determine later developmental defects and yet still observed YAP MO-mediated developmental delays (Jiang, Q. *et al.*, 2009). Thus, in three different vertebrates, loss of early YAP function interferes with the developmental networks that allow the embryo to progress through the process of gastrulation.

To determine whether the MO-mediated gastrulation defects correlated with an effect on genes required for germ-layer formation, we performed qPCR analyses on well-established markers of each germ layer. Control MO (80 ng) or the xYAP MO cocktail (80 ng) were injected into one-cell *Xenopus laevis* embryos, and the embryos were collected when uninjected siblings reached mid-gastrulation (stage 11), a stage when germ layer markers are abundantly expressed. Genes normally expressed in the organizer at the onset of gastrulation were either unaffected (*siamois*) or moderately increased (*nodal-related 3*). In contrast, the expression levels of endodermal (*sox17*, $p<0.013$), neural ectodermal (*sox11*, $p<0.021$), and three out of five mesodermal (*brachyury*, $p<0.013$; *goosecoid*, $p<0.011$; *wnt8* $p<0.018$) genes were significantly reduced in YAP MO-injected embryos (Figure 2A). However, analyses of several mesodermal markers by *in situ* hybridization in *Xenopus laevis* showed that these quantitative changes resulted from delayed expression rather than loss of mesoderm induction. While *brachyury*, *eomesodermin*, and *chordin* expression was markedly

Figure 13: Phenotype resulting from zYAP MO. zYAP MO-injected embryos are delayed in development beginning at gastrulation, as evidenced by failure of the epiboly front (*) to surround the yolk plug as seen in the uninjected sibling controls.

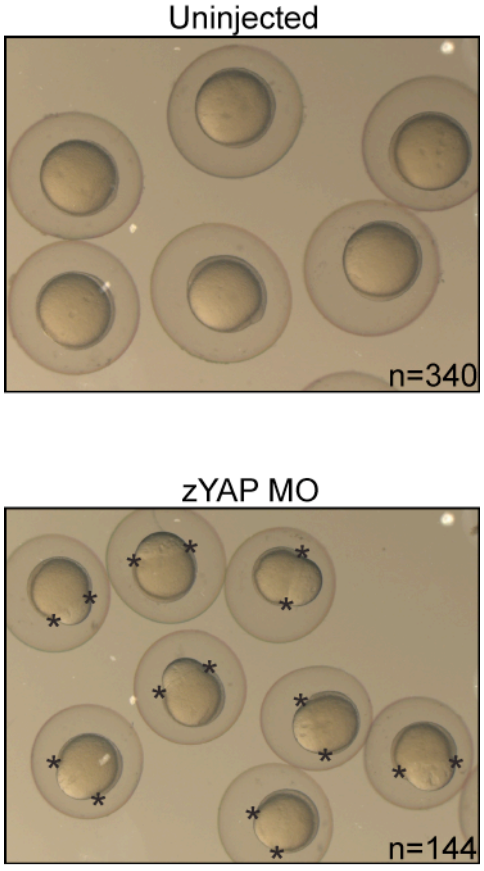
Uninjected
n=340
zYAP MO
n=144

Figure 14: Time-lapse video of 1-cell zYAP-MO injection. Time-lapse video microscopy showed that zYAP MO (16 ng) injected embryos exhibit delayed gastrulation. Asterisks mark the tissue front of epiboly movements. In uninjected and cMO-injected embryos, this front completely envelops the yolk by 10 hours post-fertilization (hpf). These fronts are still in the equatorial region in the 7.7-10 hpf YAP MO-injected embryos.

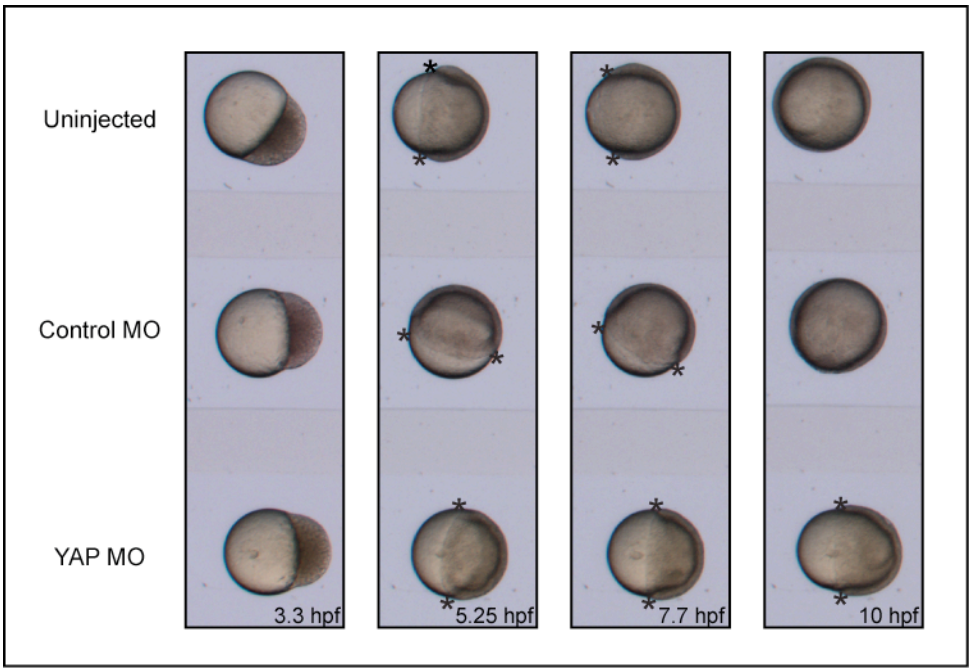
Uninjected
Control MO
YAP MO
3.3 hpf
5.25 hpf
7.7 hpf
10 hpf

Figure 15: qPCR analysis of the expression of genes required for germ layer formation in *Xenopus laevis*. qPCR analysis of mRNA levels from uninjected, control MO-injected, and xYAP MO-injected *Xenopus* embryos collected when sibling controls reached stage 10.5/11. *brachyury*, *goosecoid*, *wnt8*, *sox11*, and *sox17* mRNA levels were reduced, *nodal-related 3* mRNA levels were increased and *siamois* mRNA levels remained unchanged in xYAP morphant embryos.

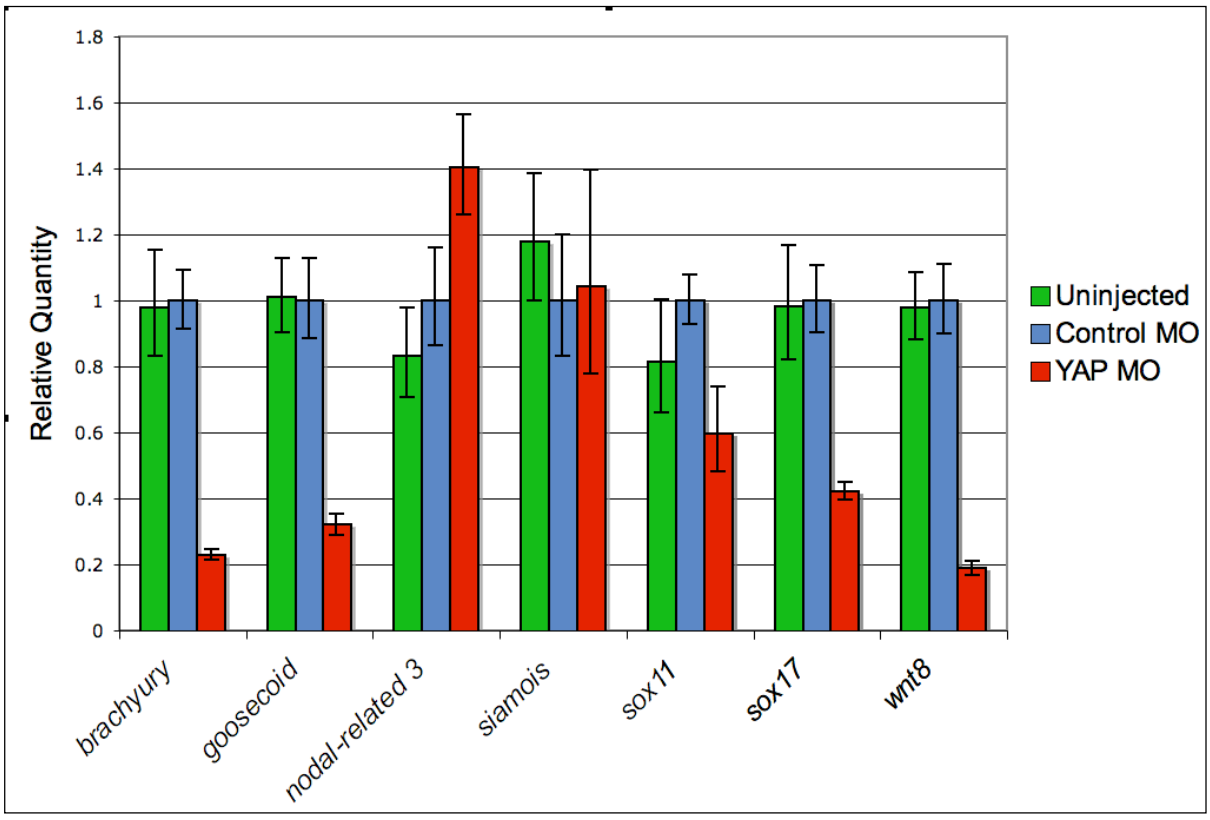
Relative Quantity
1.8
1.6
1.4
1.2
1
0.8
0.6
0.4
0.2
0
brachyury
goosecoid
nodal-related 3
siamois
sox11
sox17
wnt8
Uninjected
Control MO
YAP MO

reduced in xYAP MO-injected embryos compared to sibling stage 11 embryos (Figure 2B), at sibling stage 13 these genes, as well as several others, were expressed in patterns similar to control stage 11 embryos (Figure 16, n=14-25 per sample, 100% for all markers). Thus, eliminating endogenous xYAP protein does not prevent mesodermal gene induction, but does delay the expression of a number of mesodermal genes. These results indicate that the failure to progress through gastrulation in the absence of YAP is due to some developmental process other than germ layer induction.

YAP gain-of-function also causes axis elongation defects

From these results, we predicted that increasing YAP protein above endogenous levels may cause gastrulation to be completed more rapidly. However, time-lapse video recordings of gastrulation movements in zebrafish embryos injected with 2 different doses of *zyap* mRNA did not detect any differences in the amount of time required for epiboly movements to close around the yolk plug (Figure 17; n=5 per group). When these *zyap* mRNA injected embryos developed to later stages, however, significant perturbations were observed (Figure 18; 300 pg, n=111, 100%; 600 pg, n=94; 100%), including shortened and malformed body axes and perturbed somitic, eye, and head morphologies. Likewise, injection of *xyap*, *myap*, or *hyap* (2 ng) mRNAs all caused similar phenotypes in *Xenopus laevis* embryos (Figure 12B; n=155 (*xyap*), n=102 (*myap*), n=93 *(hyap*), 100% affected). Because YAP gain-of-function experiments produced a shortened and malformed body axis, we tested whether there was a defect in somite formation. Whole embryo immunostaining for Tropomyosin, a marker of cardiac and skeletal muscle, revealed that somites in *xyap*-injected *Xenopus laevis* embyos lost their typical chevron shape but instead exhibited an ill-defined,

Figure 16: *In situ* characterization of xYAP morphants. *In situ* characterization of gene expression in uninjected, control MO-, and xYAP MO-injected *Xenopus* embryos. Controls and sibling age-matched injected embryos are at the equivalent of stage 11 on the left and of stage 13 on the right. xYAP morphant embryos express each gene in the correct location, but the spatial pattern resembles an earlier developmental stage. For example, *brachyury* expression in the stage 11 YAP MO embryo is only faintly detected, but in the stage 13 YAP MO embryo it is indistinguishable from the control stage 11 pattern. *chordin* expression in the stage 11 YAP MO embryos is not detected, but in the stage 13 YAP MO embryo it remains confined to the dorsal blastopore lip (arrow), as in the controls at stage 11; it has not elongated along the A-P axis as in the stage 13 controls. *eomesodermin* expression in the stage 11 YAP MO embryo remains on the surface in the uninvoluted mesoderm (arrow), whereas in controls, *eomesodermin*-expressing cells have migrated internally (Ryan *et al.*, 1996). For *vent2*, *myoD*, and *not*, the stage 13 expression patterns are consistent with published patterns of early gastrulation stages, indicating developmental delay rather than loss of mesoderm. In the stage 11 panel, all views are vegetal; in the stage 13 panel, the views of *brachyury* and *vent2* embryos and of the YAP MO *chordin* embryos are vegetal and the remainder are dorsal.

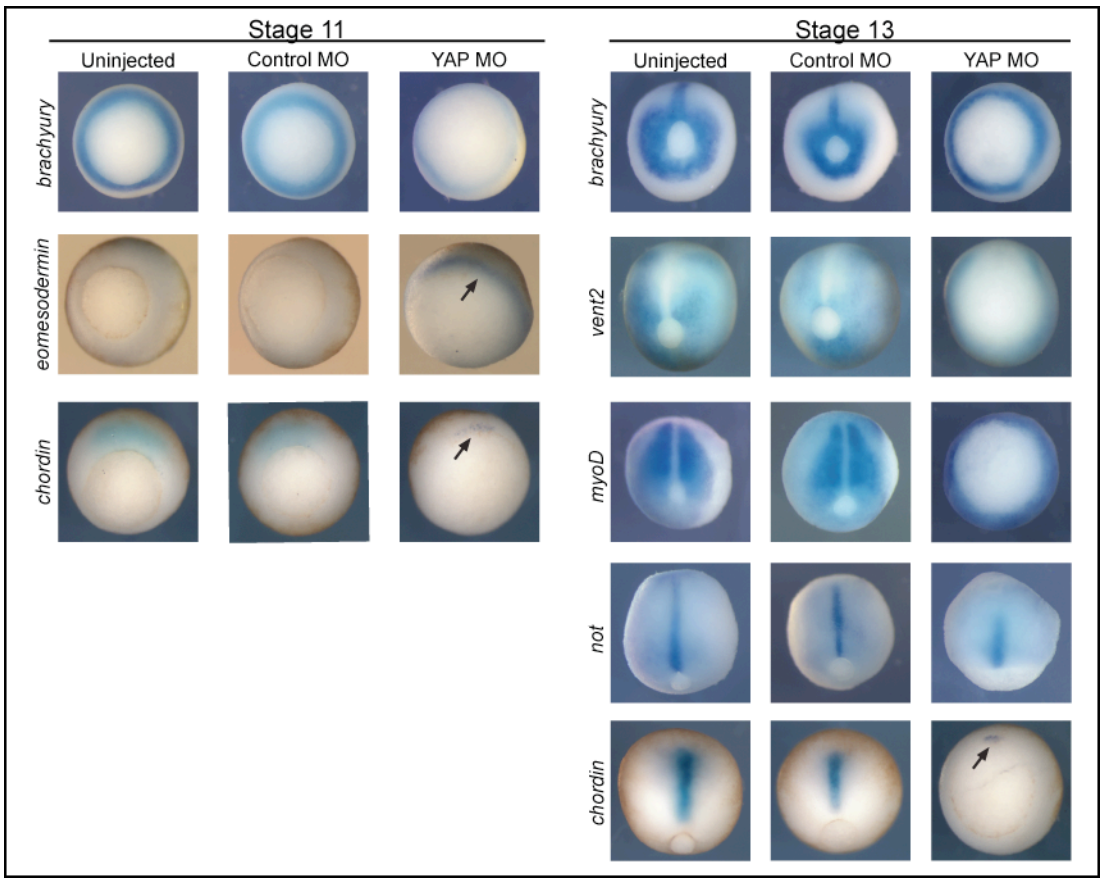
Stage 11
Uninjected
Control MO
YAP MO
brachyury
eomesodermin
chordin
Stage 13
Uninjected
Control MO
YAP MO
brachyury
vent2
myoD
not
chordin

Figure 17: Time-lapse video of epiboly progression in *zyap* mRNA injected *Danio rerio* embryos. Time-lapse videomicroscopy shows that zYAP gain-of-function does not alter the timing of gastrulation movements, as evidenced by in the progression of epiboly (asterisks mark the fronts of tissue movement around the yolk) after injection of two mRNA doses (300 pg and 600 pg) of *zyap* mRNA.

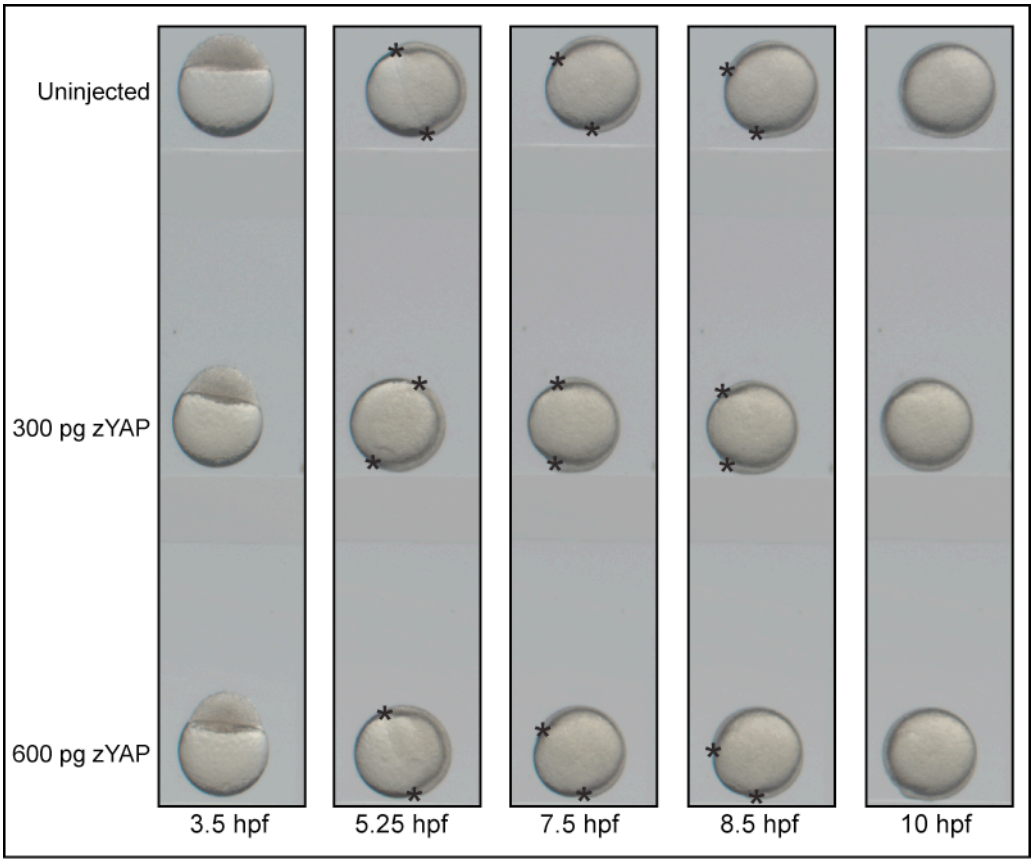
Uninjected
300 pg zYAP
600 pg zYAP
3.5 hpf
5.25 hpf
7.5 hpf
8.5 hpf
10 hpf

Figure 18: Effects of zYAP gain-of-function in *Danio rerio* embryos. zYAP gain-of-function in *Danio rerio* embryos resulted in head and eye deformities and shortened, malformed body axes. Examples of two different mRNA doses are shown.

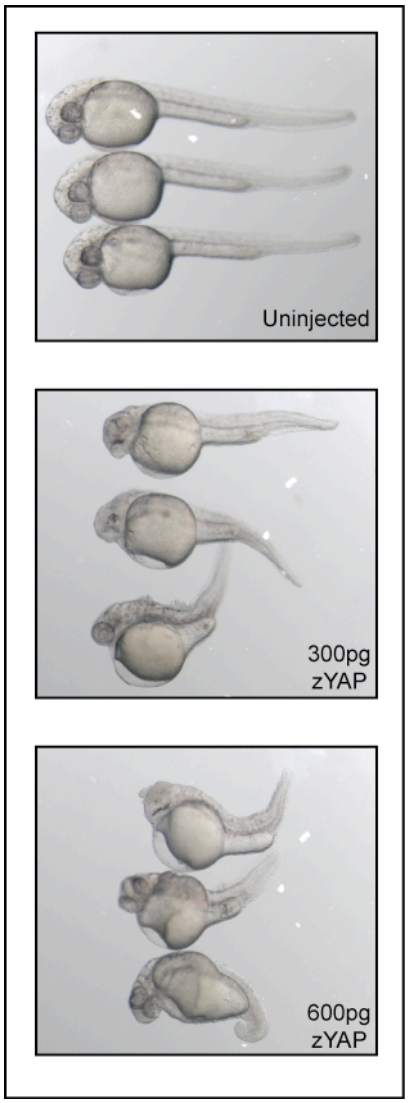
Uninjected
300pg
zYAP
600pg
zYAP

curved shape (Figure 19). Nonetheless there were no obvious changes in the arrangement of the sarcomeres at the ultrastructural level (Figure 20). Given that YAP is a well-described transcriptional co-activator, we predicted that increasing YAP levels may alter the expression of genes involved in patterning and/or elongation of the A-P axis.

YAP expands neural progenitors and inhibits neural differentiation

Because vertebrate A-P axis elongation is accomplished in part by elongation of the neural plate (Keller *et al.*, 2003, Wallingford *et al.*, 2001), we investigated whether neural progenitor fields were altered in YAP gain-of-function *Xenopus laevis* embryos. Given that our previous YAP gain-of-function experiments were injected into one-cell *Xenopus laevis* embryos, we chose to more closely monitor where our injected mRNA ended up in the embryo by co-injecting *xyap* and *β-galatosidase* (β-gal; as a lineage tracer) mRNAs into one blastomere of the 2-cell embryo. The neural progenitor field, indicated by *sox2* expression, was expanded as evidenced by a darker, longer, and/or wider expression domain compared to the uninjected side of the same embryo (Figure 21A). Consistent with this result, injection of the YAP MO cocktail (40 ng) caused a loss of *sox2* expression on the injected side (Figure 21A). YAP gain-of-function caused a concomitant reduction of neural differentiation marker expression (Figure 21B). *neuroD*, a bHLH neural differentiation transcription factor, $p27^{Xic1}$, a cdk inhibitor shown to be important for cell cycle exit and subsequent neural differentiation (Hardcastle *et al.*, 2000), and *n-tubulin*, a post-mitotic neuronal marker, each were strongly repressed (Figure 21B). Interestingly, the expression of a muscle-specific bHLH differentiation marker, *myoD*, also was strongly repressed (Figure 21D). It is well documented that increased Notch expression and/or signaling correlates with increased

Figure 19: Altered Tropomyosin staining in xYAP gain-of-function *Xenopus laevis* embryos. Whole embryo immunostaining for Tropomyosin, a marker of cardiac and skeletal muscle, revealed that somites in *xyap*-injected *Xenopus laevis* embyos exhibited an ill-defined, curved shape, rather than the typical chevron shape seen in uninjected embryos.

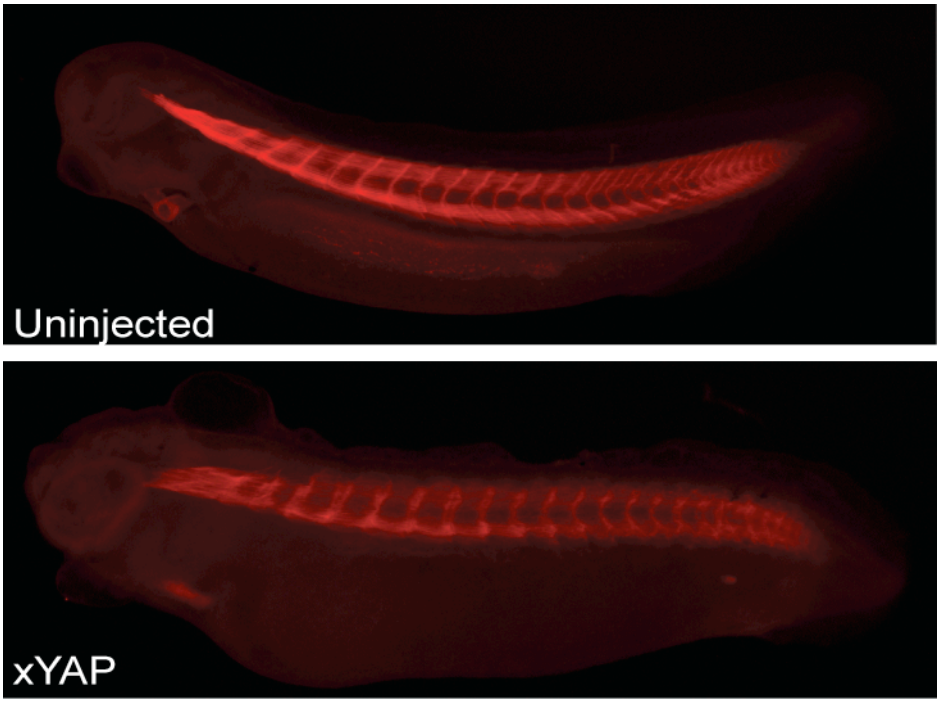
Uninjected
xYAP

Figure 20: TEM analysis of somitic muscle in xYAP gain-of-function *Xenopus laevis* embryos. Transmission electron micrographs of skeletal muscle taken from control and *xyap*-injected *Xenopus laevis* embyos (stage 30) exhibited no obvious changes in the arrangement and makeup of the sarcomeres (arrows), which run from one Z line to the next.

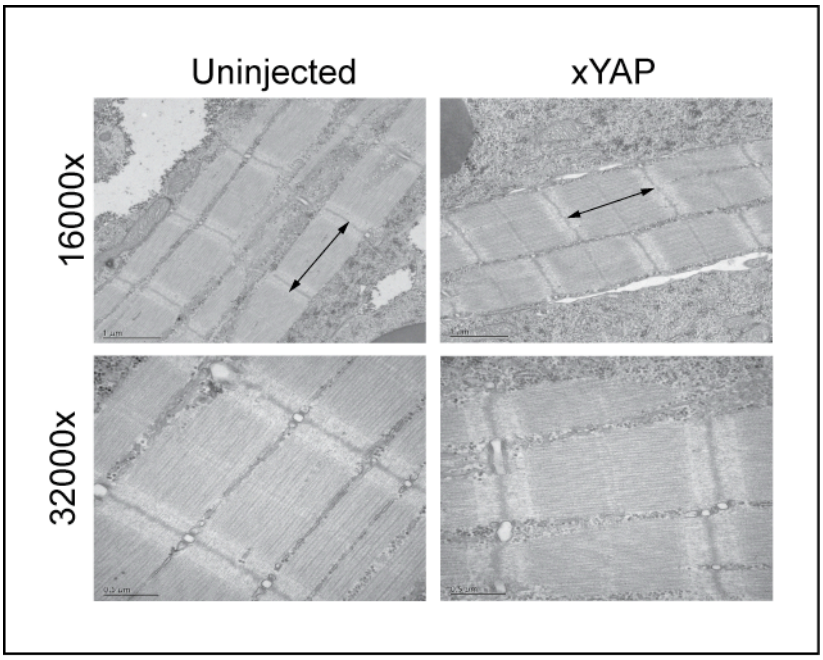
Uninjected
xYAP
16000x
32000x

Figure 21: xYAP gain-of-function expands neural progenitor fields, while neural differentiation is inhibited. (A) The neural plate progenitor field marked by *sox2* expression (blue stain) was darker, longer, and/or wider on the *xyap*-injected side (arrow, red β-gal staining) compared to the uninjected side of the same embryo. xYAP MO-mediated knockdown (40 ng) eliminated *sox2* expression on the injected side, whereas a control MO (cMO) did not. In this and all subsequent panels: n=sample size; %=frequency of the phenotype; arrow indicates injected side. (B) Expression of three genes indicative of neural differentiation (*neuroD*, *n-tubulin*, $p27^{Xic1}$) were inhibited by xYAP gain-of-function. (C) xYAP gain-of-function reduced *notch* and *hes1* expression. (D) Expression of *myoD*, a muscle differentiation marker, was reduced by xYAP gain-of-function. All views are dorsal-anterior.

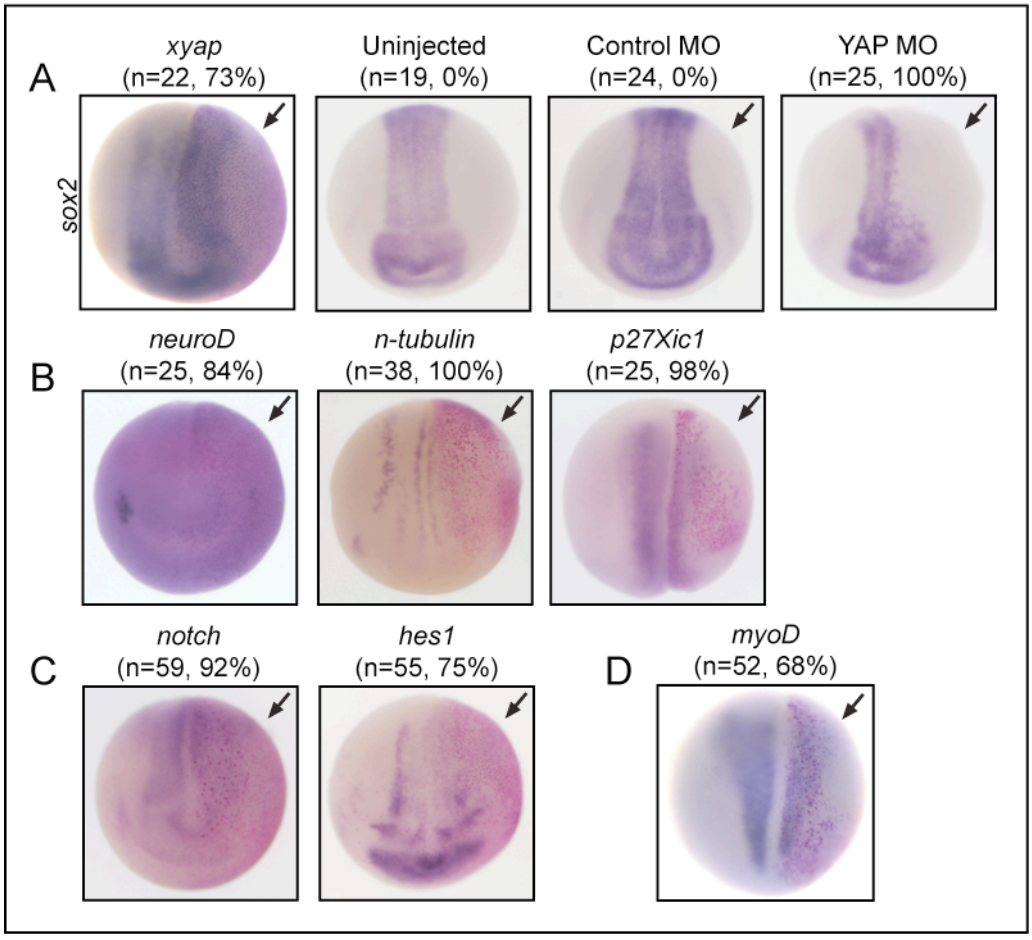
A
xyap
(n=22, 73%)
Uninjected
(n=19, 0%)
Control MO
(n=24, 0%)
YAP MO
(n=25, 100%)
sox2
B
neuroD
(n=25, 84%)
n-tubulin
(n=38, 100%)
p27Xic1
(n=25, 98%)
C
notch
(n=59, 92%)
hes1
(n=55, 75%)
D
myoD
(n=52, 68%)

numbers of neural progenitors, decreased numbers of differentiated neurons (Coffman, C. *et al.*, 1990, Coffman, C. R. *et al.*, 1993, Taranova *et al.*, 2006), and increased YAP expression (Camargo *et al.*, 2007). Therefore, we were surprised to observe that xYAP gain-of-function reduced the mRNA levels of *notch* and *hes1*, a direct Notch signaling target gene (Jarriault *et al.*, 1995, Jarriault *et al.*, 1998, Kuroda *et al.*, 1999) (Figure 21C). These results indicate that YAP's ability to repress neural differentiation is likely independent of Notch signaling.

The expansion of neural progenitors by increased YAP levels also reduced the expression domain of the differentiated epidermis, as marked by an epidermal-specific *cyto-keratin* (Jonas *et al.*, 1985) (Figure 22B). Because interactions between the neural plate and the epidermis lead to the formation of a neural plate border zone that gives rise to the precursors of the peripheral nervous system, the pre-placodal ectoderm (PPE), and the neural crest (Schlosser, 2006), we analyzed whether these tissues were properly formed. In fact, the expression of two PPE genes (*six1*; *sox11*; Brugmann et al., 2004) and two genes that are expressed by premigratory neural crest (*foxD3*; *zic1*) were dramatically reduced (Figure 22A, B). In addition, the *pax3*$^{+}$ precursors of the hatching gland were virtually eliminated (Figure 22D). Thus, in *xyap*-injected embryos there was a failure to form three different precursor populations that contribute to the formation of peripheral cranial structures. The perturbations in these three embryonic cell populations likely account for the severe defects in head morphology seen in the YAP gain-of-function tadpoles (Figure 12B).

YAP cooperates with TEAD to expand pax3^{+} *neural crest progenitors*

While the *pax3*$^{+}$ hatching gland progenitor cells were virtually eliminated, *pax3* expression in the neural plate border zone that is required for neural crest specification

Figure 22: xYAP gain-of-function inhibits the expression of genes in the pre-placodal ectoderm, epidermis, pre-migratory neural crest and hatching gland. (A) The expression of genes in the pre-placodal ectoderm (PPE), *sox11* and *six1*, are dramatically reduced on the *xyap*-injected sides. Brackets indicate the laterally located PPE expression domains on both sides the embryos. Anterior views. (B) Expression of the epidermis-specific *cyto-keratin* gene is lost on the *xyap*-injected side. Anterior view. (C) The expression of genes characteristic of premigratory neural crest (*foxD3*, *zic1* at bracket) are repressed on the *xyap*-injected sides. Anterior-dorsal views. (D) *pax3* expression in the surface ectodermal A-P stripe, which indicates the hatching gland progenitors (vertical arrows) is repressed on the *xyap*-injected side. In contrast, *pax3* expression in the underlying neural crest progenitors is expanded (see Figure 23). Dorsal view.

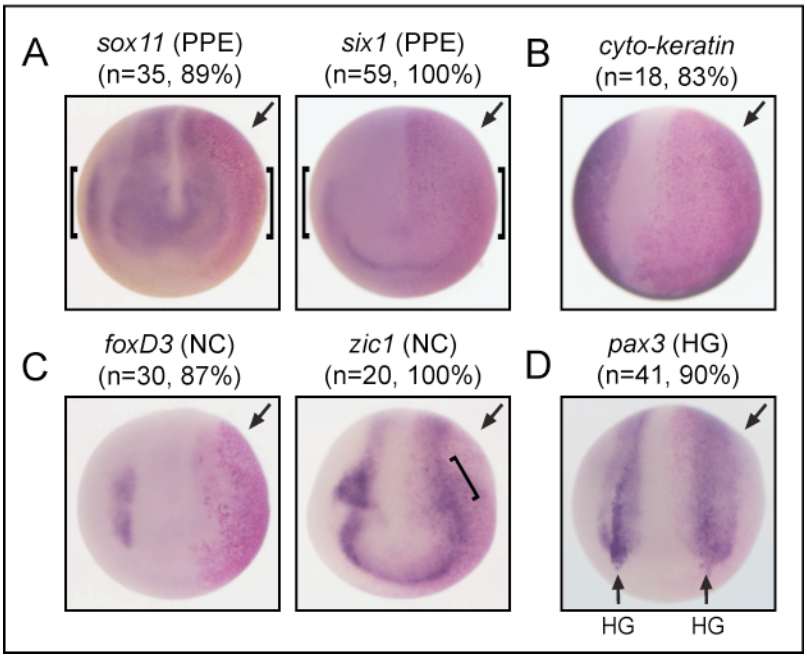
A
sox11 (PPE)
(n=35, 89%)
six1 (PPE)
(n=59, 100%)
B
cyto-keratin
(n=18, 83%)
C
foxD3 (NC)
(n=30, 87%)
zic1 (NC)
(n=20, 100%)
D
pax3 (HG)
(n=41, 90%)
HG
HG

(Monsoro-Burq *et al.*, 2005) was extended, broadened, and/or stronger compared to the uninjected, control side of the embryo (Figures 22D and 23A). This expansion of the *pax3*$^{+}$ neural crest progenitor field was concomitant with a decrease in genes expressed by specified neural crest (*zic1*, *foxD3*; Figure 22C), suggesting that increased YAP holds these cells in a progenitor-like, undifferentiated state. Consistent with these gain-of-function results, embryos that were injected with the xYAP MO cocktail (40 ng) exhibited a complete loss of *pax3* expression in both neural crest and hatching gland progenitors (Figure 23B). The loss of *pax3* in the neural crest progenitors, but not in the hatching gland precursors, could be rescued with *xyap* mRNA (Figure 23B).

Much of the *in vivo* transcriptional co-activator activity of YAP results from interactions with members of the TEAD transcription factor family (Li, Z. *et al.*, 2010). Recently, Naye *et al*. (2007) characterized two *Xenopus* TEADs, *xtead1* (*xn-tef*) and *xtead3* (*xd-tef*). Injection of *xtead1* (100 pg) mRNA alone expanded the *pax3*$^{+}$ neural crest progenitors, while a low dose of *xyap* (100 pg) mRNA alone had little effect (Figure 23C). However, upon co-injection of equal amounts of *xtead1* (100 pg) and *xyap* (100 pg) mRNAs, the percentage of embryos with an expanded domain of *pax3*$^{+}$ neural crest progenitors was greatly increased (Figure 23C), indicating cooperativity between these proteins. Although TEAD gain-of-function alone expanded the *pax3*$^{+}$ neural crest progenitors, the above experiments show that YAP enhances this effect, and the YAP MO experiments indicate that YAP is required for this effect. Therefore, we predicted that YAP acts as a transcriptional co-factor with xTEAD1 in regulating *pax3* expression.

Results from a series of *pax3* promoter transgenic deletions led Milewski *et al*. (2004) to suggest that a TEAD-binding site within a neural crest enhancer region was responsible for

Figure 23: xYAP expands *pax3*-expressing neural crest progenitors. (A) The *pax3*-expressing neural crest progenitor field (NCP) is darker, longer, and/or wider (bracket) on the *xyap*-injected side. Dorsal view, stage 15. (B) xYAP MO-mediated knockdown (40 ng) eliminated *pax3* expression in both neural crest progenitors and hatching gland (HG) precursors. Addition of exogenous *xyap* (YAP MO + *xyap*) rescued *pax3* expression in neural crest progenitors (NCP), but not in hatching gland. Dorsal views, stage 17. (C) *tead1* mRNA injection (100pg) expands *pax3*-expressing neural crest progenitors (width of bar compared to control side) at a moderate frequency (see row labeled NCP above images). *xyap* mRNA injection (100pg) rarely expands this population. In combination (*tead1*/*xyap*, 100pg each), this population is expanded in nearly every embryo. The repression of the *pax3*-expressing hatching gland progenitors (see row labeled HG above images) also was greatest when TEAD/xYAP were co-expressed. Dorsal anterior views at stage 16.

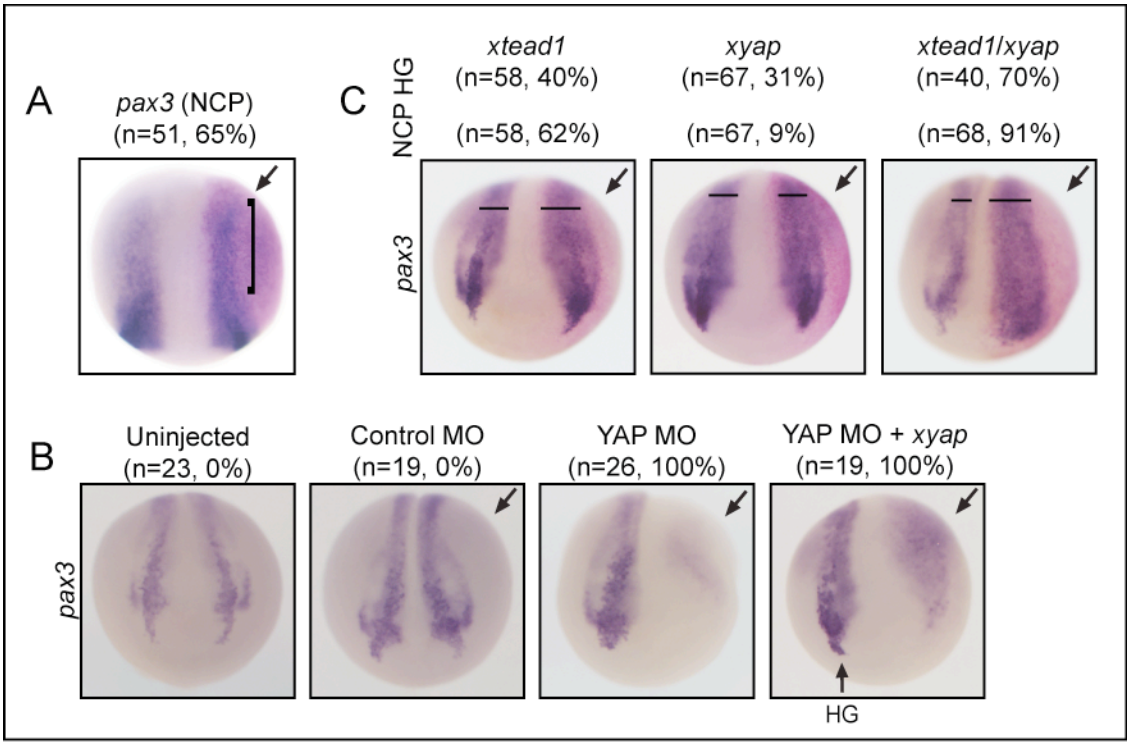
A
pax3 (NCP)
(n=51, 65%)
C
NCP HG
xtead1
(n=58, 40%)
(n=58, 62%)
xyap
(n=67, 31%)
(n=67, 9%)
xtead1/xyap
(n=40, 70%)
(n=68, 91%)
pax3
B
Uninjected
(n=23, 0%)
Control MO
(n=19, 0%)
YAP MO
(n=26, 100%)
YAP MO + xyap
(n=19, 100%)
pax3
HG

neural crest expression of *pax3*. However, we failed to find conservation of this previously described TEAD-binding site in the *Xenopus tropicalis* genome (Figure 24A). Using the genomic alignment and conserved transcription factor binding site prediction program, ConTra (Hooghe *et al.*, 2008), a predicted TEAD-binding site that was highly conserved in 15 different vertebrates was identified 58 base pairs upstream of the previously described mouse neural crest enhancer TEAD2-binding site (Figure 24A). To demonstrate direct involvement of xYAP in the control of *pax3* transcription, we performed a ChIP analysis of the *xpax3* promoter from wild-type stage 14-16 *Xenopus laevis* embryo DNA that was sheared to an appropriate size (Figure 24B). Using primers made specifically to amplify the genomic region containing the conserved TEAD-binding site (yellow box in Figure 24A), endogenous xYAP co-immunoprecipitated with this region, illustrating the direct involvement of xYAP in regulating *xpax3* transcription (Figure 24C). This TEAD binding site was specific since primers to another portion of the *pax3* promoter were not pulled down with the YAP antibody (Figure 25A). Likewise, a region of the *sox2* promoter, which possesses a putative TEAD binding site, also failed to be pulled down with the YAP antibody (Figure 25B). To confirm the presence of the TEAD-binding site within the YAP chromatin-immunoprecipitated piece of *Xenopus laevis* genomic DNA, a proofreading *Taq* polymerase was used to amplify and subclone the product (Figure 24D). Interestingly, the conserved TEAD-binding site but not the proposed mouse TEAD2-binding site, was located in this amplified fragment (Figure 24D).

To determine the functionality of this site, we subcloned this genomic region and a previously described three-base pair mutant (wild type: AA**AT**T**C**CT, mutant: AA**GG**T**A**CT) of the putative TEAD-binding site (Figure 24A) into a luciferase reporter and

Figure 24: Endogenous xYAP resides at a novel 5' regulatory region of *pax3*. (A) A highly conserved putative TEAD-binding site (yellow boxes) is present in the 5' regulatory region of the *pax3* gene in 15 different vertebrates. A previously described mouse TEAD-binding site (red box) appears less conserved. (B) Chromatin isolated from 300 wild type stage 14-16 *Xenopus laevis* embryos was sheared to a size range of 150 to 900 base pairs. (C) Chromatin immunoprecipitations (ChIPs) from 12.5 μg or 25 μg of sheared chromatin immunoprecipitated a band at the expected size for the putative novel TEAD-binding site region with the hYAP antibody but not with a control IgG antibody. (D) Sequencing of this band from three different clones verified that the genomic region pulled down by the hYAP antibody contained the novel TEAD-binding site (yellow) when compared to the *Xenopus tropicalis* genomic sequence.

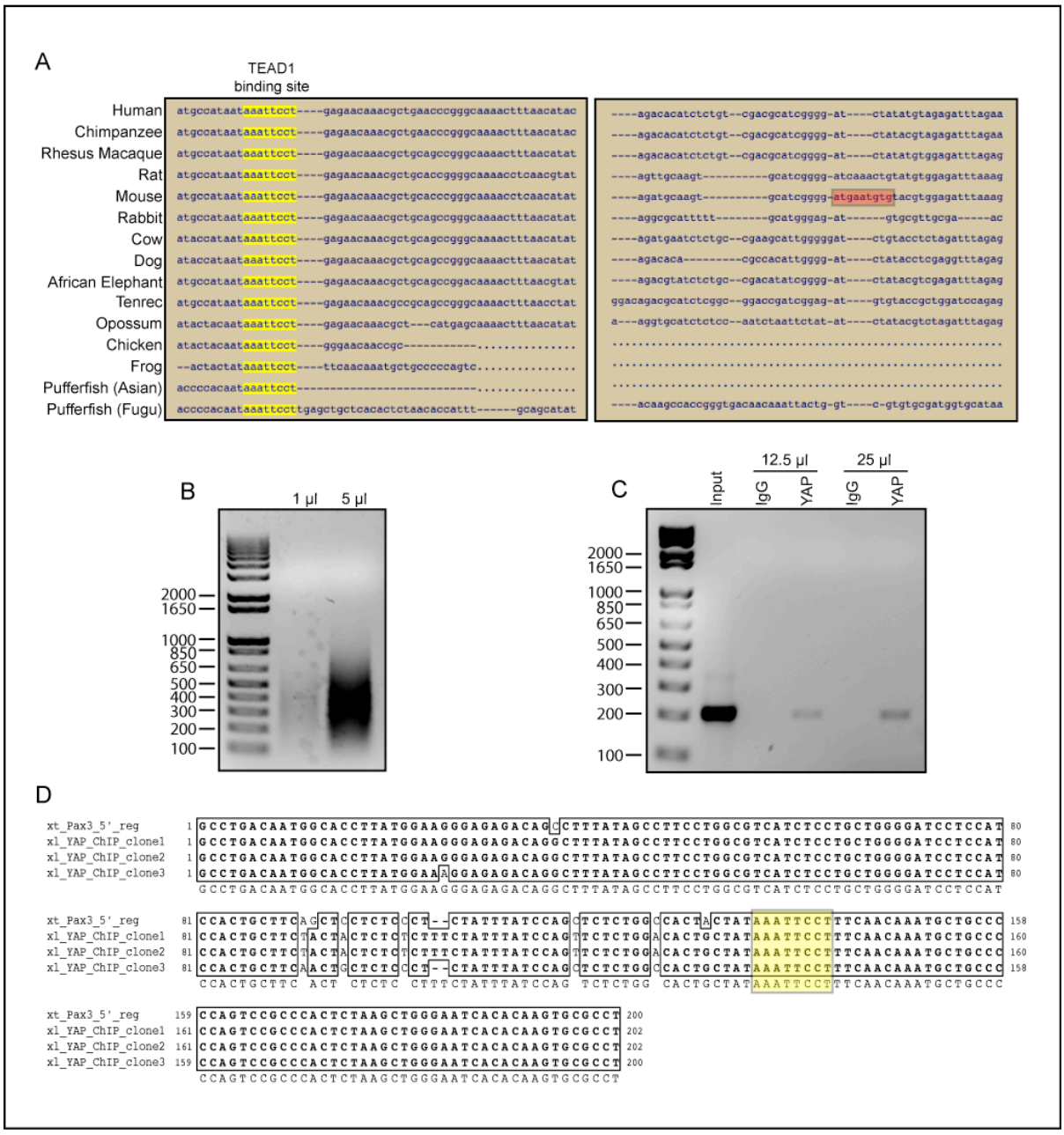
A
TEAD1
binding site
Human
Chimpanzee
Rhesus Macaque
Rat
Mouse
Rabbit
Cow
Dog
African Elephant
Tenrec
Opossum
Chicken
Frog
Pufferfish (Asian)
Pufferfish (Fugu)
B
1 µl
5 µl
2000
1650
1000
850
650
500
400
300
200
100
C
Input
12.5 µl
25 µl
IgG
YAP
IgG
YAP
2000
1650
1000
850
650
500
400
300
200
100
D
xt_Pax3_5'_reg
xl_YAP_ChIP_clone1
xl_YAP_ChIP_clone2
xl_YAP_ChIP_clone3

Figure 25: YAP does not co-immunoprecipitate with two other regions of *Xenopus laevis* genomic DNA. (A) Another region of the *pax3* promoter, not containing putative TEAD binding sequences, failed to co-immunoprecipitate with YAP or the control IgG, yet a band of the expected size was amplified in the input lane. (B) A region of the *sox2* promoter, containing a putative TEAD binding site, did not co-immunoprecipitate with YAP or the control IgG, yet a band of the expected size was amplified in the input lane. The positive control for the co-immunoprecipitation is shown in Figure 24C.

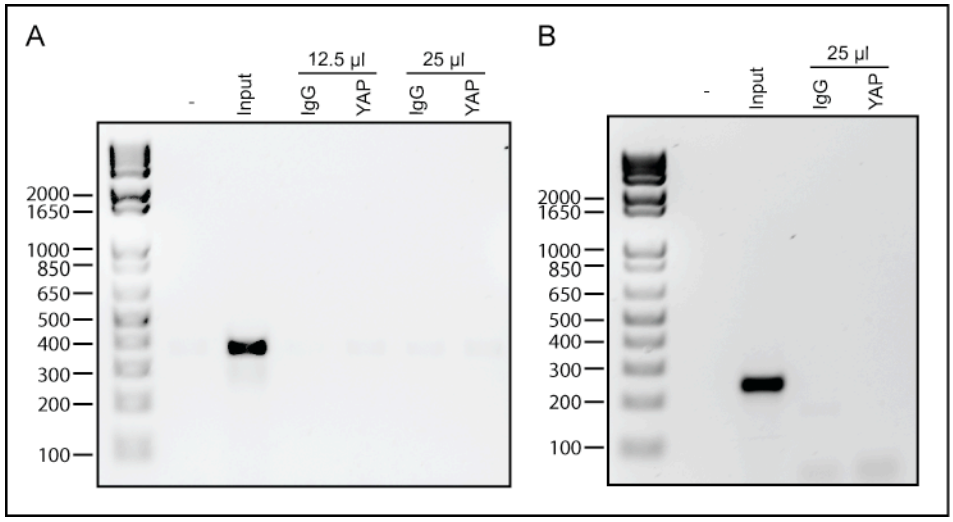
A
-
Input
12.5 µl
IgG
YAP
25 µl
IgG
YAP
2000
1650
1000
850
650
500
400
300
200
100
B
-
Input
25 µl
IgG
YAP
2000
1650
1000
850
650
500
400
300
200
100

with or without xTEAD1 and xYAP mRNAs into 1-cell *Xenopus laevis* embryos. These injected embryos (stage 14-16) were then collected and harvested for subsequent luciferase and β-gal assays. Results from these assays revealed that while the wild-type *pax3* 5'-flanking region clearly produced strong luciferase activity (35-fold greater than control) and mutation of the TEAD-binding site only slightly reduced the luciferase activity (32-fold greater than control), the addition of 100 pg of *xtead1* and *xyap* mRNAs strongly inhibited both luciferase activities (25-fold greater than control for the wild-type *pax3* 5'-flanking region and 7-fold greater than control for the TEAD-binding site mutation) (Figure 26). Although mutation of the TEAD-binding site did present a slight repression of luciferase activity, repression of the activity with the addition of xTEAD1 and xYAP was surprising, although similar effects on luciferase assays have been reported (Vassilev *et al.*, 2001) and observed by us for other putative TEAD/YAP target promoters when TEADs and YAP are added into the system. Thus, it is likely that xTEAD1 and xYAP are not the only proteins that drive *pax3* expression. Because YAP is a multifunctional protein, it may require multiple interactions for its role in regulating *pax3* transcription.

PDZ-binding motif of xYAP plays a role in epidermal and muscle differentiation

To better define which protein-protein interaction domain of xYAP is responsible for the expansion of the neural plate and neural crest progenitors as well as the correlative inhibition of neural, epidermal, and somitic muscle differentiation, we performed a series of structure-function analyses whereby mutant forms of xYAP (Figure 27) were expressed on one side of the embryo (Table 1). Using the constitutively active form of xYAP (cActive xYAP) in which the LATS phosphorylation site was mutated, we confirmed that this nuclear

Figure 26: Luciferase assay of the *pax3* 5' regulatory region. Luciferase reporter constructs containing either the wild type *pax3* 5' regulatory region or a mutation of the TEAD-binding site and a β-gal reporter with or without xTEAD1 and xYAP mRNAs were injected into 1-cell *Xenopus laevis* embryos, harvested at stage 14-16, and assayed for luciferase and β-gal activity. These assays revealed that the wild type *pax3* 5'-flanking region (*pax3* promoter) produced strong luciferase activity (35 fold activity above control), while the TEAD-binding site mutation (Mut *pax3* promoter) was only slightly reduced (32 fold activity above control). Furthermore, the addition of 100 pg of *xtead1* and *xyap* mRNAs strongly inhibited luciferase activities for both the wild type and TEAD-binding mutant reporter constructs (25 fold above control for the wild type *pax3* 5'-flanking region and 7 fold above control for the TEAD-binding site mutation).

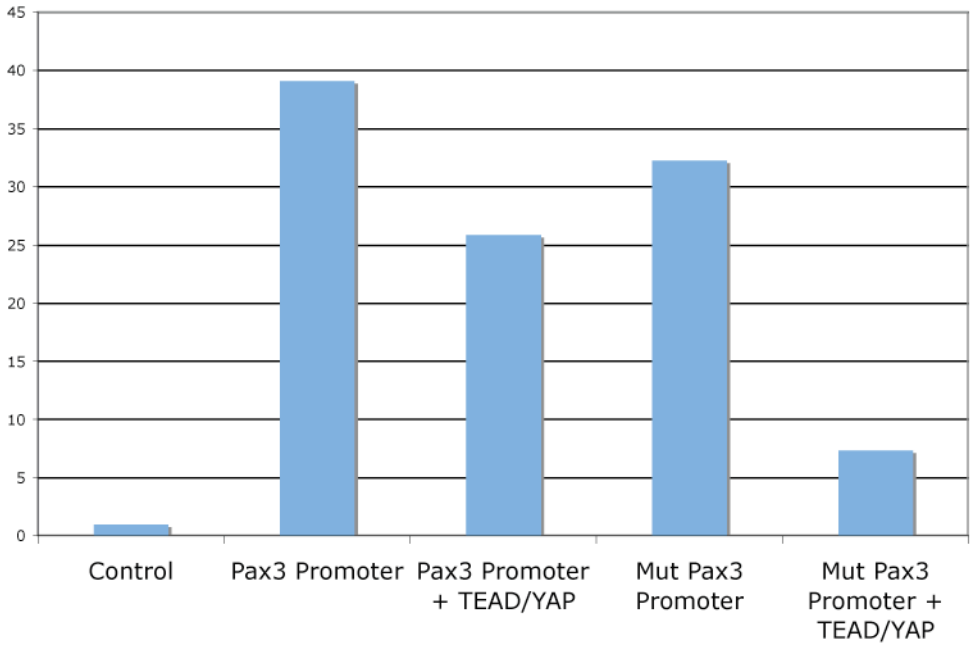
45
40
35
30
25
20
15
10
5
0
Control
Pax3 Promoter
Pax3 Promoter + TEAD/YAP
Mut Pax3 Promoter
Mut Pax3 Promoter + TEAD/YAP

Figure 27: xYAP mutants used for experiments listed in Table 1. Cartoons of the xYAP mutants created to determine which protein-protein interaction domain(s) is important for the *in vivo* gain-of-function phenotypes described in Figures 21-23. Deletions or mutations are indicated by color loss: the TEAD-binding site (xYAPΔTBS, purple), the LATS phosphorylation site (cActive xYAP, orange), the two WW domains (xYAPΔWW, red), the N-terminus (xYAP, ΔN-term) containing both the hnRNP U and TEAD binding sites, and the PDZ-binding motif (xYAPΔC-term, fuchsia) at the C-terminus.

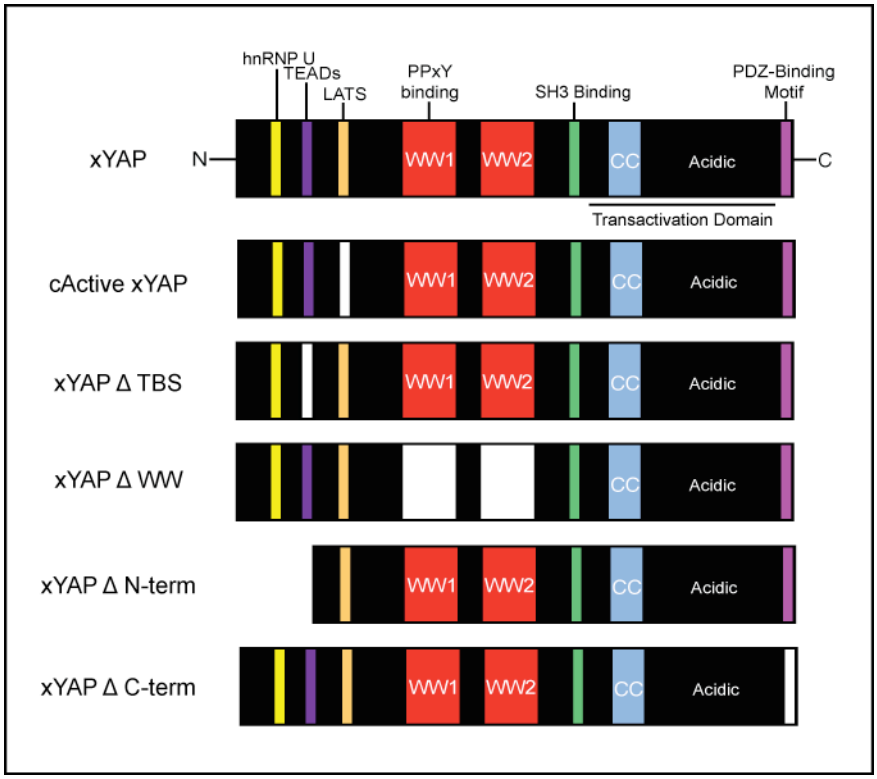
hnRNP U
TEADs
LATS
PPxY binding
SH3 Binding
PDZ-Binding Motif
xYAP
N
C
WW1
WW2
CC
Acidic
Transactivation Domain
cActive xYAP
xYAP Δ TBS
xYAP Δ WW
xYAP Δ N-term
xYAP Δ C-term

localized form of xYAP caused expansion of neural plate (*sox2*) and neural crest (*pax3*) progenitors and reduction of *pax3*$^{+}$ hatching gland precursors at frequencies comparable to wild type xYAP (Figure 28A, B). In contrast, deletion of the TEAD-binding site (TBS), WW domains, N-terminus, or C-terminus each resulted in a dramatic (*sox2*) to moderate (*pax3*-NCP, *pax3*-HG) reduction in the frequency of the respective phenotypes, indicating that an intact protein is required. These results implicate multiple binding partners. In contrast, loss of neural plate differentiation (*p27*^{xic1}) and the PPE (*sox11*) were maintained at high frequencies with each xYAP mutant, indicating that interactions at one or more of the remaining domains are sufficient to downregulate these genes. Interestingly, xYAP-mediated loss of somitic muscle (*myoD*) and epidermal (*cyto-keratin*) differentiation was specifically reduced by deletion of its PDZ-binding motif. These results implicate the involvement of a PDZ-containing interacting protein in the effects on these two tissues. The requirements for different YAP domains for the effects on these diverse embryonic tissues indicate that different binding partners are likely to mediate them.

Discussion

YAP is well conserved

Through evolution, proteins within the WW domain-containing family have functionally diversified. Although no YAP homologue exists in yeast, the closest YAP relative, Rsp5, is a WW-containing protein exhibiting ubiquitin ligase activity. The *Drosophila* YAP homologue, Yorkie, exhibits little sequence conservation when aligned with its vertebrate YAP counterparts, especially at its C-terminal end where this protein lacks the conserved vertebrate transcriptional activation domain and the SH3- and PDZ-binding

Figure 28: Bar graphs for data listed in Table 1. (A) The percentage of embryos showing expansion of *sox2*-expressing neural plate cells or expansion of *pax3*-expressing neural crest progenitor (NCP) cells after injection of each mutant form of xYAP. Note that cActive xYAP, which prevents YAP from leaving the nucleus, is as effective as wild type YAP. However, all other mutant forms reduce these phenotypes. Sample sizes are presented in Table 1. (B) The percentage of embryos showing reduced gene expression after injection of each mutant form of xYAP. Deletion of the WW domains or of the PDZ-binding motif interfered the most with repression of $pax3^{+}$ hatching gland (HG) progenitors. Loss of neural plate differentiation ($p27^{xic1}$) and a PPE marker (*sox11*) were maintained at high frequencies with each xYAP mutant, indicating that interactions at one or more of the remaining domains are sufficient to downregulate these genes. However, xYAP-mediated loss of somitic muscle (*myoD*) and epidermal (*cyto-keratin*) differentiation was specifically reduced by deletion of its PDZ-binding motif.

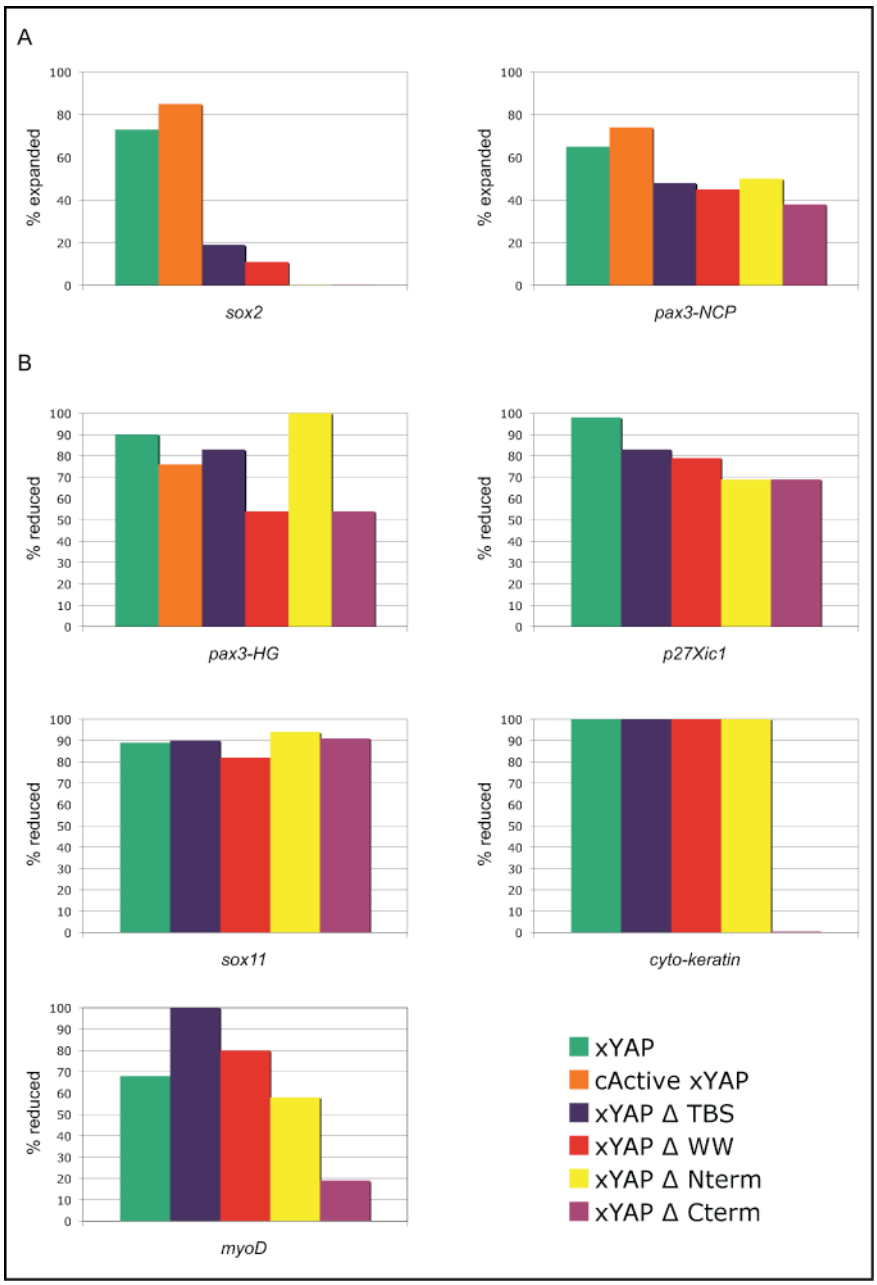
A
% expanded
sox2
pax3-NCP
B
% reduced
pax3-HG
p27Xic1
sox11
cyto-keratin
myoD
xYAP
cActive xYAP
xYAP Δ TBS
xYAP Δ WW
xYAP Δ Nterm
xYAP Δ Cterm

Table 1: PDZ-binding motif of xYAP plays a role in epidermal and muscle differentiation. Sample sizes and frequencies of genes that were expanded (*sox2*, *pax3*$^{+}$ neural crest progenitors [NCP]) or reduced (*pax3*$^{+}$ hatching gland [HG] progenitors, *p27*^{xic1}, *sox11*, *myoD*, and *cyto-keratin*) after injection of wild type *xyap* or mutant (defined in Figure 27) *xyap* mRNAs.

Probe	RNA Injected	% Change
sox2	xYAP	n=22, 73% expanded
sox2	cActive xYAP	n-20, 85% expanded
sox2	xYAP Δ TBS	n=42, 19% expanded
sox2	xYAP Δ WW	n=62, 11% expanded
sox2	xYAP Δ N-term	n=18, 0% expanded
pax3 (NCP)	xYAP	n=51, 65% expanded
pax3 (NCP)	cActive xYAP	n=19, 74% expanded
pax3 (NCP)	xYAP Δ TBS	n=68, 48% expanded
pax3 (NCP)	xYAP Δ WW	n=64, 45% expanded
pax3 (NCP)	xYAP Δ N-term	n=16, 50% expanded
pax3 (NCP)	xYAP Δ C-term	n=18, 38% expanded
pax3 (HG)	xYAP	n=41, 90% reduced
pax3 (HG)	cActive xYAP	n=17, 76% reduced
pax3 (HG)	xYAP Δ TBS	n=68, 83% reduced
pax3 (HG)	xYAP Δ WW	n=67, 54% reduced
pax3 (HG)	xYAP Δ N-term	n=8, 100% reduced
pax3 (HG)	xYAP Δ C-term	n=13, 54% reduced
$p27^{xic1}$	xYAP	n=25, 98% reduced
$p27^{xic1}$	xYAP Δ TBS	n=35, 83% reduced
$p27^{xic1}$	xYAP Δ WW	n=42, 79% reduced
$p27^{xic1}$	xYAP Δ N-term	n=35, 69% reduced
$p27^{xic1}$	xYAP Δ C-term	n=35, 69% reduced
sox11	xYAP	n=35, 89% reduced
sox11	xYAP Δ TBS	n=31, 90% reduced
sox11	xYAP Δ WW	n=33, 82% reduced
sox11	xYAP Δ N-term	n=34, 94% reduced
sox11	xYAP Δ C-term	n=35, 91% reduced
myoD	xYAP	n=52, 68% reduced
myoD	xYAP Δ TBS	n=34, 100% reduced
myoD	xYAP Δ WW	n=81, 80% reduced
myoD	xYAP Δ N-term	n=71, 58% reduced
myoD	xYAP Δ C-term	n=50, 19% reduced
cyto-keratin	xYAP	n=32, 100% reduced
cyto-keratin	xYAP Δ TBS	n=42, 100% reduced
cyto-keratin	xYAP Δ WW	n=47, 100% reduced
cyto-keratin	xYAP Δ N-term	n=41, 100% reduced
cyto-keratin	xYAP Δ C-term	n=38, 0.03% reduced

motifs. However, other invertebrates, such as the acorn worm, honeybee, wasp, sea anemone, sea urchin, and sea squirt, which also exhibit low vertebrate YAP identity (~40%), do possess the PDZ-binding motif. In order to utilize frog and fish to elucidate a common functional role in vertebrate development, it is important to establish that the YAP proteins in these animals contain similar functional domains. Indeed, xYAP and zYAP are 78% identical to the mouse homologue and contain all of the functional domains described in mammals. Interestingly, the proline-rich region present at the N-terminus of the human homologue, which allows for hnRNP U binding, contains fewer prolines in non-mammals (human, 18; mouse, 15; frog, 6; zebrafish, 3).

The functional diversity of YAP *in vivo*, however, is just now beginning to be unraveled. In particular, there is a paucity of information regarding its function in early vertebrate developmental processes. Previously, we reported that mice lacking YAP exhibit severe developmental phenotypes that result in early lethality (Morin-Kensicki *et al.*, 2006). Given that the A-P axis defects may result from the extra-embryonic tissue defects, we exploited two more amenable models, *Xenopus laevis* and *Danio rerio*, to investigate the function of YAP during early development. Herein, we provide the first description of the mechanism by which YAP regulates the completion of gastrulation and the elongation of the A-P body axis. This protein is required for the proper timing of expression of early mesodermal genes, and for the expansion of the *sox2*$^{+}$ neural plate and *pax3*$^{+}$ neural crest progenitors at the neural plate border. We demonstrate that the effects of YAP, a transcriptional co-activator, on *pax3*$^{+}$ neural crest progenitors are accomplished, at least in part, by co-regulation of the *pax3* gene via interaction with the transcription factor, TEAD1.

YAP is required for progression through gastrulation

The MO-mediated elimination of xYAP *in vivo* resulted in a failure of the embryo to close its blastopore, and while a hypomorphic knockdown allowed gastrulation to procede, these embryos had a reduced A-P body axis. A similar defect was observed in zebrafish embryos, indicating conservation of a role for YAP in completion of gastrulation and axis elongation across frog, fish, and mouse. While germ layer inductions occurred in the absence of xYAP, the onset of mesodermal gene expression was perturbed, indicating that YAP is required during the early steps of mesodermal fate specification. These results demonstrate that the previously described A-P axis defect in YAP mutant mice is not simply due to nutritional deficiencies.

Increasing YAP expands progenitors and inhibits their differentiation

When wild type *xyap*, *myap*, or *hyap* RNAs were injected into *Xenopus laevis* embryos, major morphological defects became apparent at tail bud stages, when tissue progenitors are differentiating into functional cell types. Because the tissue perturbations were widespread, we predicted that gene expression changes occurred during earlier patterning events. In fact, we observed that at neural plate stages two progenitor populations were expanded (*sox2*$^+$ neural plate; *pax3*$^+$ neural crest), whereas differentiation markers of these tissues as well as of somitic muscle and epidermis were repressed. These results are consistent with the report that the small intestinal progenitor pool was expanded when YAP was specifically overexpressed in the small intestines of mice (Camargo *et al.*, 2007). The mechanism by which the expansion of progenitors in frog embryos is accomplished is not yet known. The expansion of mouse intestinal progenitors is mediated by activation of the Notch pathway by YAP

(Camargo *et al.*, 2007); however, frog embryos injected with *xyap* mRNA showed reduced *notch* and *hes1* RNA expression. Interestingly, xYAP did not expand all progenitors or all *pax3*-expressing cells. YAP gain-of-function inhibited *pax3* expression in hatching gland precursors, and reduced the expression of *six1*, a transcription factor that maintains the PPE in a progenitor state (Brugmann *et al.*, 2004, Schlosser *et al.*, 2008). These results demonstrate that YAP-mediated expansion of progenitor populations has tissue specificity, even within the embryonic ectoderm.

xYAP directly regulates pax3 transcription

The effects of altering YAP levels on *pax3* expression in the neural crest progenitors suggested that YAP directly regulates *pax3* transcription. Increasing evidence suggests that the interaction of YAP with the TEAD family of transcription factors is critically important for proper vertebrate development (Cao *et al.*, 2008, Nishioka *et al.*, 2009, Sawada *et al.*, 2005, Yagi *et al.*, 2007). Therefore, we searched for highly conserved TEAD binding sites in the 5' regulatory region of *pax3* and found a previously undescribed, TEAD-binding site within this region. Increased expression of TEAD1 phenocopied the xYAP-mediated expansion of *pax3* in the neural crest progenitors and significantly enhanced this phenotype following coexpression of *xtead1* with levels of *xyap* mRNA that were ineffective on their own. Importantly, we demonstrated the *in vivo* relevance of this predicted association by ChIP analysis. Endogenous YAP localized to this newly identified TEAD-binding site within the 5' regulatory region of *pax3*, but not to a region of the *pax3* promoter lacking putative TEAD binding sites. In addition, a region of the *sox2* promoter containing a putative TEAD binding site also did not co-immunoprecipitate with YAP. We have yet to confirm whether

endogenous TEAD1 resides on this region or whether other TEADs are present. For example, there is evidence that TEAD1 and TEAD2 can functionally compensate for each other in early mouse development (Chen, Z. *et al.*, 1994, Sawada *et al.*, 2008). Nonetheless, these experiments demonstrate a new developmental role for both TEAD and YAP in cooperatively driving *pax3* expression in neural crest progenitors.

Our structure/function analyses, however, indicate that the expansion of the *pax3* neural crest progenitors likely involves YAP binding to proteins in addition to TEADs, because deletion of domains other than the TEAD-binding site also reduced this effect. In fact, the different effects of YAP on different ectodermal and mesodermal genes appear to require different protein interaction domains, confirming that the ability of YAP to bind to multiple proteins endows this protein with diverse functions. Here, we have illuminated a few key developmental roles for YAP, which appear to be consistent across three vertebrates. Moving forward, it will be interesting to see whether it is YAP's transcriptional activation abilities or its function as a scaffolding protein that is more important for each specific effect. An intriguing notion is that YAP may act as a critical scaffolding protein within the nucleus to assist in the regulation of transcription or regulate the state and/or remodeling of chromatin.

Chapter III – Transcriptional control of YAP

Introduction

Regulation of gene expression is critically important in development, as it controls the growth, survival, mobility, and function of each cell. Improper regulation of gene expression can lead to a variety of developmentl defects, such as loss of conceptus, birth defects, and cancer (Gavert *et al.*, 2007, Jacob *et al.*, 2007, Semenza, 2000). Determining the spatial and temporal expression of genes in different cells provides insight into a gene's involvement in these processes (Andersson *et al.*, 2007, Zurita *et al.*, 2008). Due to the high level of conservation in developmental processes across mammals, the mouse is a favored model organism for studying the functions of genes whose presence is critical for proper embryogenesis.

From our work, we concluded that Yes-associated protein (YAP) is critical for early embryonic development (Morin-Kensicki *et al.*, 2006). YAP is a modular adaptor protein with multiple protein interaction domains and can function as both a scaffolding protein and a transcriptional co-activator. To determine the *in vivo* importance of this scaffolding complex, we used homologous recombination to remove YAP from the mouse and found that few embryos survived past E8.5. YAP expression is also shown to be elevated in cancer (Dong *et al.*, 2007, Overholtzer *et al.*, 2006). Studying the transcriptional regulation of YAP provides insight into the mechanisms by which it functions. To understand *yap* at the RNA level, it is important to identify and characterize the regulatory elements of the *yap* promoter.

The *yap* promoter does not contain a canonical TATA or CAAT box, which are traditionally known to regulate transcription. Thus, *yap* is controlled by a TATA-less promoter, which is common among maternally expressed and/or housekeeping genes (Figure 29). To better understand the transcriptional regulation of *yap*, deletion analysis of the *yap*

Figure 29: Comparison between a TATA-containing and a TATA-less promoter. There are two types of promoters, TATA-containing promoters and TATA-less promoters. TATA boxes are typically located 25-30 bp upstream of the transcriptional start site and direct transcription by interacting with a transcription factor known as TATA-binding protein (TBP) (Parker *et al.*, 1984). TBP is one component of a larger complex known as transcription factor IID (TFIID). When TFIID binds to a TATA box, it initializes the formation of a larger pre-initiation complex, which contains RNA polymerase II (Buratowski *et al.*, 1989). RNA polymerase II is responsible for the transcription of almost every gene. Sometimes, a CAAT box accompanies the TATA box to enhance binding of the transcriptional machinery for transcriptional initiation; however, CAAT boxes are not always necessary for transcriptional initiation. TATA-less promoters contain a control element known as an initiator (Inr) (Smale *et al.*, 1989). An Inr is considered a functional analog of the TATA box, and is sufficient alone for directing the initiation of transcription (Chen, W. *et al.*, 1985, Smale *et al.*, 1989). Another type of TATA-less promoter is one that contains CpG islands.

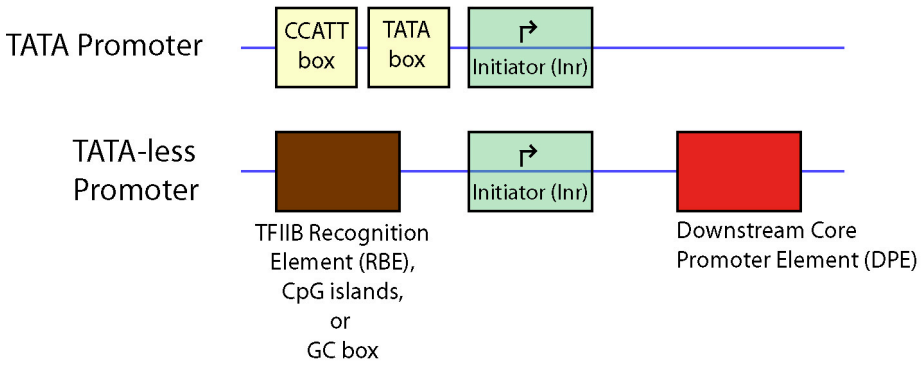
TATA Promoter
CCATT box
TATA box
Initiator (Inr)
TATA-less Promoter
Initiator (Inr)
TFIIB Recognition Element (RBE), CpG islands, or GC box
Downstream Core Promoter Element (DPE)

promoter was performed based around repetitive regions of the genomic DNA. Promoter activity for the various deletion constructs of the *yap* promoter was tested by directionally cloning the construct into a luciferase reporter vector and transfecting them into established fibroblast and epithelial cell lines. Based on these data, our analysis was narrowed to a specific, conserved region of the *yap* promoter. This conserved region was further studied to identify sites controlling promoter activity, and specific sites were characterized to identify a transcription factor regulating *yap* expression at the RNA level.

Methods and Materials

Cloning of yap Promoter Constructs into a Luciferase Reporter Vector

Primers were designed to include *Mlu*I and *Xho*I sites such that the resulting PCR-amplified fragment could be easily cloned into the multicloning site of the pGL3-basic vector (Promega). Various 5' upstream fragments, (-2828/+28), (-1819/+28), (-1374/+28), (-500/+28), and (-141/+28), of *yap* were amplified by PCR and inserted in front of the luciferase reporter gene in the pGL3-basic expression vector. The numbering of the fragments was based on the currently accepted transcriptional start site. The fragments were ligated into the pGL3-basic vector at the *Mlu*I and *Xho*I sites. To construct a mutant promoter fragment, primers containing a point mutation in the putative Sp1 binding site were constructed. The primers were used with the QuikChange® Site-Directed Mutagenesis Kit (Stratagene) to amplify a mutated yap promoter fragment (-141/+28). The yap promoter region and the inserts were sequenced to confirm proper amplification and ligation into the reporter vector (UNC-CH Genome Analysis Facility).

Cell Culture

NIH-3T3 cells, a mouse fibroblast cell line, and M1 cells, a mouse epithelial cell line derived from a microdissected cortical collecting duct of a mouse transgenic for the early region of simian virus 40 (SV40), Tg(SV40E)Bri/7, were grown on 100 mm plates in Dulbecco's Complete Growth Serum with 10% fetal bovine serum (FBS) and penicillin/streptomycin antibiotics (Stoos *et al.*, 1991).

Transfection and Luciferase Assay

Cells were grown to approximately 90-95% confluence on a 16 mm-diameter plate and transfected with Lipofectamine 2000 (Invitrogen) using 0.4 μg of plasmid DNA containing the *yap* promoter fragment. To normalize for transfection efficiency, 0.4 μg of plasmid vector containing the lacZ gene was cotransfected. The lacZ gene was under the control of the *actin* promoter. The transfected cells were lysed in 110 μL of Glo Lysis Buffer (Promega). The luciferase assay was performed according to the protocol for the luciferase assay system (Promega), and the relative activity was measured with a luminometer (Berthold Detection Systems).

For the β-galactosidase (β-gal) assay, 30 μL of cell lysate was added to 201 μL of sodium phosphate buffer (0.1 M, pH 7.5), 3 μL of 100x Mg^{2+} solution (0.1 M $MgCl_2$, 4.5 M β-mercaptoethanol), and 66 μL of 1x ONPG (Sigma) in sodium phosphate buffer (Sambrook *et al.*, 2001). The reaction was carried out in a 37°C incubator for at least 30 minutes and stopped by adding 500 μL of 1 M sodium carbonate. β-gal activity was determined by measuring the level of the hydrolysis product of ONPG at a wavelength of 420 nm (μQuant,

Bio-Tek Instruments, Inc.). The luciferase activity was normalized according to the β-gal activity by taking the ratio of luciferase activity to β-gal expression in the cells.

Preparation of Nuclear Extracts

Nuclear extracts were prepared from NIH-3T3 and M1 cells according to established methods (Sambrook *et al.*, 2001). Briefly, the cells were collected by centrifugation at 250 x g for 10 minutes at room temperature and rinsed with phosphate-buffered saline several times. The cells were then resuspended in ice-cold cell homogenization buffer (10 mM HEPES-KOH pH 7.9, 1.5 mM $MgCl_2$, 10 mM KCl, 0.5 M dithiothreitol, 0.5 mM phenylmethylsulfonyl fluoride), incubated on ice for 10 minutes, and then collected again by centrifugation. The cell pellet was resuspended in ice-cold cell homogenization buffer containing 0.05% Nonidet P-40 and the cells were homogenized in ice with 20 strokes of a tight-fitting Dounce homogenizer. The nuclei were then collected by centrifugation at 250 x g for 10 minutes at 4°C. The nuclei pellet was resuspended in 1 mL of ice-cold cell resuspension buffer (40 mM HEPES-KOH pH 7.9, 0.4 M KCl, 1 mM dithiothreitol, 10% (v/v) glycerol, 0.1 mM phenylmethylsulfonyl fluoride, 1x Complete-EDTA protease inhibitor), 5 M NaCl was added to a final concentration of 300 mM, and the suspension was incubated on ice for 30 minutes. The nuclear extract was then recovered by centrifugation at 104,000 x g for 20 minutes at 4°C and stored at -80°C. Protein concentrations were determined using the Bradford method (Bio-Rad Laboratories).

Electrophoretic mobility shift assay (EMSA)

The oligonucleotides *myap* f 5'-CGA GGC GCG CGG GCG GGC GCT CCT CGC AAC-3' and *myap* r 5'-GTT GCG AGG AGC GCC CGC CCG CGC GCC TCG-3' were synthesized (LI-COR) and annealed to generate a double-stranded *myap* promoter fragment corresponding to the region in (-141/+28) containing the putative Sp1 binding site. A 2% agarose gel was run to confirm that the oligonucleotide was double-stranded. An oligonucleotide containing the consensus Sp1 binding sequence was obtained for use as a positive control (LI-COR). The oligonucleotides were end labeled with an infrared dye that fluoresces at 700 nm (LI-COR). The binding reaction was performed according to a standardized protocol (LI-COR) using 1.5 μg of NIH-3T3 and M1 nuclear lysates. A 4% nondenaturing polyacrylamide gel was prepared and the products of each binding reaction were run at 10 V/cm in 1X TBE (89 mM tris, 89 mM boric acid, 2 mM Na_4EDTA, pH 8.3) for 180 minutes and the gel was imaged using the Odyssey Imaging System (LI-COR). A supershift of the binding was performed by incubating the binding reaction for an additional 30 minutes at room temperature in the presence of a Sp1 antibody (Santa Cruz Biotechnologies, Inc.). A competition assay was performed, in which the binding reaction was incubated with an unlabeled double-stranded *myap* promoter oligonucleotide at a concentration of 50x and 100x.

Results

Deletion construct (-141/+28) maintained yap promoter activity

An online database, RepeatMasker, was utilized to design primers around the repetitive sequences of genomic DNA, which contained the *yap* promoter. Primers were obtained to amplify the constructs (-2828/+28), (-1819/+28), (-1374/+28), and (-500/+28) of

the *yap* promoter. The different deletion constructs were directionally cloned into the multiple cloning site of a pGL3-basic reporter vector using the restriction enzymes *Xho*I and *Mlu*I. Each clone of the deletion construct was sequenced to ensure proper insertion. The pGL3-basic vector contains the luciferase gene, whose transcription is initiated by activators in the deletion constructs. The empty pGL3-basic vector provided a baseline for promoter activity. The highest level of promoter activity initially observed was in the (-500/+28) deletion construct (data not shown).

According to the UCSC Genome Browser, the fragment of greatest interest in this experiment was the (-141/+28) deletion construct because it was highly conserved across species, such as mouse, rat, dog, and human (Figure 30). In NIH-3T3 cells, the deletion construct (-141/+28) maintained a 15-fold increase in luciferase activity relative to the baseline (Figure 31). Similarly, in M1 cells, the highest relative activity was observed in (-141/+28) (Figure 32).

Mutation of a putative Sp1 binding site in (-141/+28) reduced YAP promoter activity

An online database, Proscan, identified multiple putative Sp1 binding sites within a region of the (-141/+28) deletion construct. A putative Sp1 binding site 34 bp upstream of the transcriptional start site was chosen for study based on the match attained in Proscan, and two adjacent nucleotides were mutated (Table 2).

After confirming proper mutation of the putative Sp1 binding site by sequencing, promoter activity in NIH-3T3 and M1 cells was analyzed by performing the luciferase and β-gal assays. The deletion construct of (-141/+28) with the first mutated putative Sp1 binding

Figure 30: Alignment of *myap* proximal promoter region. Alignment of proximal promoter region 150 bp upstream of *yap* transcriptional start site in different species. Conservation across species is shown in the solid blue peaks.

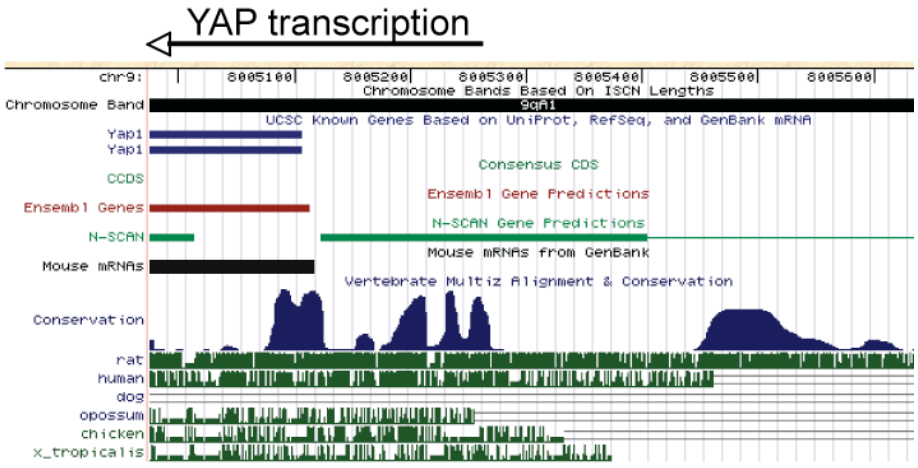
YAP transcription
chr9:
8005100
8005200
8005300
8005400
8005500
8005600
Chromosome Bands Based On ISCN Lengths
Chromosome Band
9qA1
UCSC Known Genes Based on UniProt, RefSeq, and GenBank mRNA
Yap1
Yap1
Consensus CDS
CCDS
Ensembl Gene Predictions
Ensembl Genes
N-SCAN Gene Predictions
N-SCAN
Mouse mRNAs from GenBank
Mouse mRNAs
Vertebrate Multiz Alignment & Conservation
Conservation
rat
human
dog
opossum
chicken
X_tropicalis

Figure 31: Relative *myap* promoter activity in NIH-3T3 fibroblasts. Relative *yap* promoter activity over the baseline vector. The activities were normalized by taking the ratio of luciferase activity to β-gal activity in NIH-3T3 cells. Error bars represent standard error (n = 12).

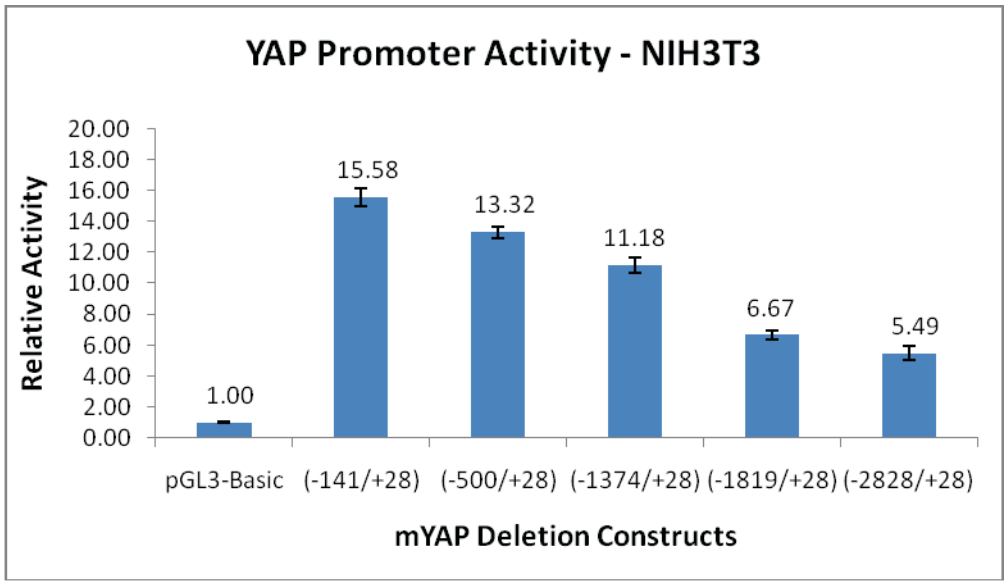
YAP Promoter Activity - NIH3T3
Relative Activity
20.00
18.00
16.00
14.00
12.00
10.00
8.00
6.00
4.00
2.00
0.00
1.00
15.58
13.32
11.18
6.67
5.49
pGL3-Basic
(-141/+28)
(-500/+28)
(-1374/+28)
(-1819/+28)
(-2828/+28)
mYAP Deletion Constructs

Figure 32: Relative *myap* promoter activity in M1 epithelial cells. Relative *yap* promoter activity over the baseline vector. The activities were normalized by taking the ratio of luciferase activity to β-gal activity in M1 cells. Error bars represent standard error (n = 12).

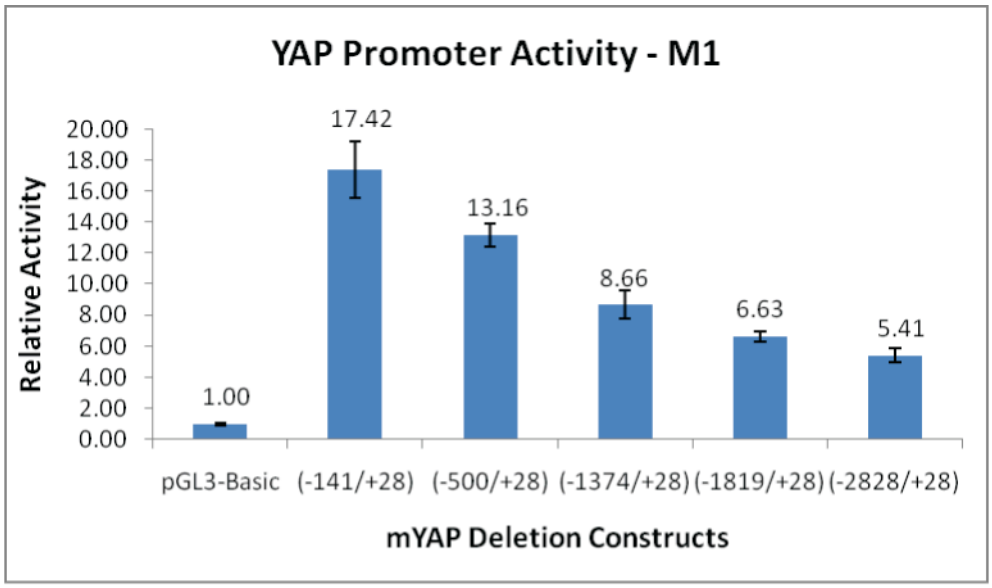
YAP Promoter Activity - M1
Relative Activity
20.00
18.00
16.00
14.00
12.00
10.00
8.00
6.00
4.00
2.00
0.00
1.00
17.42
13.16
8.66
6.63
5.41
pGL3-Basic
(-141/+28)
(-500/+28)
(-1374/+28)
(-1819/+28)
(-2828/+28)
mYAP Deletion Constructs

Table 2. Comparison of the sequence of wild type to first mutated *yap* (-141/+28) fragment. The region highlighted in blue represents the putative Sp1 binding site based on a consensus sequence for the antibody produced by Santa Cruz Biotechnologies, Inc (5'-GGG GCG GGG C-3').

	Sequence
yap (-141/+28)	5' – CGC GGG CGG GCG CGC GGA GCG - 3'
yap Sp1 mutant 1 (-141/+28)	5' – CGC GGG CTT GCG CGC GGA GCG - 3'

site had a significantly lower amount of *yap* promoter activity in NIH3T3 (Figure 33, $P < 0.0001$, $n = 12$) and M1 (Figure 34, $P < 0.0003$, $n = 9$) cells.

Another putative Sp1 binding site was analyzed in order to identify what was controlling the remaining promoter activity. Two adjacent base pairs in a second site 48 bp upstream of the transcriptional start site were mutated (Table 3). The Sp1 mutant 2 of (-141/+28) did not significantly reduce promoter activity in NIH-3T3 (Figure 33) or M1 (Figure 34) cells. These results indicate that while the first Sp1 site is important for YAP transcription in both fibroblasts and epithelial cells, it is not solely responsible for YAP transcription, suggesting that other proteins may be involved in forming a transcriptional complex for recruiting the RNA polymerase II transcriptional machinery.

Sp1 is responsible for shifing a yap promoter oligonucleotide

An EMSA (Electrophoretic Mobility Shift Assay) was performed to show that Sp1 specifically binds to the promoter at the first putative Sp1-binding site. When nuclear extracts, from NIH-3T3 and M1 cells, are incubated in the presence of oligonucleotides, they bind to the DNA to form a protein-DNA complex. When labeled oligonucleotides are separated by electrophoresis, any proteins binding to these oligonucleotides will reduce the mobility of these IRdye-labeled oligonucleotides.

A 30-bp forward and reverse oligonucleotide was designed to contain the first putative Sp1-binding site that resulted in reduced promoter activity in both NIH-3T3 and M1 cells. Single-stranded and double-stranded oligonucleotides were electrophoresed on an agarose gel and imaged at 700 nm with an Odyssey Imaging System to confirm annealing of the IRdye labeled olignucleotides (Figure 35). Using these oligonucleotides, binding

Figure 33: Mutation of Sp1 site reduced *myap* promoter activity in fibroblasts. Percentage of promoter activity relative to the normal (-141/+28) deletion construct in NIH-3T3 cells. Sp1 Mutant 1 represents the construct with two adjacent nucleotides mutated 36 bp upstream of the transcriptional start site. Sp1 Mutant 2 represents the construct with two adjacent nucleotides mutated 48 bp upstream of the transcriptional start site. Promoter activity was significantly reduced in the presence of Sp1 Mutant 1 ($P < 0.0001$, $n = 12$). Sp1 Mutant 2 had no effect on promoter activity.

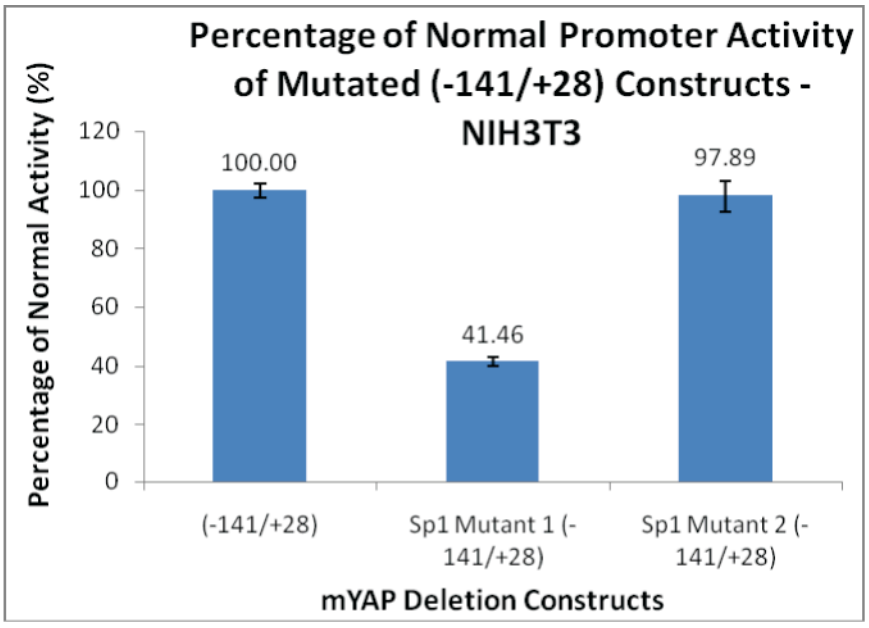
Percentage of Normal Promoter Activity of Mutated (-141/+28) Constructs - NIH3T3
Percentage of Normal Activity (%)
120
100
80
60
40
20
0
100.00
41.46
97.89
(-141/+28)
Sp1 Mutant 1 (-141/+28)
Sp1 Mutant 2 (-141/+28)
mYAP Deletion Constructs

Table 3. Comparison of the sequence of wild type to second mutated *yap* (-141/+28) fragment. The region highlighted in blue represents the putative Sp1 binding site based on a consensus sequence for the antibody produced by Santa Cruz Biotechnologies, Inc (5'-GGG GCG GGG C-3').

	Sequence
yap (-141/+28)	5' – GCG GAG CCC GCG AGG - 3'
yap Sp1 mutant 2 (-141/+28)	5' – GCG GAG CTT GCG AGG - 3'

Figure 34: Mutation of one putative Sp1 site reduced *myap* promoter activity in epithelial cells. Percentage of promoter activity relative to the normal (-141/+28) deletion construct in M1 cells. Sp1 Mutant 1 represents the construct with two adjacent nucleotides mutated 36 bp upstream of the transcriptional start site. Sp1 Mutant 2 represents the construct with two adjacent nucleotides mutated 48 bp upstream of the transcriptional start site. Promoter activity was significantly reduced in the presence of Sp1 Mutant 1 ($P < 0.0003$, $n = 9$). Sp1 Mutant 2 did not reduce promoter activity.

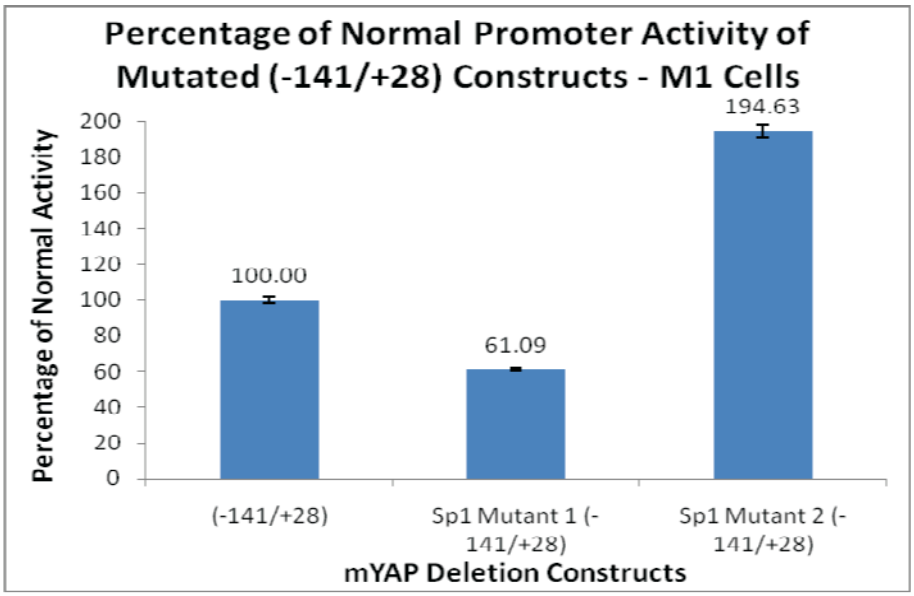
Percentage of Normal Promoter Activity of Mutated (-141/+28) Constructs - M1 Cells
Percentage of Normal Activity
200
180
160
140
120
100
80
60
40
20
0
100.00
61.09
194.63
(-141/+28)
Sp1 Mutant 1 (-141/+28)
Sp1 Mutant 2 (-141/+28)
mYAP Deletion Constructs

reactions with nuclear extracts from NIH-3T3 and M1 cells were performed and run out on a 4% nondenaturing polyacrylamide gel. Based on the results of the EMSA assay, a complex containing the *yap* promoter oligonucleotide and bound transcription factors co-migrated with the positive control oligonucleotide containing a consensus Sp1-binding site (Figure 36, upper band), while several nonspecific, lower bands also migrated in the presence of the oligonucleotides. To determine the reason for the nonspecific binding, nuclear extracts were incubated individually with the forward and reverse oligonucleotides (Figure 37). Results from this experiment illustrated that these nonspecific bands are due to the binding of residual single-stranded oligonucleotides. The specific Sp1 shift was present and consistent in both cell types. A competition assay was performed using unlabeled *yap* promoter oligonucleotide at concentrations of 50 and 100 times that of the labeled *yap* promoter oligonucleotide. When the unlabeled *yap* promoter oligonucleotide was added to the labeled consensus Sp1 oligonucleotide, the intensity of the shifted band was reduced. The same reduction was seen when the unlabeled *yap* promoter oligonucleotide was added to the labeled *yap* promoter oligonucleotide (Figure 36). There was greater reduction in the intensity of the shifted band with 100x excess compared to 50x excess unlabeled *yap* promoter oligonucleotide. These combined results suggest that the electromobility shift of the labeled oligonucleotides is due to Sp1.

To further confirm that the transcription factor binding to the *yap* promoter oligonucleotide was Sp1, the binding reaction was incubated with an Sp1 antibody. Normally, the antibody will bind to the protein-DNA complex, leading to what is called a supershift, whereby the mobility is further reduced. However, no supershift was observed

Figure 35: Annealing of *myap* promoter oligos for gel-shift analysis. Annealing of the two oligos (mYAPf and mYAPr) containing the putative Sp1 binding site within the *myap* promoter fragment was confirmed by gel electroporesis. Both single-stranded oligos, mYAPf and mYAPr, at two different quantities (1 μl and 2 μl) migrated faster than that of the slower, double-stranded oligo (annealed lane).

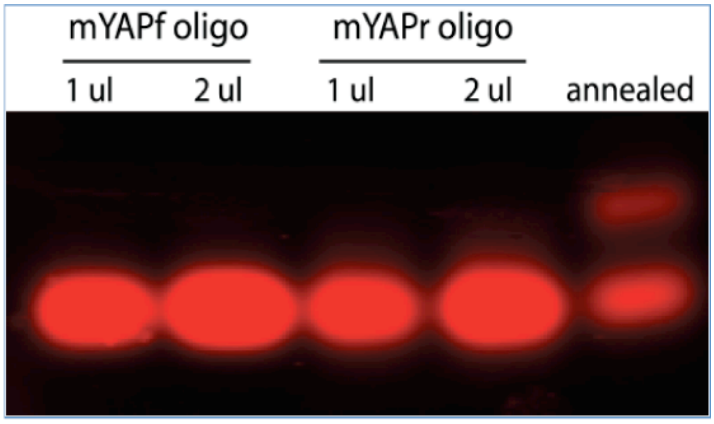
mYAPf oligo
mYAPr oligo
1 ul
2 ul
1 ul
2 ul
annealed

Figure 36: Competitive gel-shift assay for Sp1 site in the mYAP promoter. Gel shift assay shows competition between labeled and unlabeled YAP oligos for Sp1 binding. Lane A shows the IRdye labeled double-stranded YAP oligo. Lane B shows the inhibited migration of a positive control IRdye labeled Sp1-binding site containing double-stranded oligo in the presence of nuclear extracts from NIH-3T3 or M1 cells. Lane C shows that 50x excess of the unlabeled YAP oligo competes for Sp1 binding to the positive control, Sp1 oligo. Lane D shows the inhibited migration of the YAP oligo in the presence of nuclear extracts from NIH-3T3 and M1 cells, containing Sp1 (top band) as well as unknown or nonspecific (NS, lower bands) proteins. Comparing this lane with the positive control (Lane B) suggests that Sp1 can bind to the YAP oligo. Lanes E and F show both 50x and 100x unlabeled YAP oligo, respectively, competes for Sp1 binding to the YAP oligo.

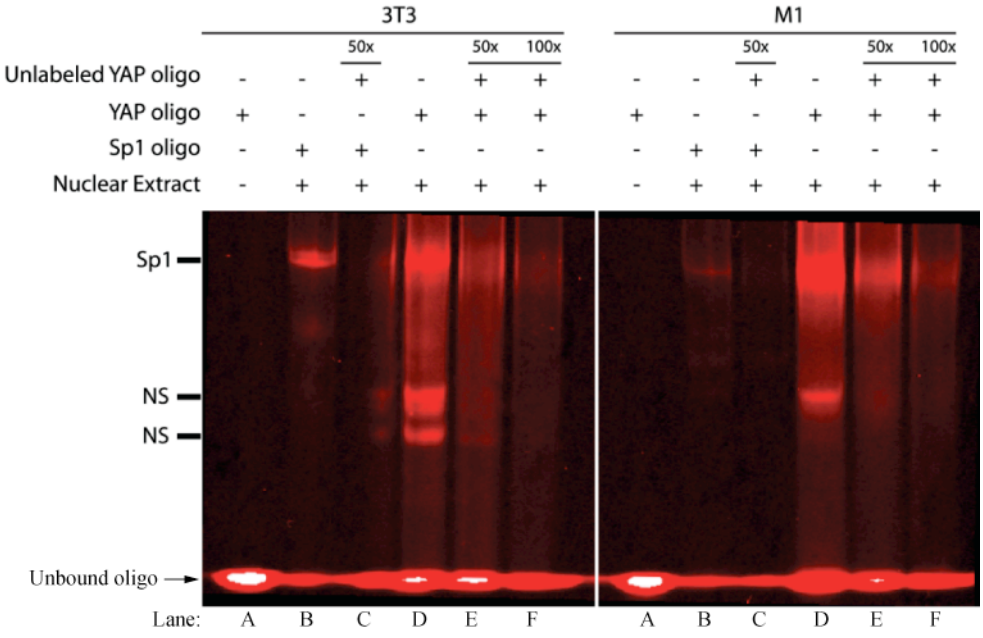
3T3
M1
50x
50x
100x
Unlabeled YAP oligo
YAP oligo
Sp1 oligo
Nuclear Extract
Sp1
NS
NS
Unbound oligo
Lane:
A B C D E F
A B C D E F

with the addition of Sp1 antibody with either the consensus Sp1 or *yap* promoter oligonucleotides (Figure 37). Instead, the intensity of the band was reduced, suggesting that the Sp1 antibody competes for Sp1 with the DNA. Other studies have shown similar results using Sp1 antibody in a gel supershift assay (Dean *et al.*, 2000).

Discussion

To identify and characterize the elements of the *yap* promoter, an analysis of the promoter was performed to narrow the focus of study to a small region containing potential regulatory elements. Different deletion constructs of the *yap* promoter up to 3 kbp upstream of the transcriptional start site were designed using RepeatMasker, an online database that searches for repeated sequences in genomic DNA. When the luciferase reporter vector containing each deletion construct was transfected into cells, the transcriptional machinery bound to the reporter construct and initiated transcription of the luciferase gene. A luciferase substrate was utilized to determine the promoter activity of each deletion construct. Analysis of the promoter was narrowed to 500 bp upstream of the transcriptional start site for *myap* after it maintained the highest levels of promoter activity. A search on the UCSC Genome Browser indicated that the region 150 bp upstream of the transcriptional start site was highly conserved across species; thus it was hypothesized that this region was sufficient for high levels of *yap* promoter activity.

In both NIH3T3 and M1 cells, the deletion construct (-141/+28) maintained the highest level of promoter activity, while the larger constructs had much lower levels of activity. These lower levels of activity could be due to the presence of repressors or other

Figure 37: Competitive gel-shift assay and supershift of Sp1. Lane A shows the IRdye labeled double-stranded YAP oligo. Lane B shows the inhibited migration of a positive control IRdye labeled, Sp1-binding site containing, double-stranded oligo in the presence of nuclear extracts from NIH-3T3 or M1 cells. Lane C shows that addition of a Sp1 antibody competes for Sp1 binding to the Sp1 oligo. Lanes D and E illustrate that the nonspecific bands (NS) that inhibit the YAP oligo migration are due to proteins binding to the single-stranded, unannealed oligos (YAP reverse oligo and YAP forward oligo). Lane F shows the inhibited migration of the YAP oligo in the presence of nuclear extracts from NIH-3T3 and M1 cells, containing the Sp1 (top band) protein as well as the nonspecific (NS, lower bands) proteins. Comparing this lane with the positive control (Lane B) suggests that Sp1 can bind to this oligo. Lane G shows that addition of a Sp1 antibody competed for Sp1 (top band) binding to the YAP oligo as it did in the presence of the positive control Sp1 oligo.

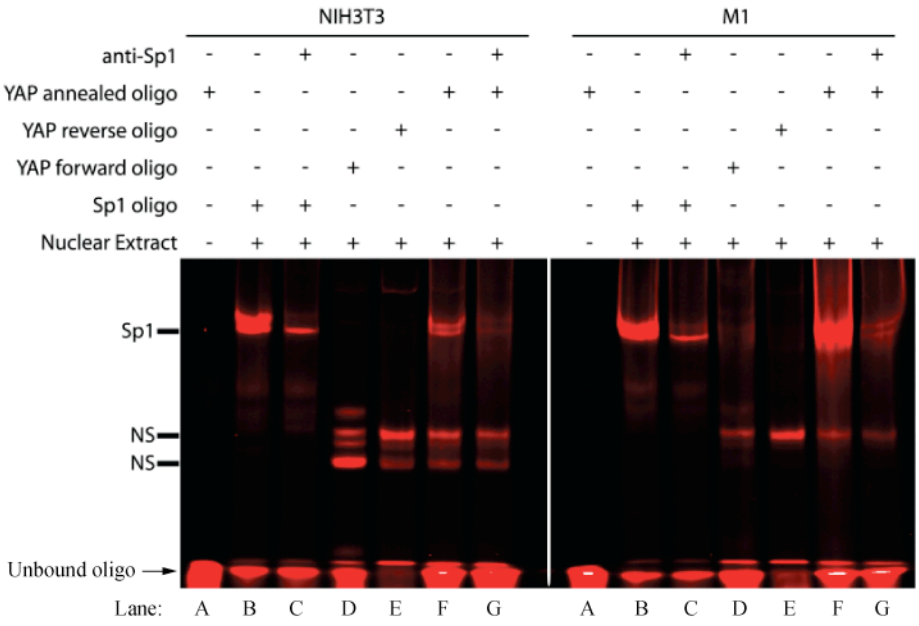
NIH3T3
M1
anti-Sp1 - - + - - - + - - + - - - +
YAP annealed oligo + - - - - + + + - - - - + +
YAP reverse oligo - - - - + - - - - - - + - -
YAP forward oligo - - - + - - - - - - + - - -
Sp1 oligo - + + - - - - - + + - - - -
Nuclear Extract - + + + + + + - + + + + + +
Sp1
NS
NS
Unbound oligo
Lane: A B C D E F G A B C D E F G

processes of regulation, such as epigenetic marks. After demonstrating that the (-141/+28) construct maintained the highest level of promoter activity, the next step was to identify potential activators within the region of the (-141/+28) construct. According to an online database, Proscan, the region up to 150 bp upstream of the transcriptional start site contains several putative Sp1 binding sites. Sp1 is a transcription factor that binds to GC boxes. The *yap* promoter is rich in guanine and cytosine, nucleotides of which GC boxes are composed. Sp1 is associated with TATA-less promoters that contain regions rich in guanine and cytosine, and can recruit the components of the transcriptional machinery, such as RNA polymerase II, to the promoter (Smale, 1994). In addition, Sp1, like YAP, is ubiquitously expressed in most cells during development. Sp1 is present in the early stages of embryonic development, and is known to regulate transcription of other genes during embryogenesis (Smale, 1994). Promoters whose transcription is regulated by Sp1 usually contain multiple Sp1 binding sites, each having slightly different DNA sequences and thus different binding affinities for Sp1 (Dynan *et al.*, 1983, Gidoni *et al.*, 1985). The possibility for Sp1 regulating *yap* transcription is further supported by evidence that mice lacking Sp1 are always smaller than their littermates and exhibit a range of defects including defective body axis symmetry, incomplete turning, and growth outside the yolk sac; however, these mice were stated to survive to E10-11 (Marin *et al.*, 1997). The extended life span of the Sp1-null mice compared with the YAP-null mice could be due to compensation from another protein, such as Sp3. Interestingly, the differentiative capacity of *Sp1*$^{-/-}$ cells does not appear to be severely impeded, since many of the structural hallmarks of normal E8.5–9.5 embryos in the best-developed *Sp1*$^{-/-}$ embryos remain.

Based on the results obtained, Sp1 Mutant 1, which was a mutation in a putative site 36 bp upstream of the start site, significantly reduced promoter activity in both NIH-3T3 and M1 cells. These data suggest that the site located in Sp1 Mutant 1 is essential for activating promoter activity. Sp1 Mutant 2, which was a mutation in the potential site 48 bp upstream of the start site, had no effect on promoter activity in NIH-3T3 cells, but actually increased promoter activity in M1 cells. It is likely that the two adjacent point mutations made in Sp1 Mutant 2 created an activation site for another transcription factor unique to M1 cells, leading to an increase in promoter activity. The activity reduced by Sp1 Mutant 1 in NIH-3T3 and M1 cells was only 40 to 60 percent, respectively, so there must be another site in the region controlling the remaining promoter activity. This coincides with previous studies indicating that there are usually multiple Sp1 binding sites regulating transcription (Dynan *et al.*, 1983, Gidoni *et al.*, 1985).

Although these results are highly suggestive that Sp1 plays a critical role in YAP expression, they are not yet definitive. To further characterize the role of Sp1 in controlling *yap* transcription, YAP expression could be analyzed when Sp1 is overexpressed or knocked out of cells. In the future, other regulatory elements that regulate *yap* transcription are likely to be identified. Based on an online database, UCSC Genome Browser, the first intron of *yap* is also highly conserved, and thus, could possibly serve as a site of transcriptional regulation.

Further studies of *yap* expression and regulation will be beneficial in determining YAP's role in development. For example, different elements of the *yap* promoter could be used to drive the expression of Green Fluorescence Protein (GFP) or LacZ to determine what regions of the promoter are sufficient to mediate *yap* expression in localized regions of the mouse, zebrafish, or frog embryos. Identification of these elements can then be used to

determine whether transgenic expression of YAP is sufficient to rescue defects observed in YAP-deficient mice, zebrafish, or frog. The ability to rescue the developmental defects associated with YAP-deficient mice, zebrafish, or frog would demonstrate specificity in YAP's diverse roles during development.

Chapter IV – Identification of putative YAP transcriptional target genes

Introduction

Although we knocked out the transcriptional co-activator, YAP, in mouse, frog, and zebrafish and confirmed the presence of YAP on the *pax3* promoter *in vivo*, the number of known gene targets associated with YAP mediated transcription remains limited. Given that we possessed a mouse lacking the YAP gene, I created an immortalized cell line of mouse embryonic fibroblasts (MEFs) isolated from the YAP mutant mice. The rationale for creating these cells was that gene targets should be easily identified by comparing gene expression profiles between wild type and YAP mutant immortalized cell lines. Similar efforts have been succussful, for example the Src, Yes, Fyn (SYF) triple mutant MEF cell lines were created from similarly aged mutant embryos as YAP mutant embryos (Klinghoffer *et al.*, 1999). With assistance from Elizabeth Morin-Kensicki and Jim Bear, immortalized MEF cell lines were created from our YAP mutant mice, and in so doing, at least one potential new YAP gene target was identified.

Methods and Materials

Isolation and immortalization of mouse embryonic fibroblasts (MEFs)

Embryonic day 8.5 (E8.5) mice were isolated from pregnant CD57BL/6J females heterozygous for the targeted *Yap*^{tm1Smil} allele (Morin-Kensicki *et al.*, 2006), dissected in 1X PBS, exposed to trypsin for 10 min at 37°C, physically dissociated by pipetting up and down, and each embryo was plated in a single well of 24-well fibronectin coated tissue culture plate. Subsequently, the cells were passaged to normal tissue culture plates and maintained in DMEM-High glucose and 10% FBS at 37°C.

At passage two, cells were exposed to SV40 large T antigen retrovirus conditioned media from Ψ2 packaging cells and supplemented with polybrene (4 μg/mL) at 32°C overnight (Brown *et al.*, 1986). A well of cells isolated from each wild type or heterozygous embryo was not exposed to the retroviral-conditioned media and served as a control for determining immortalization of the cell lines. The retroviral and MEF conditioned media was removed and inactivated with bleach. The control cells hit their crisis point by passage 8, while the cells exposed to the SV40 Large T antigen retrovirus continued to multiply and were considered to be immortalized by passage 10. To properly genotype the isolated cell lines, genomic DNA was isolated from each immortalized cell line and PCR was performed as previously described (Morin-Kensicki *et al.*, 2006).

Western blot

Cells from each immortalized MEF cell lines were lysed in RIPA buffer and the insoluble fraction was pelleted at 13,000 x g for 5 min at 4°C. Total protein concentrations were quantified using the BCA Protein Assay Kit (Pierce), according to the manufacturer's protocol. Equal amounts of protein were loaded onto a 10% SDS-PAGE gel, separated by electrophoresis, transferred to a PVDF membrane, blocked in Odyssey Blocking Buffer (Li-Cor) for 1 hour at room temperature, and co-probed for mYAP using an affinity purified rabbit anti-YAP antibody (1:1000), which was generated against human YAP (274-454) (Howell *et al.*, 2004) and a mouse anti-Actin antibody (Clontech), for 1 hr at room temperature. The blots were washed three times with TBST at room temperature and exposed to anti-rabbit IRDye 800 (1:20,000) and anti-mouse IRDye 680 (1:20,000) secondary antibodies for 1 hour at room temperature. The blots were washed three times with TBST and

once with 1X PBS to remove the Tween 20 (Sigma). The blots were then scanned on a Li-Core Odyssey.

Removal of mutant mYAP from YAP$^{-/-}$ MEFs

Turbo-Cre was removed by restriction digestion with *Eco*RI and subcloned into the bicistronic mammalian retroviral expression vector, pMIG-RI. Because subcloning with one restriction enzyme may result in concatemers, restriction digests with *Sal*I and *Xho*I confirmed the identity of a single copy. Similarly, proper gene orientation within the vector was confirmed by restriction digest with *Nco*I.

Phoenix cells, a retroviral packaging cell line, were maintained in DMEM-high glucose and 10% FBS. Transfection of the pMIG-RI and pMIG-RI-Turbo-Cre recombinase into the packaging line was performed using lipofectamine (Invitrogen), according to manufacturer's protocol. After three days, the conditioned media from the transfected packaging cell line was removed and filtered through a 0.45 micron filter and stored at 4°C. Media from mutant YAP MEFs plated at sixty percent confluence was removed and replaced with warm (32°C) retroviral conditioned media (pMIG-RI or pMIG-RI-Turbo-Cre-recombinase) supplemented with 4 μg/ml polybrene. After four hours, the retroviral-conditioned media was removed, inactivated with bleach, and replaced with DMEM-high glucose and 10% FBS. After two days, the retroviral infected mutant YAP MEFs were split and further propagated. To confirm viral integration of the pMIG-RI and pMIG-RI-Turbo-Cre recombinase vectors into the mutant YAP MEFs genome, cells were trypsinized, washed with 1X PBS, well resuspended in 1X PBS with 1% FBS plus P/S, filtered to single cell suspension (5 x 10^6 cells/mL), and cell sorted by the NHGRI cell sorting core facility. Only

1% of the each of the sorted cells was GFP positive, but they were plated into two 12-well sized wells. These cells were expanded and sorted for GFP positive cells three more times in attempts to retrieve as pure of a cell population as possible that lacked the mutant mYAP.

Microarray

High quality RNA was isolated from a wild type MEF cell line and a $YAP^{-/-}$ cell line using the RNeasy Plus Qiagen kit, according to the manufacturer's protocol. The RNA was treated with DNase (Promega) according to the manufacturer's specifications and quantified using a Nanodrop. The isolated RNA was considered to be of high quality if the A_{260}/A_{280} ratio was above 1.8. The RNA was given to the NHLBI Microarray facility, which amplified the product by reverse transcribing the RNA into cDNAs and probed full genome mouse microarrays with the resulting cDNAs. The NHLBI MicroArray facility then provided a list of genes that showed greater than two fold changes in either direction.

RT-PCR

Total RNA was isolated from MEF cell lines (two wild type YAP MEF lines and one $YAP^{-/-}$ MEF line) as described above, and 1 μg of RNA was reverse transcribed using random hexamer priming and Superscript II reverse transcriptase (Invitrogen), according to the manufacturer's specifications, while a control for each sample was exposed to all reagents except the reverse transcriptase. For PCR analyses, 1 μl of the resulting RT products were used in 25 μl reactions. Gene specific primers for *adrenomedullin* (Forward: GAG CGA AGC CCA CAT TCG T, Reverse: GAA GCG GCA TCC ATT GCT), *rasgap3* (Forward: GTG GAG CCA ATT GTC ACA AAC AGT G, Reverse: GCC TGT AAC CAG

TGT GAT GGC TCT G), *follistain-like 3* (Forward: GTT CCT GGG CCT CGT CCA C, Reverse: CGG TAC ATG ACG CGC AAG), *arhgap22* (Forward: TCC TAA CAT TCT TCG GCC AC, Reverse: CTG GTG ACC TCT TCA GAG CC), *edg7* (Forward: GAA TTG CCT CTG CAA CAT CTC, Reverse: GAG TAG ATG ATG GGG TTC A), *ephA1* (Forward: GCC TGG CCC TTT CTC CCC TG, Reverse: TCT CTG TCT CTG GCC TCT CC), and *actin* (Forward: GCT CCG GCA TGT GCA A, Reverse: AGG ATC TTC ATG AGG TAG T) were used to amplify the gene specific products using REDTaq DNA polymerase Ready Mix (Sigma) and the following PCR program: ((95°C for 5 min, 25 cycles of: (95°C for 30 sec, 57°C for 30 sec, 72°C for 45 sec), 72°C for 10 min, and overnight at 4°C)), except for the *actin* primers, which followed this PCR program: ((95°C for 5 min, 18 cycles of: (95°C for 30 sec, 55°C for 30 sec, 72°C for 45 sec), 72°C for 10 min, and overnight at 4°C)). The PCR products were then resolved on 2% agarose gels and viewed and photographed under UV illumination.

Addition of mYAP back to YAP$^{-/-}$ MEF-Turbo-Cre cells

YAP$^{-/-}$ MEF-Turbo-Cre cells that were sorted four times and passaged 36 times were trypsinized and counted. Two million cells were placed in 50 mL conical tubes, pelleted by slow centrifugation (700 rpm) for ten minutes, and resuspended in 100 μl of a room temperature mixture of the MEF1 stock solution (Lonza) and the included supplement. After resuspension, 5 μg of pCMV-HA-mYAP endotoxin-free maxi prepped (Qiagen) plasmid DNA was added to the cell/MEF1 solution. This cell resuspension was then transferred to a cuvette and electroporated in an Amaxa electroporator with program T-20. After electroporation, 500 μl of warm culture media (DMEM-high glucose with 10% FBS and P/S)

was added to the cells and transferred to T-75 tissue culture plates containing 8 mL of warm culture media, then placed back into the 37°C incubator.

Cell Culture

Jurkat (Clone E6-1) cells are human T cells that were originally isolated from the peripheral blood of a 14-year old male with acute T cell leukemia. They are maintained in RPMI-1640 culture media supplemented with 10% FBS at a cell concentration of 1 x 10^5 and 1 x 10^6 cells/mL.

In order to transfect Jurkat cells with pCMV-HA-mYAP endotoxin-free maxi prepped DNA (Qiagen), the cells were electroporated with an Amaxa electorporator. 12-well plates with 1 mL of prewarmed growth media were prepared and 1 x 10^6 cells were pelleted at 90 x g for 10 min. The cell pellet was then suspended in 100 μl prewarmed NF solution V precombined with the Amaxa supplement with 2 μg of pCMV-HA-mYAP endotoxin-free maxi prepped DNA (Qiagen). The cell/DNA suspension was transferred to a cuvette and electroporated with program X-05. The transfected cells were then added to one 12-well containing the prewarmed growth media. After 24 hours, total RNA was isolated from the transfected Jurkat cells with the RNeasy Plus kit (Qiagen). Quantity and quality of the RNA was determined using a Nanodrop and was treated with DNase (Promega) according to the manufacturer's protocol. 1 μg of RNA was reverse transcribed using random hexamer priming and Superscript II reverse transcriptase (Invitrogen), according to the manufacturer's specifications, while a control for each sample was exposed to all reagents except the reverse transcriptase. For PCR analyses, 1 μl of the resulting RT products was used in 25 μl reactions. Gene specific primers for human *adrenomedullin* (Forward: CTG GGT TCG CTC

GCC TTC CTA, Reverse: GTT GTC CTT GTC CTT ATC TGT), human *actin* (Forward: GCT CCG GCA TGT GCA A, Reverse: AGG ATC TTC ATG AGG TAG T), and mouse *yap* (Forward: GGG AGC TCT GAC TCC ACA GCA TGT TCG, Reverse: GGC AGA ATT CAT CAG CGT CTG GGG C) were used to amplify the gene specific products using REDTaq DNA polymerase Ready Mix (Sigma) and the following PCR program: ((95°C for 5 min, 27 cycles of: (95°C for 30 sec, 55°C for 30 sec, 72°C for 45 sec), 72°C for 10 min, and overnight at 4°C)), except for the *actin* and *myap* primers, which followed the same program except with 20 cycles. The PCR products were resolved on 2% agarose gels then viewed and photographed under UV illumination.

Cloning of mouse and human adrenomedullin promoters

Genomic DNA was isolated from NIH-3T3 (mouse) and Jurkat (human) cells according to established methods. Mouse and human *adrenomedullin* (*adm*) promoter regions were amplified from the isolated genomic DNA with specific primers containing restriction enzyme sites for the subsequent cloning of the *madm* promotor (Forward: CCG CTC GAG GCG AGG AGG CAA CGA GGT CCA GCC, Reverse: CCC AAG CTT GCA AAA CCC CAA AGT CCA AG) and *hadm* promoter (Forward: CGG GGT ACC GCG AGG TGG CAG CGA GGT ACA GTC, Reverse: TCC CCC GGG GCA AAA CTC CGA AGT CCA AG) into the pGL3-basic luciferase vector (Promega). The resulting PCR products were electrophoresed on a 0.8% agarose gel and gel-purified using the QIAquick Gel Extraction Kit (Qiagen). The gel-purified products and the pGL3-basic luciferase vector (Promega) were then restriction digested with *Xho*I and *Hind*III for the *madm* promoter and *Kpn*I and *Sma*I for the hADM promoter and subcloned using T4 DNA ligase (NEB) and

transformed into competent cells (Invitrogen). Positive clones were sent for sequencing and confirmed correct based on alignments with the NCBI deposited genomic sequences.

Results and Discussion

Creation of immortalized MEF cell lines

To properly genotype the isolated cell lines, genomic DNA was isolated from each immortalized cell line and PCR was performed as previously described (Morin-Kensicki *et al.*, 2006). PCR analysis confirmed that two wild type, one heterozygous, and one targeted *Yap*^{tm1Smil} allele MEF-SV40 large T antigen cell lines were obtained (Figure 38A). These cell lines were continuously passaged and stored in liquid nitrogen.

Identification and correction of error with the targeted YAP^{tm1} *allele*

After confirming the genotypes of the MEF cell lines, to be comprehensive in our analysis, a western blot to illustrate the lack of mYAP within our isolated MEF cell lines was performed. Indeed, a band corresponding to the full length YAP was missing from the YAP-null targeted cell line, but an equally strong band slightly lower than the wild type band for YAP was present in both the heterozygous and homozygous YAP targeted cell lines (Figure 38B,C). Given that the neomycin resistence gene within the targeted gene allele was not removed from the ES cells before they were put into pseudopregnant female mice, we were concerned that the promoter of the neomycin resistant gene was not sufficiently stalled and allowed continued in-frame transcription of the *yap* gene. Elizabeth Morin-Kensicki performed a series of RACE experiments to determine exactly what *yap* transcript was produced at the targeted *Yap*^{tm1Smil} allele. The resulting mutant YAP protein was missing the

Figure 38: PCR and western blot analyses identify the genotype of the MEF immortalized cell lines. A) PCR analysis of isolated genomic DNA from the respective MEF cell lines show the identity of two wild type immortilized MEF cell lines (+/+ A, B), a heterozygous line (+/-), and a homozygous targeted YAP allele line (-/-). B) Western blot analysis using our polyclonal YAP antibody (green bands) revealed that our YAP targeted mouse was not a true null as evidenced by the lower YAP bands in the null MEF cell lines. A monoclonal antibody aganst Actin (red bands) was used as a loading control. Note: mYAP was added back to the YAP null/mutant cell line using a retrovirus (-/- w/ YAP virus). C) Western blot analysis of the MEF cell lines after stabling expressing Cre recombinase (-/- MEF + Cre virus) via retroviral infection showed that removal of the neomycin resistant gene prevented the mutant YAP transcript from being transcribed and/or translated, but not in the YAP -/- MEF cell line exposed to virus lacking Cre recombinase (-/- MEF + virus).

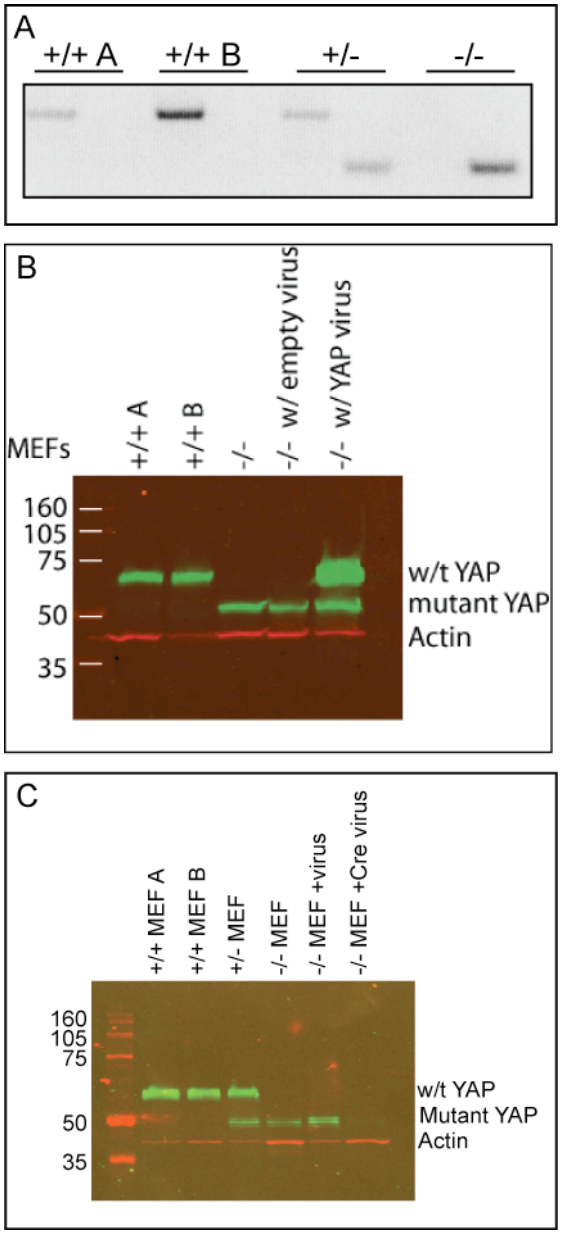
A
+/+ A
+/+ B
+/-
-/-
B
MEFs
+/+ A
+/+ B
-/-
-/- w/ empty virus
-/- w/ YAP virus
160
105
75
50
35
w/t YAP
mutant YAP
Actin
C
+/+ MEF A
+/+ MEF B
+/- MEF
-/- MEF
-/- MEF +virus
-/- MEF +Cre virus
160
105
75
50
35
w/t YAP
Mutant YAP
Actin

extreme N-terminus, where hnRNP U binding was shown to occur, and part of the TEAD binding site, which was disrupted to the point that TEAD binding would likely no longer occur. Although these results and realization that our mouse was not a true null were disappointing, we realized that the neomycin resistant gene could still be removed because two loxP sites were present on either side of the gene. In the presence of Cre recombinase, these loxP sites allow for removal of the intervening genomic sequence and hopefully truly disrupt the transcription of the *myap* transcript. Therefore, to correct the YAP-null immortalized MEF cell line, Cre recombinase was subcloned into a retroviral bicistronic vector. The resulting retrovirus was used to infect the wild type and YAP-null MEF cell lines. These lines were then sorted for GFP^+ cells indicating that the cells were infected with the virus and stably producing the Cre recombinase. In order to obtain a pure population of cells lacking the mutant YAP form (Figure 38C), four cycles of sorting were needed.

Microarray analysis

From these sorted, YAP-null cells, total RNA was isolated and submitted to the NHLBI Microarray Facility, who performed the probing of entire mouse genome microrarrays. Thousands of genes were changed between the wild type and YAP-null MEF cell lines and analyses of these changes did not point towards the involvement of a single signaling cascade. To choose a reasonably sized set of genes to verify the results from the microarray analysis by RT-PCR, I screened the list for those genes that could potentially play a role in the phenotypes associated with the mouse, frog, or zebrafish embryos lacking YAP. In addition, these chosen genes exhibited a range of fold differences and were lower in YAP-

null cells compared to wild types. Given that YAP is a transcriptional co-activator, the rationale was that genes lower in YAP-null cells could be potential gene targets of YAP.

follistatin-like 3 was chosen because its expression was 85 fold less in the YAP-null cells compared to wild type cells. It is structurally and functionally similar to follistatin in that they both bind and antagonize the actions of activin and myostatin, both members of the TGF-β family (Xia *et al.*, 2009). Overexpression of activin in mice leads to cancer, liver necrosis, and cachexia, whereas overexpression of myostatin in mice also leads to cachexia as well as reduced muscle and adipocyte mass (Lee, S. J. *et al.*, 2005, Matzuk *et al.*, 1992, Matzuk *et al.*, 1994, Reisz-Porszasz *et al.*, 2003, Zimmers *et al.*, 2002). However, mice without Follistatin-like 3 exhibited no changes in body weight or muscle composition, but instead showed increases in pancreatic islet cell number as well as enhanced glucose tolerance and sensitivity to insulin (Mukherjee *et al.*, 2007).

arhgap22 was chosen because its expression was 42 fold less in the YAP-null cells compared to wild type cells. It is a Rho GTPase activating protein (Rho-GAP), which associates with a zinc finger transcription factor, Vascular endothelial zinc-finger 1 (Vezf1) to inhibit Vezf1 activation of the *endothelin-1* promoter, inhibits Rac1 signaling, and regulates endothelial cell capillary tube formation (Aitsebaomo *et al.*, 2004). In addition, Arhgap22 plays a role in regulating the transition between mesenchymal or amoeboid movements associated with cancerous melanoma cells (Sanz-Moreno *et al.*, 2008). In this case, Arhgap22 inactivates Rac through Rho signaling via ROCK, which suppresses mesenchymal movements.

rasGRP3 was chosen because its expression was 26 fold less in the YAP-null cells compared to wild type cells. RasGRP3 is a guanine exchange factor (GEF), which facilities

the exchange of GDP and GTP and thus promotes active Ras-GTP. Although RasGRP3 knockout mice exhibited no overt phenotype other than hypogammaglobulinemia, a loss of function gene trap for RasGRP3 revealed that RasGRP3 is a VEGF-responsive GEF, which important for responses to phorbal esters in endothelial cells (Coughlin *et al.*, 2005, Roberts *et al.*, 2004).

adrenomedullin was chosen because its expression was 25 fold less in the YAP-null cells compared to wild type cells. Adrenomedullin is a multifunctional peptide hormone best known for its ability to act as a vasodilator, angiogenic factor, regulator of bone metabolism, and as tumor growth promoter. Mice lacking Adrenomedullin or its receptor, calcitonin receptor-like receptor (Calcrl), did not survive by E14.5 due to cardiovascular defects and hydrops fetalis (Caron *et al.*, 2001, Dackor *et al.*, 2006). However, it was noted that reduced levels of Adrenomedulin in female heterozygotes resulted in defects in placental development resulting in fetal growth restriction (Dackor *et al.*, 2006).

edg7 was chosen because its expression was 25 fold less in the YAP-null cells compared to wild type cells. Edg7 or lysophosphatidic acid (LPA) receptor (LPA_3) is a G protein-coupled receptor for its ligand, LPA, a lipid-signaling molecule. Deletion of Edg7 from mice leads to reduced litter sizes due to delayed implantation and altered embryo spacing. These defects ultimately resulted in delayed embryonic development, hypertrophic placentas, embryos sharing of the placenta, and death by E10.5 (Ye *et al.*, 2005). The delay in implantation was likely due to reduced cyclooxygenase-2 (COX-2) levels, which led to reduced levels of prostaglandins.

Figure 39: RT-PCR validation of microarray results. RT-PCR analysis confirmed that *follistatin-like3*, *arhGAP22*, *adrenomedullin*, *rasGRP3*, *edg7*, and *ephA1* were present in the two wild type immortalized MEF cell lines (+/+ MEF A,B), but were missing in the $YAP^{-/-}$ MEF cell line.

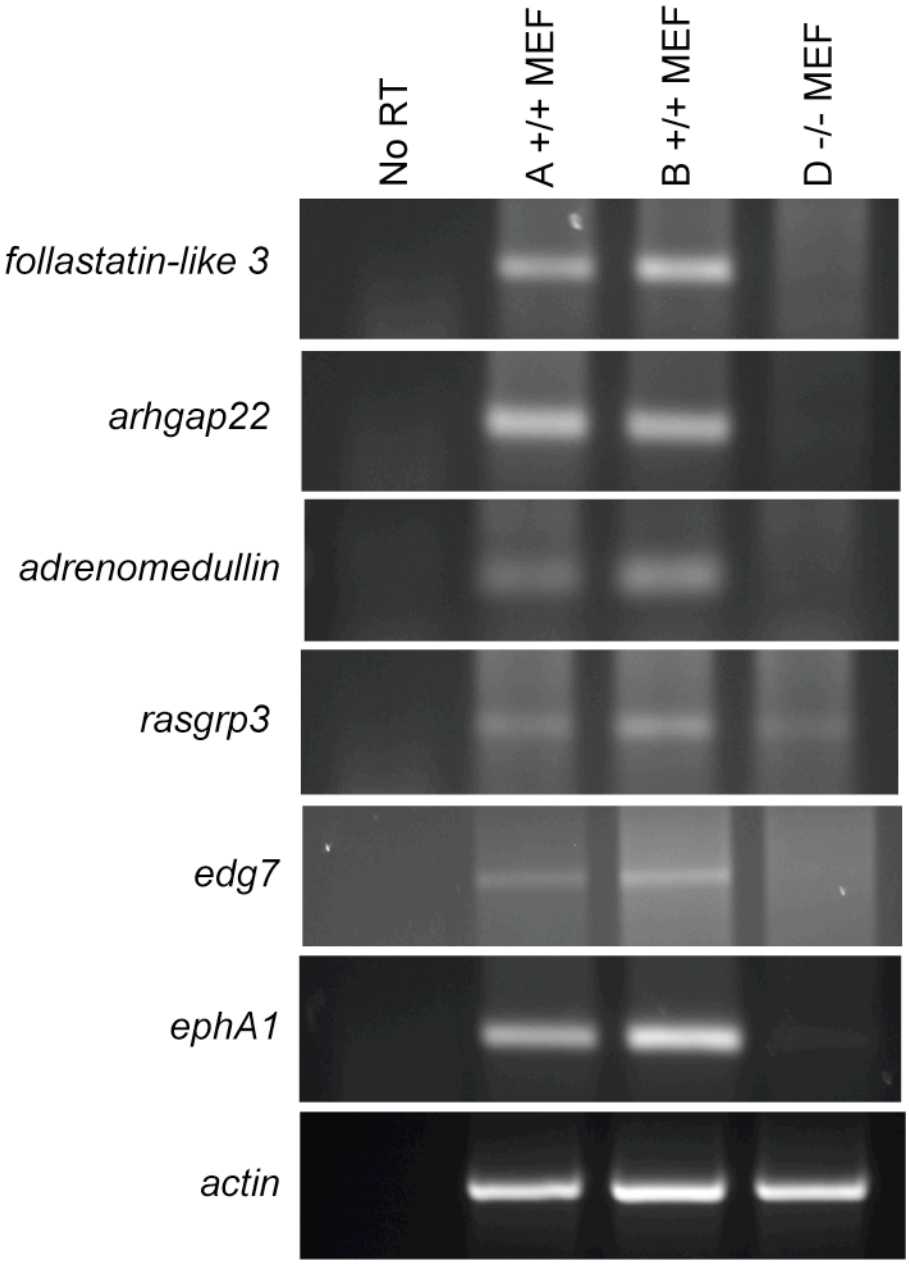
No RT
A +/+ MEF
B +/+ MEF
D -/- MEF
follastatin-like 3
arhgap22
adrenomedullin
rasgrp3
edg7
ephA1
actin

EphA1 was chosen because its expression was 20 fold less in the YAP-null cells compared to wild type cells. EphA1 is a receptor for ephrins A1-A6 and is overexpressed in breast, liver, lung, and colon carcinomas (Himanen *et al.*, 2007). In general, these receptors and ligands are linked to regulating cell activity within the nervous and vascular systems through cell-to-cell interactions. Upon ligand binding to the receiving cell, a forward signaling cascasde is activated in the receptor-containing cell as well as a reverse signal within the ligand-expressing cell.

RT-PCR analyses revealed that *follistatin-like3*, *arhGAP22*, *adrenomedullin*, *rasGRP3*, *edg7*, and *ephA1* were confirmed to be present in both wild type MEF cell lines and absent or dramatically reduced in the $YAP^{-/-}$ MEF cell line (Figure 39). To test whether these genes were YAP gene targets, YAP was added back to the $YAP^{-/-}$ MEF cells via retroviral integration. Of these genes, *adrenomedullin* was the only gene that was increased in the $YAP^{-/-}$ MEF cells after the addition of exogenous YAP to these cells (Figure 40A). Addition of YAP to Jurkat cells, which also lack endogenous YAP expression, increased *adrenomedullin* expression as well (Figure 40B). To test whether YAP could regulate the *adrenomedullin* promoter directly, I subcloned the mouse *adrenomedullin* promoter (-2054/+94) from the genomic DNA of NIH-3T3 fibroblast cells into a luciferase reporter. Electroporation of the promoter with or without the addition of YAP into the $YAP^{-/-}$ MEF cells, showed an increase in promoter activity on the order of two to three fold (Figure 41). In addition, maximum expression of YAP occurred at 15 hr after electroporation, while YAP expression was gone by 24 hr after electroporation. Although the fold change in *adrenomedullin* promoter activity was only two to three fold, extension of exogenous YAP expression might offer larger fold changes in *adrenomedullin* promoter activity; therefore,

Figure 40: Adding YAP back to YAP$^{-/-}$ MEFs and Jurkat cells increased *adrenomedullin* expression. RT-PCR analysis showed that the addition of mYAP back to the YAP-null MEF cell line (A) and to a T-cell line (Jurkat cells) that lack endogenous YAP (B) upregulated *adrenomedullin* transcription.

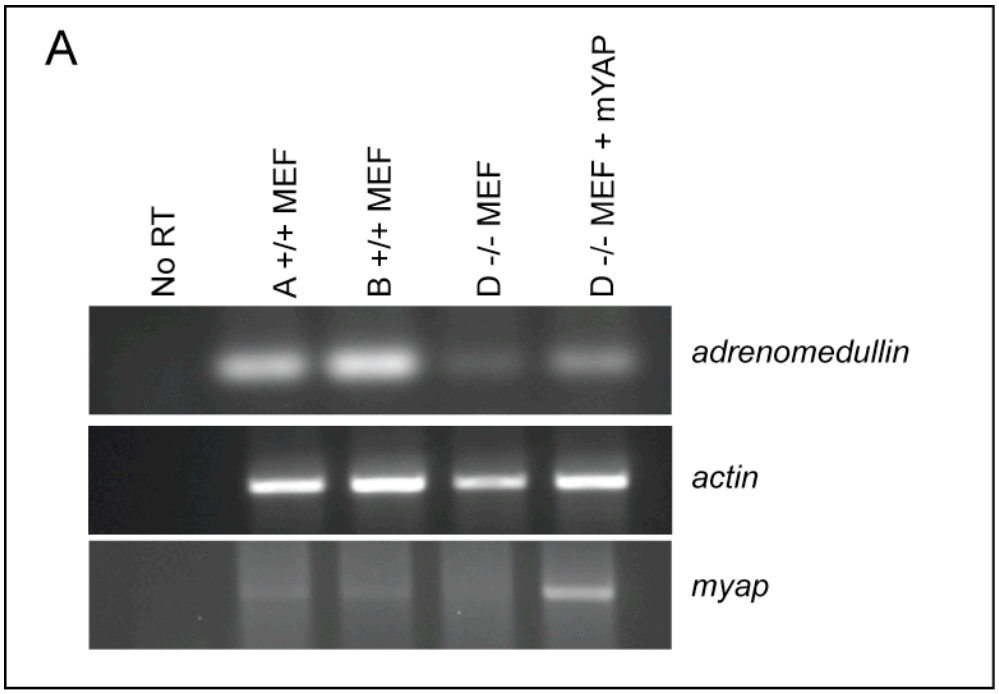
A
No RT
A +/+ MEF
B +/+ MEF
D -/- MEF
D -/- MEF + mYAP
adrenomedullin
actin
myap

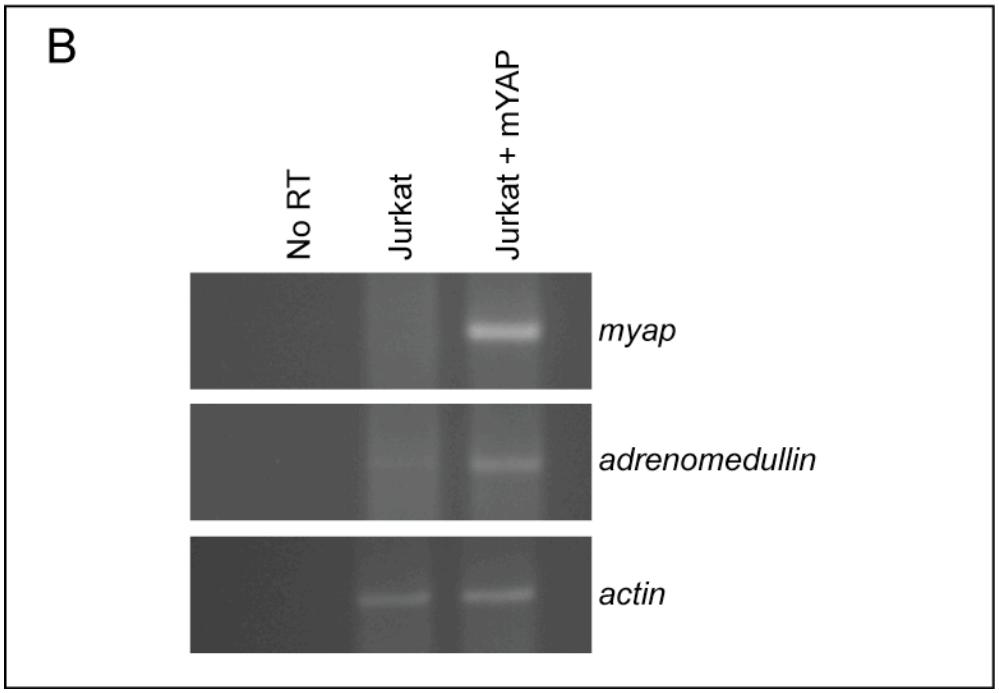
B
No RT
Jurkat
Jurkat + mYAP
myap
adrenomedullin
actin

Figure 41: Time course for mouse *adrenomedullin* promoter activity in MEF cell lines. $YAP^{-/-}$ MEFs were electroporated with the mouse *adrenomedullin* luciferase and β-gal reporter constructs with (+) or without (-) the addition of an expression vector containing mYAP. Luciferse and β-gal reporter assays revealed maximum promoter activity at fifteen hours, but exogenous YAP expression and *adrenomedullin* promoter activity was eliminated by twenty-four hours.

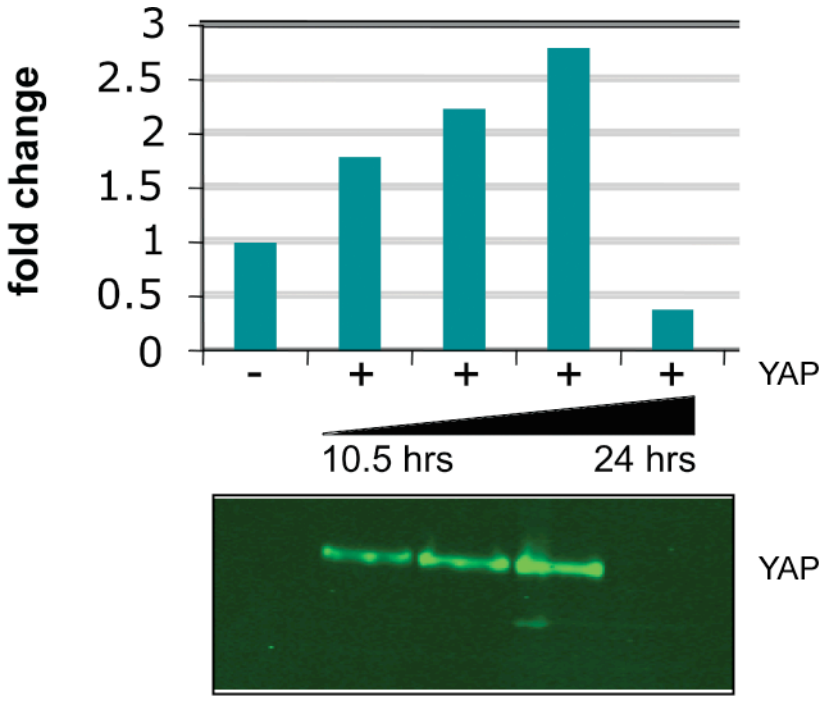
fold change
3
2.5
2
1.5
1
0.5
0
-
+
+
+
+
YAP
10.5 hrs
24 hrs
YAP

Figure 42: YAP is present on the mouse *adrenomedullin* promoter. A) Chromatin isolated from the wild type MEF cell line was sheared to sizes between 650 bp and 100 bp. (B) Chromatin immunoprecipitations (ChIPs) from sheared wild type MEF chromatin using the YAP antibody revealed the presence of YAP at two locations on the *adrenomedullin* 5' regulatory region, but was not present when a control IgG antibody was used.

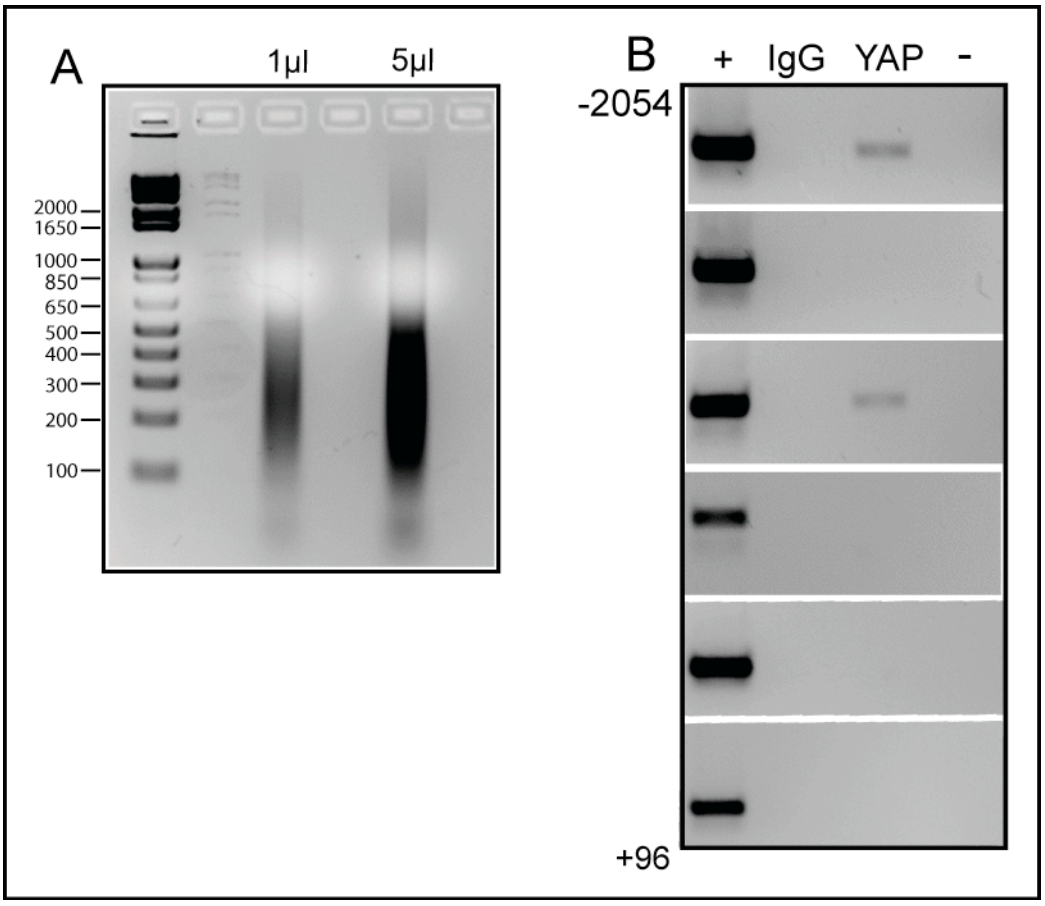
A
1µl
5µl
2000
1650
1000
850
650
500
400
300
200
100
B
+
IgG
YAP
-
-2054
+96

activation of the *adrenomedullin* promoter under these conditions suggests that YAP is involved in regulating *adrenomedullin* gene expression. To determine whether endogenous YAP was present within this 5' regulatory region, six primer sets encomposing the *adrenomedullin* promoter (-2054/+94) were used in chromatin immunoprecipitations. ChIP analyses revealed that YAP was present endogenously at two locations on the *adrenomedullin* promoter, confirming that *adrenomedullin* is likely a YAP gene target (Figure 42). However, more luciferase assays and *in vivo* transgenic approaches need to be performed to confirm YAP's transcriptional control over the *adrenomedullin* gene.

Chapter V – Summary and Perspectives

I provided evidence for YAP playing an important role during early vertebrate development by utilizing a series of knockdown and gain-of-function approaches in *Xenopus laevis* and *Danio rerio* embryos. I found that YAP morpholino (MO)-mediated loss-of-function prevented further developmental progression at gastrulation, and reduced YAP levels resulted in a delay of mesoderm induction. Increasing YAP function expanded the neural plate and early neural crest, while concomitantly inhibiting the induction and expansion of the preplacodal ectoderm (PPE). In addition, YAP gain-of-function maintained and expanded progenitor domains, while inhibiting differentiation. Next, I presented preliminary work on the regulation of the *yap* promoter by Sp1. Finally, I identified *adrenomedullin* as a putative transcriptional target of YAP.

Although these three diverse projects are interwoven only by their association and relevance to understanding the function of YAP in vertebrate development, much time was spent contemplating the potential functions of YAP *in vivo*. Even with the knowledge gained from this work and from others, there are still many unanswered questions regarding this complicated protein. With that being said, some preliminary data that I collected leads me to consider that understanding the role of YAP *in vivo* revolves around its function as both a transcriptional co-activator and a scaffolding protein and that these functions should not be separated based on the protein's localization in the cell. At the beginning of this project, I associated YAP's role as a scaffolding protein with its cytoplasmic location, while its role as transcriptional co-activator I associated with its nuclear location. I now believe, however, that understanding YAP's role *in vivo* involves both functions and that these functions are interdependent. More importantly, I believe the scaffolding properties of YAP within the nucleus needs further attention and here are several reasons why.

According to the current literature, YAP's interaction with the TEAD family of transcription factors clearly has a profound affect on developmental outcomes; however, the canonical definition of classifying nuclear proteins as transcription factors or repressors is becoming obsolete. We are now moving toward a more realistic view that takes into account the clustering of protein complexes present or absent on exposed pieces of chromatin. Not only must these clusters of proteins link themselves to one another and to their DNA targets, but they must also assist in recruiting chromatin remodeling complexes and the RNA polymerase II pre-initiation complex. Although we know a great deal about the cell nucleus, we still lack some key pieces of information for understanding the processes of cellular differentiation and aging. The nuclear architecture is finally coming into its own as an emerging field in cell and developmental biology (Misteli, 2009, Misteli, 2010). There are two opposing lines of thought on how the nucleus is organized. One line suggests that the architecture of the nucleus is set up and maintained by scaffolding proteins, which link structural portions of the nucleus together. The other line suggests that the nuclear architecture is a self-organizing entity instructed to regulate internal nuclear processes via instructive signals from outside the cell. Although experiments to define which of these two opposing lines of thinking are true can be difficult to interpret, I currently prefer to accept the possibility that both lines of thinking are true and not mutually exclusive. Furthermore, I think that YAP is a good example of how both of these lines of thinking could be true.

For example, our lab previously identified hnRNP U as a specific binding partner of YAP, but not TAZ; however, the functional importance of this interaction was difficult to delineate (Howell *et al.*, 2004). This was especially true given that the ascribed functions for hnRNP U include regulating pre-RNA processing, mRNA transport, mRNA translation,

mRNA stability, and transcription. Furthermore, hnRNP U interacts with RNP particles allowing for its association with histone acetylases (HATs), p300, and chromosomal attachment regions. The mechanistic details and significance of these interactions are still being worked out. hnRNP U can be divided into three main interacting protein pieces. The amino terminus of hnRNP U interacts with DNA, the middle interacts with the phosphorylated C terminal domain (CTD) of RNA polymerase II, and the carboxy terminus interacts with nuclear actin and mRNA (Kukalev *et al.*, 2005). Although this hnRNP U-YAP interaction was thoroughly analyzed and published, I repeated the co-immunoprecipitations both ways and found that the interaction was quite robust (not shown). Given these reassuring results of YAP's interaction with hnRNP U, I was curious as to which portion of hnRNP U YAP interacted. Afterall, where YAP binds to hnRNP U could potentially compete with other potential interactions and affect the function of hnRNP U. In addition, further support for the putative importance of YAP's interaction with hnRNP U came from the hnRNP U hypomorph, which clearly exhibited a delay in development and thus was similar to the *in vivo* results we observed in the mouse, frog, and zebrafish (Roshon *et al.*, 2005). Because of these anecdotal observations, I decided to perform a GST pulldown with the proline-rich N-terminus of YAP and [^{35}S] radiolabeled portions of hnRNP U. I found that YAP bound specifically to the carboxy terminus of hnRNP U (Figure 43), which is shown to also interact with nuclear actin and mRNA. However, I did not further pursue the details regarding the functional outcome of such an interaction, yet I feel that it may be worth pursuing in the future (Kukalev *et al.*, 2005).

Another example of YAP's putative role in the nuclear architecture came from my literature searches for evidence of phenotypes similar to those I observed in my YAP

Figure 43: YAP binds to the C-terminus of hnRNP U. Three different portions (N-terminus (1-250), middle (251-550), and the C-terminus (551-823)) of hnRNP U were *in vitro* translated in the presence of [^{35}S] radio-labeled methionine. GST pulldowns using purified GST, GST-YAP-PR (proline rich N-terminus) proteins, and the three different portions of hnRNP U showed that the C-terminus of hnRNP U strongly binds to the proline rich N-terminus of YAP.

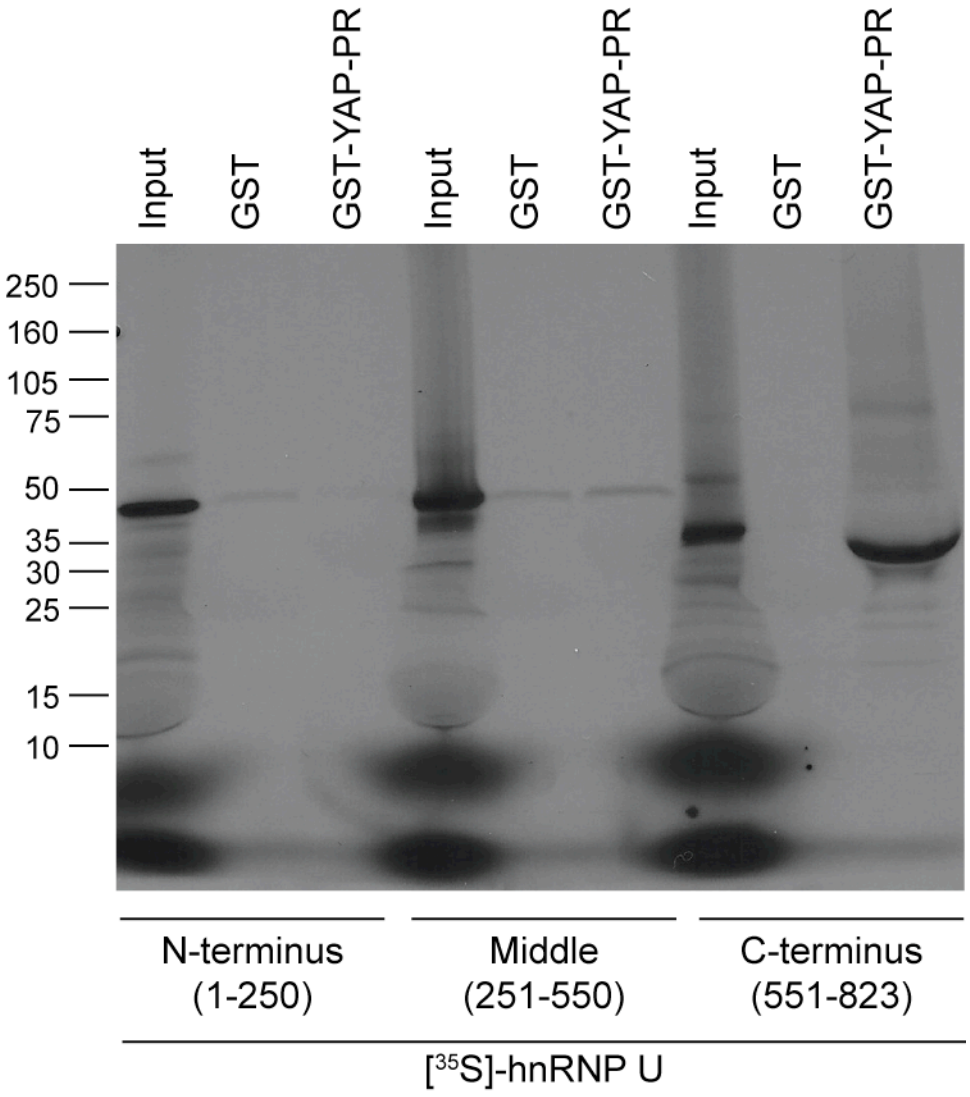
Input
GST
GST-YAP-PR
Input
GST
GST-YAP-PR
Input
GST
GST-YAP-PR
250
160
105
75
50
35
30
25
15
10
N-terminus
(1-250)
Middle
(251-550)
C-terminus
(551-823)
[35S]-hnRNP U

morphant or mutant *Xenopus laevis embryos*. I serendipitously came across a paper whereby loss of Brg1, the catalytic subunit of the SWI/SNF chromatin remodeling complex, resulted in expansion of $sox2^{+}$ neural progenitors and loss of neural differentiation as evidence by reduced *n-tubulin in situ* staining (Seo *et al.*, 2005). This paper was of particular interest because we were previously contacted by Dr. Bernard Weissman (UNC) regarding the possibility that YAP may bind to another member of the SWI/SNF chromatin remodeling complex, BAF155. We provided Dr. Weissman with some of our purified YAP antibody, but never heard the outcome of their co-immunoprecipitation experiments. However, given these two pieces of anecdotal information, I looked at the proteins to see if Brg1 and/or BAF155 contained a PPxY motif, which would allow their binding to the WW domains of YAP. In fact, both Brg1 and BAF155 possess PPxY motifs and bound to the WW domain of YAP in GST pulldowns using endogenous HeLa cell lysates (Figure 44). Endogenous co-immunoprecipitations were more difficult and could not be confirmed. However, I obtained an hBrg1construct from Dr. Keji Zhao and co-expressed HA-Brg1 and Myc-mYAP in HeLa cells. By immunoprecipitating HA-Brg1 from isolated nuclear extracts, I obtained a modest amount of YAP binding from the resulting co-immunoprecipitations (Figure 45). Based on these results, I conclude that YAP is capable of binding to the SWI/SNF chromatin-remodeling complex; however, I was unable to define the functional importance of such an interaction.

I believe these interactions further support the hypothesis that YAP is more than just a transcriptional co-activator that associates with TEAD transcription factors to activate target genes. I hypothesize that YAP plays a more prominent role in regulating the fundamental interworkings of the nucleus through its interaction with other nuclear proteins and protein

Figure 44: BAF155 and Brg1 can bind to the YAP WW1 domain. Western blot analyses of GST pulldowns using purified GST, GST-YAP-WW1, and nuclear lysates from HeLa cells showed that both BAF155 and Brg1 could bind to the WW1 domain of YAP, but not to GST.

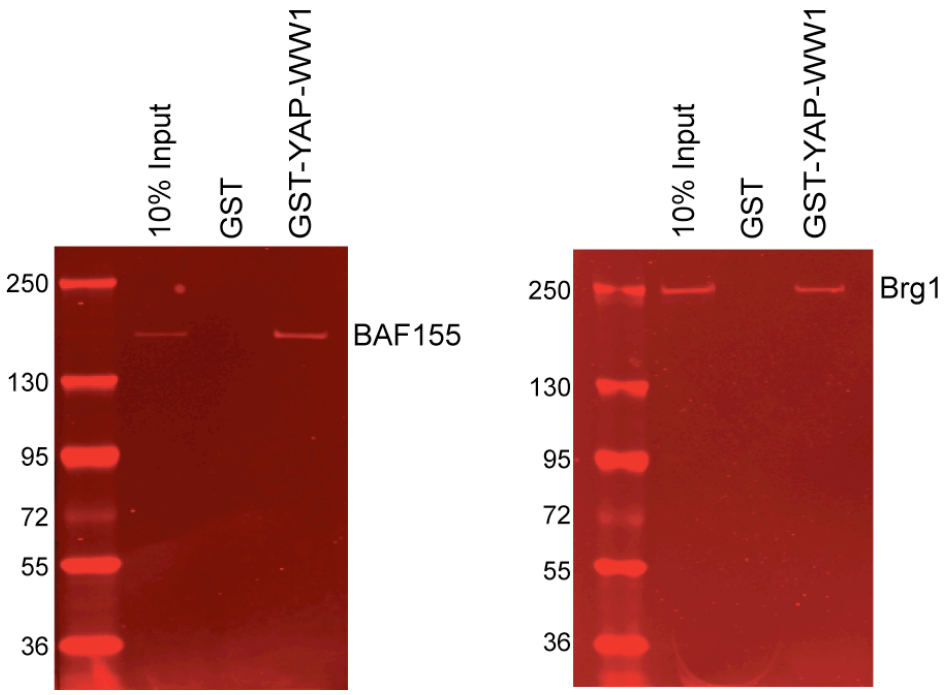
10% Input
GST
GST-YAP-WW1
250
130
95
72
55
36
BAF155
10% Input
GST
GST-YAP-WW1
250
130
95
72
55
36
Brg1

Figure 45: Co-immunoprecipitation of YAP with Brg1. HA-Brg1 and Myc-mYAP-cAct, the constitutively active, nuclear form of YAP, were co-transfected into HeLa cells. Immunoprecipitations using beads conjugated with an HA antibody and subsequent western blot analyses using a HA antibody showed that HA-Brg1 was immunoprecipitated and a YAP antibody illustrated that YAP co-immunoprecipitated with Brg1.

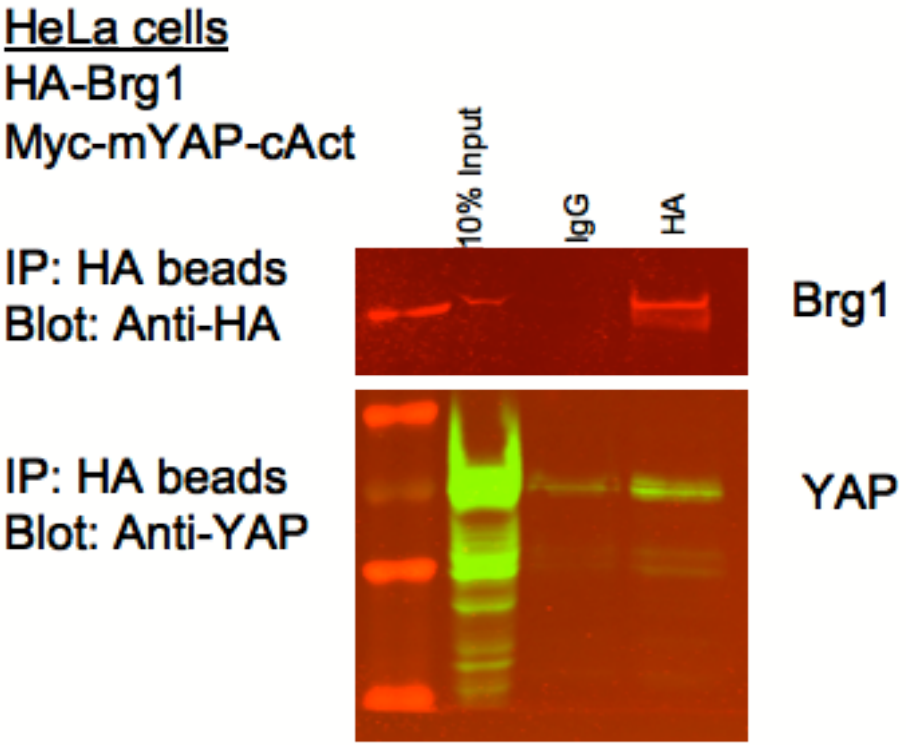
HeLa cells
HA-Brg1
Myc-mYAP-cAct
10% Input
IgG
HA
IP: HA beads
Blot: Anti-HA
Brg1
IP: HA beads
Blot: Anti-YAP
YAP

complexes than is currently appreciated. Not only do these preliminary data suggest a possible role in linking nuclear pieces together for a common goal, but my functional analyses of YAP deletions reveal that the PDZ-binding motif may play a role in regulating muscle and epidermal differentiation. Although an affinity peptide pulldown with whole *Xenopus laevis* lysates and the PDZ-binding motif of YAP was previously performed, the experimental outcome was extremely dirty; therefore, such an experiment deserves revisiting in light of these current findings.

Finally, I would like to briefly point out an evolutionary perspective on the presence and function of YAP and TAZ, especially given how important YAP appears to be for proper vertebrate development. By constructing a phylogenetic tree for YAP and TAZ, I was able to find a YAP and TAZ homolog for most every vertebrate, illustrating that there was a clear duplication event that occurred between the invertebrate and vertebrate branches on this phylogenetic tree (Figure 46). Invertebrates only have a single YAP/TAZ protein, which is actually more similar to YAP than TAZ as they have two WW domains. Surprisingly, all the invertebrate YAP/TAZ homologs contained the traditional PDZ-binding motif at its C-terminus. I say this was surprising because the fly homolog, Yorkie, does not have this conserved domain. Therefore, some functional data obtained from the fly may not be conserved in the rest of the animal kingdom. However, what I found most interesting is that the conserved signaling pathway, the Hippo signaling pathway, of which YAP is a part, and its components, are conserved all the way down to the base of the evolutionary tree. These members are first present in the placozoan, *Trichoplax adhaerens* (Srivastava *et al.*, 2008). The simplicity of this organism is astounding. It is only one millimeter thick, is made of only three layers, and feeds on microbes by absorption on their underside. In addition, these

Figure 46: Evolutionary conservation of YAP and TAZ. A phylogenetic tree for YAP and TAZ was constructed using MEGA 4.1. Although all vertebrate homologs of YAP and TAZ are not listed on this tree, a homolog could be found for every vertebrate tested; however, only one YAP/TAZ homolog could be found in the genomes of the listed invertebrates, suggesting that the prescence of TAZ in vertebrates is the result of a duplication event that occurred between the invertebrate and vertebrate branches.

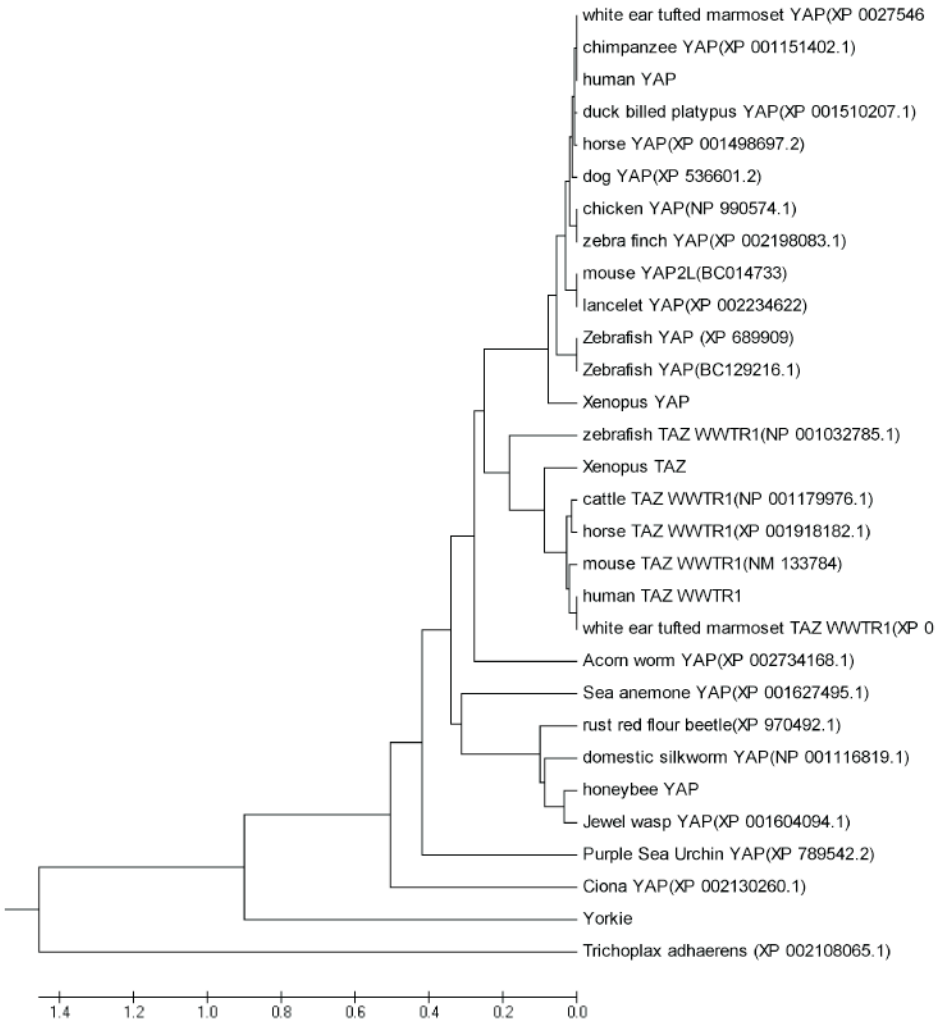
white ear tufted marmoset YAP(XP 0027546
chimpanzee YAP(XP 001151402.1)
human YAP
duck billed platypus YAP(XP 001510207.1)
horse YAP(XP 001498697.2)
dog YAP(XP 536601.2)
chicken YAP(NP 990574.1)
zebra finch YAP(XP 002198083.1)
mouse YAP2L(BC014733)
lancelet YAP(XP 002234622)
Zebrafish YAP (XP 689909)
Zebrafish YAP(BC129216.1)
Xenopus YAP
zebrafish TAZ WWTR1(NP 001032785.1)
Xenopus TAZ
cattle TAZ WWTR1(NP 001179976.1)
horse TAZ WWTR1(XP 001918182.1)
mouse TAZ WWTR1(NM 133784)
human TAZ WWTR1
white ear tufted marmoset TAZ WWTR1(XP 0
Acorn worm YAP(XP 002734168.1)
Sea anemone YAP(XP 001627495.1)
rust red flour beetle(XP 970492.1)
domestic silkworm YAP(NP 001116819.1)
honeybee YAP
Jewel wasp YAP(XP 001604094.1)
Purple Sea Urchin YAP(XP 789542.2)
Ciona YAP(XP 002130260.1)
Yorkie
Trichoplax adhaerens (XP 002108065.1)
1.4
1.2
1.0
0.8
0.6
0.4
0.2
0.0

organisms reproduce asexually although there is some scant data suggesting they may have evolved some primitive sexual reproduction. Notably, sponge and hydra did not contain components of the conserved Hippo signaling pathway (Chapman *et al.*, 2010, Srivastava *et al.*, 2010). This observation makes one wonder how those organisms survive without this pathway, yet almost all other organisms possesses such a pathway. Furthermore, given the complexity of YAP's diverse and overlapping function with other signaling pathways in vertebrates, it may be useful to study its earliest, most fundamental cellular function in *Trichoplax adhaerens*.

In summary, I characterized the effects of YAP loss-of-function and gain-of-function approaches in *Xenopus laevis* and *Danio rerio* embryos. YAP morpholino (MO)-mediated loss-of-function resulted in a delay of mesoderm induction and impaired axis formation, similar to the mouse phenotype. YAP gain-of-function in *Xenopus laevis* expanded the progenitor populations in the neural plate and neural plate border zone, while concomitantly inhibiting markers for the neural crest, preplacodal ectoderm, hatching gland, epidermis, and somitic muscle. I found that *yap* expression is controlled by a TATA-less promoter, which includes a GC box where Sp1 binds and regulates *yap* transcription. I also found that *adrenomedullin*, a multifunctional peptide hormone known to act as a vasodilator, angiogenic factor, regulator of placental development, and tumor growth promoter, is a newly identified, putative target of YAP. These studies demonstrate that YAP is involved in the process of cell differentiation and the lack or overabundance of YAP protein disrupts the developmental time line of vertebrates with grievous consequences. Understanding the mechanistic details of these effects involve understanding the transcriptional control of YAP and its target genes.

In the future, understanding the linkage between YAP, the nuclear architecture, and transcriptional regulation will bolster our understanding of cell differentiation.

References

Aitsebaomo, J., Wennerberg, K., Der, C. J., Zhang, C., Kedar, V., Moser, M., Kingsley-Kallesen, M. L., Zeng, G. Q., and Patterson, C. (2004) p68RacGAP is a novel GTPase-activating protein that interacts with vascular endothelial zinc finger-1 and modulates endothelial cell capillary formation. *J Biol Chem* 279(17): 17963-17972.

Alarcon, C., Zaromytidou, A. I., Xi, Q., Gao, S., Yu, J., Fujisawa, S., Barlas, A., Miller, A. N., Manova-Todorova, K., Macias, M. J., Sapkota, G., Pan, D., and Massague, J. (2009) Nuclear CDKs drive Smad transcriptional activation and turnover in BMP and TGF-beta pathways. *Cell* 139(4): 757-769.

Andersson, O., Bertolino, P., and Ibanez, C. F. (2007) Distinct and cooperative roles of mammalian Vg1 homologs GDF1 and GDF3 during early embryonic development. *Dev Biol* 311(2): 500-511.

Bork, P., and Sudol, M. (1994) The WW domain: a signalling site in dystrophin? *Trends Biochem Sci* 19(12): 531-533.

Brown, M., McCormack, M., Zinn, K. G., Farrell, M. P., Bikel, I., and Livingston, D. M. (1986) A recombinant murine retrovirus for simian virus 40 large T cDNA transforms mouse fibroblasts to anchorage-independent growth. *J Virol* 60(1): 290-293.

Brugmann, S. A., Pandur, P. D., Kenyon, K. L., Pignoni, F., and Moody, S. A. (2004) Six1 promotes a placodal fate within the lateral neurogenic ectoderm by functioning as both a transcriptional activator and repressor. *Development* 131(23): 5871-5881.

Brunskill, E. W., Witte, D. P., Yutzey, K. E., and Potter, S. S. (2001) Novel cell lines promote the discovery of genes involved in early heart development. *Dev Biol* 235(2): 507-520.

Buratowski, S., Hahn, S., Guarente, L., and Sharp, P. A. (1989) Five intermediate complexes in transcription initiation by RNA polymerase II. *Cell* 56(4): 549-561.

Camargo, F. D., Gokhale, S., Johnnidis, J. B., Fu, D., Bell, G. W., Jaenisch, R., and Brummelkamp, T. R. (2007) YAP1 increases organ size and expands undifferentiated progenitor cells. *Curr Biol* 17(23): 2054-2060.

Cao, X., Pfaff, S. L., and Gage, F. H. (2008) YAP regulates neural progenitor cell number via the TEA domain transcription factor. *Genes Dev* 22(23): 3320-3334.

Caron, K. M., and Smithies, O. (2001) Extreme hydrops fetalis and cardiovascular abnormalities in mice lacking a functional Adrenomedullin gene. *Proc Natl Acad Sci U S A* 98(2): 615-619.

Chapman, J. A., Kirkness, E. F., Simakov, O., Hampson, S. E., Mitros, T., Weinmaier, T., Rattei, T., Balasubramanian, P. G., Borman, J., Busam, D., Disbennett, K., Pfannkoch, C., Sumin, N., Sutton, G. G., Viswanathan, L. D., Walenz, B., Goodstein, D. M., Hellsten, U., Kawashima, T., Prochnik, S. E., Putnam, N. H., Shu, S., Blumberg, B., Dana, C. E., Gee, L., Kibler, D. F., Law, L., Lindgens, D., Martinez, D. E., Peng, J., Wigge, P. A., Bertulat, B., Guder, C., Nakamura, Y., Ozbek, S., Watanabe, H., Khalturin, K., Hemmrich, G., Franke, A., Augustin, R., Fraune, S., Hayakawa, E., Hayakawa, S., Hirose, M., Hwang, J. S., Ikeo, K., Nishimiya-Fujisawa, C., Ogura, A., Takahashi, T., Steinmetz, P. R., Zhang, X., Aufschnaiter, R., Eder, M. K., Gorny, A. K., Salvenmoser, W., Heimberg, A. M., Wheeler, B. M., Peterson, K. J., Bottger, A., Tischler, P., Wolf, A., Gojobori, T., Remington, K. A., Strausberg, R. L., Venter, J. C., Technau, U., Hobmayer, B., Bosch, T. C., Holstein, T. W., Fujisawa, T., Bode, H. R., David, C. N., Rokhsar, D. S., and Steele, R. E. (2010) The dynamic genome of Hydra. *Nature* 464(7288): 592-596.

Chen, Q., Chen, H., Zheng, D., Kuang, C., Fang, H., Zou, B., Zhu, W., Bu, G., Jin, T., Wang, Z., Zhang, X., Chen, J., Field, L. J., Rubart, M., Shou, W., and Chen, Y. (2009) Smad7 is required for the development and function of the heart. *J Biol Chem* 284(1): 292-300.

Chen, W., and Struhl, K. (1985) Yeast mRNA initiation sites are determined primarily by specific sequences, not by the distance from the TATA element. *Embo J* 4(12): 3273-3280.

Chen, Z., Friedrich, G. A., and Soriano, P. (1994) Transcriptional enhancer factor 1 disruption by a retroviral gene trap leads to heart defects and embryonic lethality in mice. *Genes Dev* 8(19): 2293-2301.

Chitnis, A., Henrique, D., Lewis, J., Ish-Horowicz, D., and Kintner, C. (1995) Primary neurogenesis in *Xenopus* embryos regulated by a homologue of the *Drosophila* neurogenic gene Delta. *Nature* 375(6534): 761-766.

Chong, P. A., Lin, H., Wrana, J. L., and Forman-Kay, J. D. (2006) An expanded WW domain recognition motif revealed by the interaction between Smad7 and the E3 ubiquitin ligase Smurf2. *J Biol Chem* 281(25): 17069-17075.

Coffman, C., Harris, W., and Kintner, C. (1990) Xotch, the *Xenopus* homolog of Drosophila notch. *Science* 249(4975): 1438-1441.

Coffman, C. R., Skoglund, P., Harris, W. A., and Kintner, C. R. (1993) Expression of an extracellular deletion of Xotch diverts cell fate in Xenopus embryos. *Cell* 73(4): 659-671.

Coughlin, J. J., Stang, S. L., Dower, N. A., and Stone, J. C. (2005) RasGRP1 and RasGRP3 regulate B cell proliferation by facilitating B cell receptor-Ras signaling. *J Immunol* 175(11): 7179-7184.

Cui, C. B., Cooper, L. F., Yang, X., Karsenty, G., and Aukhil, I. (2003) Transcriptional coactivation of bone-specific transcription factor Cbfa1 by TAZ. *Mol Cell Biol* 23(3): 1004-1013.

Dackor, R. T., Fritz-Six, K., Dunworth, W. P., Gibbons, C. L., Smithies, O., and Caron, K. M. (2006) Hydrops fetalis, cardiovascular defects, and embryonic lethality in mice lacking the calcitonin receptor-like receptor gene. *Mol Cell Biol* 26(7): 2511-2518.

Davis, M., Hatzubai, A., Andersen, J. S., Ben-Shushan, E., Fisher, G. Z., Yaron, A., Bauskin, A., Mercurio, F., Mann, M., and Ben-Neriah, Y. (2002) Pseudosubstrate regulation of the SCF(beta-TrCP) ubiquitin ligase by hnRNP-U. *Genes Dev* 16(4): 439-451.

Dean, G., Young, D. A., Edwards, D. R., and Clark, I. M. (2000) The human tissue inhibitor of metalloproteinases (TIMP)-1 gene contains repressive elements within the promoter and intron 1. *J Biol Chem* 275(42): 32664-32671.

Dong, J., Feldmann, G., Huang, J., Wu, S., Zhang, N., Comerford, S. A., Gayyed, M. F., Anders, R. A., Maitra, A., and Pan, D. (2007) Elucidation of a universal size-control mechanism in Drosophila and mammals. *Cell* 130(6): 1120-1133.

Dynan, W. S., and Tjian, R. (1983) Isolation of transcription factors that discriminate between different promoters recognized by RNA polymerase II. *Cell* 32(3): 669-680.

Espanel, X., and Sudol, M. (2001) Yes-associated protein and p53-binding protein-2 interact through their WW and SH3 domains. *J Biol Chem* 276(17): 14514-14523.

Ferrigno, O., Lallemand, F., Verrecchia, F., L'Hoste, S., Camonis, J., Atfi, A., and Mauviel, A. (2002) Yes-associated protein (YAP65) interacts with Smad7 and potentiates its inhibitory activity against TGF-beta/Smad signaling. *Oncogene* 21(32): 4879-4884.

Gassmann, M., Casagranda, F., Orioli, D., Simon, H., Lai, C., Klein, R., and Lemke, G. (1995) Aberrant neural and cardiac development in mice lacking the ErbB4 neuregulin receptor. *Nature* 378(6555): 390-394.

Gavert, N., and Ben-Ze'ev, A. (2007) beta-Catenin signaling in biological control and cancer. *J Cell Biochem* 102(4): 820-828.

Gidoni, D., Kadonaga, J. T., Barrera-Saldana, H., Takahashi, K., Chambon, P., and Tjian, R. (1985) Bidirectional SV40 transcription mediated by tandem Sp1 binding interactions. *Science* 230(4725): 511-517.

Gorina, S., and Pavletich, N. P. (1996) Structure of the p53 tumor suppressor bound to the ankyrin and SH3 domains of 53BP2. *Science* 274(5289): 1001-1005.

Hardcastle, Z., and Papalopulu, N. (2000) Distinct effects of XBF-1 in regulating the cell cycle inhibitor p27(XIC1) and imparting a neural fate. *Development* 127(6): 1303-1314.

Harland, R. M. (1991) *In situ* hybridization: an improved whole-mount method for *Xenopus* embryos. *Methods Cell Biol* 36: 685-695.

Himanen, J. P., Saha, N., and Nikolov, D. B. (2007) Cell-cell signaling via Eph receptors and ephrins. *Curr Opin Cell Biol* 19(5): 534-542.

Hiraoka, Y., Komatsu, N., Sakai, Y., Ogawa, M., Shiozawa, M., and Aiso, S. (1997) XLS13A and XLS13B: SRY-related genes of *Xenopus laevis*. *Gene* 197(1-2): 65-71.

Hong, J. H., Hwang, E. S., McManus, M. T., Amsterdam, A., Tian, Y., Kalmukova, R., Mueller, E., Benjamin, T., Spiegelman, B. M., Sharp, P. A., Hopkins, N., and Yaffe, M. B. (2005) TAZ, a transcriptional modulator of mesenchymal stem cell differentiation. *Science* 309(5737): 1074-1078.

Hooghe, B., Hulpiau, P., van Roy, F., and De Bleser, P. (2008) ConTra: a promoter alignment analysis tool for identification of transcription factor binding sites across species. *Nucleic Acids Res* 36(suppl 2): W128-132.

Hossain, Z., Ali, S. M., Ko, H. L., Xu, J., Ng, C. P., Guo, K., Qi, Z., Ponniah, S., Hong, W., and Hunziker, W. (2007) Glomerulocystic kidney disease in mice with a targeted inactivation of Wwtr1. *Proc Natl Acad Sci U S A* 104(5): 1631-1636.

Howell, M., Borchers, C., and Milgram, S. L. (2004) Heterogeneous nuclear ribonuclear protein U associates with YAP and regulates its co-activation of Bax transcription. *J Biol Chem* 279(25): 26300-26306.

Iwabuchi, K., Bartel, P. L., Li, B., Marraccino, R., and Fields, S. (1994) Two cellular proteins that bind to wild-type but not mutant p53. *Proc Natl Acad Sci U S A* 91(13): 6098-6102.

Jacob, L., and Lum, L. (2007) Deconstructing the hedgehog pathway in development and disease. *Science* 318(5847): 66-68.

Jarriault, S., Brou, C., Logeat, F., Schroeter, E. H., Kopan, R., and Israel, A. (1995) Signalling downstream of activated mammalian Notch. *Nature* 377(6547): 355-358.

Jarriault, S., Le Bail, O., Hirsinger, E., Pourquie, O., Logeat, F., Strong, C. F., Brou, C., Seidah, N. G., and Isra l, A. (1998) Delta-1 activation of notch-1 signaling results in HES-1 transactivation. *Mol Cell Biol* 18(12): 7423-7431.

Jiang, Q., Liu, D., Gong, Y., Wang, Y., Sun, S., Gui, Y., and Song, H. (2009) yap is required for the development of brain, eyes, and neural crest in zebrafish. *Biochem Biophys Res Commun* 384(1): 114-119.

Jiang, S. W., Wu, K., and Eberhardt, N. L. (1999) Human placental TEF-5 transactivates the human chorionic somatomammotropin gene enhancer. *Mol Endocrinol* 13(6): 879-889.

Jonas, E., Sargent, T. D., and Dawid, I. B. (1985) Epidermal keratin gene expressed in embryos of *Xenopus laevis*. *Proc Natl Acad Sci U S A* 82(16): 5413-5417.

Kampa, K. M., Acoba, J. D., Chen, D., Gay, J., Lee, H., Beemer, K., Padiernos, E., Boonmark, N., Zhu, Z., Fan, A. C., Bailey, A. S., Fleming, W. H., Corless, C.,

Felsher, D. W., Naumovski, L., and Lopez, C. D. (2009) Apoptosis-stimulating protein of p53 (ASPP2) heterozygous mice are tumor-prone and have attenuated cellular damage-response thresholds. *Proc Natl Acad Sci U S A* 106(11): 4390-4395.

Kanai, F., Marignani, P. A., Sarbassova, D., Yagi, R., Hall, R. A., Donowitz, M., Hisaminato, A., Fujiwara, T., Ito, Y., Cantley, L. C., and Yaffe, M. B. (2000) TAZ: a novel transcriptional co-activator regulated by interactions with 14-3-3 and PDZ domain proteins. *EMBO J* 19(24): 6778-6791.

Kavsak, P., Rasmussen, R. K., Causing, C. G., Bonni, S., Zhu, H., Thomsen, G. H., and Wrana, J. L. (2000) Smad7 binds to Smurf2 to form an E3 ubiquitin ligase that targets the TGF beta receptor for degradation. *Mol Cell* 6(6): 1365-1375.

Keller, R., Davidson, L. A., and Shook, D. R. (2003) How we are shaped: the biomechanics of gastrulation. *Differentiation* 71(3): 171-205.

Klinghoffer, R. A., Sachsenmaier, C., Cooper, J. A., and Soriano, P. (1999) Src family kinases are required for integrin but not PDGFR signal transduction. *EMBO J* 18(9): 2459-2471.

Komori, T., Yagi, H., Nomura, S., Yamaguchi, A., Sasaki, K., Deguchi, K., Shimizu, Y., Bronson, R. T., Gao, Y. H., Inada, M., Sato, M., Okamoto, R., Kitamura, Y., Yoshiki, S., and Kishimoto, T. (1997) Targeted disruption of Cbfa1 results in a complete lack of bone formation owing to maturational arrest of osteoblasts. *Cell* 89(5): 755-764.

Komuro, A., Nagai, M., Navin, N. E., and Sudol, M. (2003) WW domain-containing protein YAP associates with ErbB-4 and acts as a co-transcriptional activator for the carboxyl-terminal fragment of ErbB-4 that translocates to the nucleus. *J Biol Chem* 278(35): 33334-33341.

Kukalev, A., Nord, Y., Palmberg, C., Bergman, T., and Percipalle, P. (2005) Actin and hnRNP U cooperate for productive transcription by RNA polymerase II. *Nat Struct Mol Biol* 12(3): 238-244.

Kuroda, K., Tani, S., Tamura, K., Minoguchi, S., Kurooka, H., and Honjo, T. (1999) Delta-induced Notch signaling mediated by RBP-J inhibits MyoD expression and myogenesis. *J Biol Chem* 274(11): 7238-7244.

Ladher, R., Mohun, T. J., Smith, J. C., and Snape, A. M. (1996) Xom: a *Xenopus* homeobox gene that mediates the early effects of BMP-4. *Development* 122(8): 2385-2394.

Lee, H. S., Nishanian, T. G., Mood, K., Bong, Y. S., and Daar, I. O. (2008) EphrinB1 controls cell-cell junctions through the Par polarity complex. *Nat Cell Biol* 10(8): 979-986.

Lee, J. E., Hollenberg, S. M., Snider, L., Turner, D. L., Lipnick, N., and Weintraub, H. (1995) Conversion of *Xenopus* ectoderm into neurons by NeuroD, a basic helix-loop-helix protein. *Science* 268(5212): 836-844.

Lee, K. F., Simon, H., Chen, H., Bates, B., Hung, M. C., and Hauser, C. (1995) Requirement for neuregulin receptor erbB2 in neural and cardiac development. *Nature* 378(6555): 394-398.

Lee, S. J., Reed, L. A., Davies, M. V., Girgenrath, S., Goad, M. E., Tomkinson, K. N., Wright, J. F., Barker, C., Ehrmantraut, G., Holmstrom, J., Trowell, B., Gertz, B., Jiang, M. S., Sebald, S. M., Matzuk, M., Li, E., Liang, L. F., Quattlebaum, E., Stotish, R. L., and Wolfman, N. M. (2005) Regulation of muscle growth by multiple ligands signaling through activin type II receptors. *Proc Natl Acad Sci U S A* 102(50): 18117-18122.

Li, R., Rosendahl, A., Brodin, G., Cheng, A. M., Ahgren, A., Sundquist, C., Kulkarni, S., Pawson, T., Heldin, C. H., and Heuchel, R. L. (2006) Deletion of exon I of SMAD7 in mice results in altered B cell responses. *J Immunol* 176(11): 6777-6784.

Li, Z., Zhao, B., Wang, P., Chen, F., Dong, Z., Yang, H., Guan, K. L., and Xu, Y. (2010) Structural insights into the YAP and TEAD complex. *Genes Dev* 24(3): 235-240.

Lowe, C., Yoneda, T., Boyce, B. F., Chen, H., Mundy, G. R., and Soriano, P. (1993) Osteopetrosis in Src-deficient mice is due to an autonomous defect of osteoclasts. *Proc Natl Acad Sci U S A* 90(10): 4485-4489.

Lu, X., Borchers, A. G., Jolicoeur, C., Rayburn, H., Baker, J. C., and Tessier-Lavigne, M. (2004) PTK7/CCK-4 is a novel regulator of planar cell polarity in vertebrates. *Nature* 430(6995): 93-98.

Macias, M. J., Hyvonen, M., Baraldi, E., Schultz, J., Sudol, M., Saraste, M., and Oschkinat, H. (1996) Structure of the WW domain of a kinase-associated protein complexed with a proline-rich peptide. *Nature* 382(6592): 646-649.

Maeda, T., Mazzulli, J. R., Farrance, I. K., and Stewart, A. F. (2002) Mouse DTEF-1 (ETFR-1, TEF-5) is a transcriptional activator in alpha 1-adrenergic agonist-stimulated cardiac myocytes. *J Biol Chem* 277(27): 24346-24352.

Marin, M., Karis, A., Visser, P., Grosveld, F., and Philipsen, S. (1997) Transcription factor Sp1 is essential for early embryonic development but dispensable for cell growth and differentiation. *Cell* 89(4): 619-628.

Matzuk, M. M., Finegold, M. J., Su, J. G., Hsueh, A. J., and Bradley, A. (1992) Alpha-inhibin is a tumour-suppressor gene with gonadal specificity in mice. *Nature* 360(6402): 313-319.

Matzuk, M. M., Finegold, M. J., Mather, J. P., Krummen, L., Lu, H., and Bradley, A. (1994) Development of cancer cachexia-like syndrome and adrenal tumors in inhibin-deficient mice. *Proc Natl Acad Sci U S A* 91(19): 8817-8821.

Megason, S. G. (2009) *In toto* imaging of embryogenesis with confocal time-lapse microscopy. *Methods Mol Biol* 546: 317-332.

Meyer, D., and Birchmeier, C. (1995) Multiple essential functions of neuregulin in development. *Nature* 378(6555): 386-390.

Mills, A. A., Zheng, B., Wang, X. J., Vogel, H., Roop, D. R., and Bradley, A. (1999) p63 is a p53 homologue required for limb and epidermal morphogenesis. *Nature* 398(6729): 708-713.

Misteli, T. (2009) Self-organization in the genome. *Proc Natl Acad Sci U S A* 106(17): 6885-6886.

Misteli, T. (2010) Higher-order genome organization in human disease. *Cold Spring Harb Perspect Biol* 2(8): a000794.

Mizuseki, K., Kishi, M., Matsui, M., Nakanishi, S., and Sasai, Y. (1998) *Xenopus* Zic-related-1 and Sox-2, two factors induced by chordin, have distinct activities in the initiation of neural induction. *Development* 125(4): 579-587.

Mohler, P. J., Kreda, S. M., Boucher, R. C., Sudol, M., Stutts, M. J., and Milgram, S. L. (1999) Yes-associated protein 65 localizes p62(c-Yes) to the apical compartment of airway epithelia by association with EBP50. *J Cell Biol* 147(4): 879-890.

Monsoro-Burq, A. H., Wang, E., and Harland, R. (2005) Msx1 and Pax3 cooperate to mediate FGF8 and WNT signals during *Xenopus* neural crest induction. *Dev Cell* 8(2): 167-178.

Morales, F. C., Takahashi, Y., Kreimann, E. L., and Georgescu, M. M. (2004) Ezrin-radixin-moesin (ERM)-binding phosphoprotein 50 organizes ERM proteins at the apical membrane of polarized epithelia. *Proc Natl Acad Sci U S A* 101(51): 17705-17710.

Morin-Kensicki, E. M., Boone, B. N., Howell, M., Stonebraker, J. R., Teed, J., Alb, J. G., Magnuson, T. R., O'Neal, W., and Milgram, S. L. (2006) Defects in yolk sac vasculogenesis, chorioallantoic fusion, and embryonic axis elongation in mice with targeted disruption of Yap65. *Mol Cell Biol* 26(1): 77-87.

Moustakas, A., and Heldin, C. H. (2009) The regulation of TGFbeta signal transduction. *Development* 136(22): 3699-3714.

Mukherjee, A., Sidis, Y., Mahan, A., Raher, M. J., Xia, Y., Rosen, E. D., Bloch, K. D., Thomas, M. K., and Schneyer, A. L. (2007) FSTL3 deletion reveals roles for TGF-beta family ligands in glucose and fat homeostasis in adults. *Proc Natl Acad Sci U S A* 104(4): 1348-1353.

Murakami, M., Nakagawa, M., Olson, E. N., and Nakagawa, O. (2005) A WW domain protein TAZ is a critical coactivator for TBX5, a transcription factor implicated in Holt-Oram syndrome. *Proc Natl Acad Sci U S A* 102(50): 18034-18039.

Murakami, M., Tominaga, J., Makita, R., Uchijima, Y., Kurihara, Y., Nakagawa, O., Asano, T., and Kurihara, H. (2006) Transcriptional activity of Pax3 is co-activated by TAZ. *Biochem Biophys Res Commun* 339(2): 533-539.

Naye, F., Treguer, K., Soulet, F., Faucheux, C., Fedou, S., Theze, N., and Thiebaud, P. (2007) Differential expression of two TEF-1 (TEAD) genes during *Xenopus laevis* development and in response to inducing factors. *Int J Dev Biol* 51(8): 745-752.

Nejigane, S., Haramoto, Y., Okuno, M., Takahashi, S., and Asashima, M. (2011) The transcriptional coactivators Yap and TAZ are expressed during early *Xenopus* development. *Int J Dev Biol* 55: 121-126.

Nieuwkoop, P. D., and Faber, J. (1994) *Normal Table of Xenopus Laevis (Daudin)*. North Holland Publishing Company, Amsterdam.

Nishioka, N., Yamamoto, S., Kiyonari, H., Sato, H., Sawada, A., Ota, M., Nakao, K., and Sasaki, H. (2008) Tead4 is required for specification of trophectoderm in pre-implantation mouse embryos. *Mech Dev* 125(3-4): 270-283.

Nishioka, N., Inoue, K., Adachi, K., Kiyonari, H., Ota, M., Ralston, A., Yabuta, N., Hirahara, S., Stephenson, R. O., Ogonuki, N., Makita, R., Kurihara, H., Morin-Kensicki, E. M., Nojima, H., Rossant, J., Nakao, K., Niwa, H., and Sasaki, H. (2009) The Hippo signaling pathway components Lats and Yap pattern Tead4 activity to distinguish mouse trophectoderm from inner cell mass. *Dev Cell* 16(3): 398-410.

Omerovic, J., Puggioni, E. M., Napoletano, S., Visco, V., Fraioli, R., Frati, L., Gulino, A., and Alimandi, M. (2004) Ligand-regulated association of ErbB-4 to the transcriptional co-activator YAP65 controls transcription at the nuclear level. *Exp Cell Res* 294(2): 469-479.

Otto, F., Thornell, A. P., Crompton, T., Denzel, A., Gilmour, K. C., Rosewell, I. R., Stamp, G. W., Beddington, R. S., Mundlos, S., Olsen, B. R., Selby, P. B., and Owen, M. J. (1997) Cbfa1, a candidate gene for cleidocranial dysplasia syndrome, is essential for osteoblast differentiation and bone development. *Cell* 89(5): 765-771.

Overholtzer, M., Zhang, J., Smolen, G. A., Muir, B., Li, W., Sgroi, D. C., Deng, C. X., Brugge, J. S., and Haber, D. A. (2006) Transforming properties of YAP, a candidate oncogene on the chromosome 11q22 amplicon. *Proc Natl Acad Sci U S A* 103(33): 12405-12410.

Pandur, P. D., and Moody, S. A. (2000) *Xenopus* Six1 gene is expressed in neurogenic cranial placodes and maintained in the differentiating lateral lines. *Mech Dev* 96(2): 253-257.

Park, K. S., Whitsett, J. A., Di Palma, T., Hong, J. H., Yaffe, M. B., and Zannini, M. (2004) TAZ interacts with TTF-1 and regulates expression of surfactant protein-C. *J Biol Chem* 279(17): 17384-17390.

Park, S. K., Miller, R., Krane, I., and Vartanian, T. (2001) The erbB2 gene is required for the development of terminally differentiated spinal cord oligodendrocytes. *J Cell Biol* 154(6): 1245-1258.

Parker, C. S., and Topol, J. (1984) A Drosophila RNA polymerase II transcription factor contains a promoter-region-specific DNA-binding activity. *Cell* 36(2): 357-369.

Peng, L., Huang, Y., Jin, F., Jiang, S. W., and Payne, A. H. (2004) Transcription enhancer factor-5 and a GATA-like protein determine placental-specific expression of the Type I human 3beta-hydroxysteroid dehydrogenase gene, HSD3B1. *Mol Endocrinol* 18(8): 2049-2060.

Reisz-Porszasz, S., Bhasin, S., Artaza, J. N., Shen, R., Sinha-Hikim, I., Hogue, A., Fielder, T. J., and Gonzalez-Cadavid, N. F. (2003) Lower skeletal muscle mass in male transgenic mice with muscle-specific overexpression of myostatin. *Am J Physiol Endocrinol Metab* 285(4): E876-888.

Roberts, D. M., Anderson, A. L., Hidaka, M., Swetenburg, R. L., Patterson, C., Stanford, W. L., and Bautch, V. L. (2004) A vascular gene trap screen defines RasGRP3 as an angiogenesis-regulated gene required for the endothelial response to phorbol esters. *Mol Cell Biol* 24(24): 10515-10528.

Roshon, M. J., and Ruley, H. E. (2005) Hypomorphic mutation in hnRNP U results in post-implantation lethality. *Transgenic Res* 14(2): 179-192.

Ryan, K., Garrett, N., Mitchell, A., and Gurdon, J. B. (1996) Eomesodermin, a key early gene in Xenopus mesoderm differentiation. *Cell* 87(6): 989-1000.

Sambrook, J., and Russell, D. W. (2001) *Molecular cloning: a laboratory manual.* Cold Spring Harbor Laboratory Press, Cold Spring Harbor, NY.

Sanz-Moreno, V., Gadea, G., Ahn, J., Paterson, H., Marra, P., Pinner, S., Sahai, E., and Marshall, C. J. (2008) Rac activation and inactivation control plasticity of tumor cell movement. *Cell* 135(3): 510-523.

Sasai, N., Mizuseki, K., and Sasai, Y. (2001) Requirement of FoxD3-class signaling for neural crest determination in *Xenopus*. *Development* 128(13): 2525-2536.

Sasai, Y., Lu, B., Steinbeisser, H., Geissert, D., Gont, L. K., and De Robertis, E. M. (1994) *Xenopus* chordin: a novel dorsalizing factor activated by organizer-specific homeobox genes. *Cell* 79(5): 779-790.

Sawada, A., Nishizaki, Y., Sato, H., Yada, Y., Nakayama, R., Yamamoto, S., Nishioka, N., Kondoh, H., and Sasaki, H. (2005) Tead proteins activate the Foxa2 enhancer in the node in cooperation with a second factor. *Development* 132(21): 4719-4729.

Sawada, A., Kiyonari, H., Ukita, K., Nishioka, N., Imuta, Y., and Sasaki, H. (2008) Redundant roles of Tead1 and Tead2 in notochord development and the regulation of cell proliferation and survival. *Mol Cell Biol* 28(10): 3177-3189.

Schlosser, G. (2006) Induction and specification of cranial placodes. *Dev Biol* 294(2): 303-351.

Schlosser, G., Awtry, T., Brugmann, S. A., Jensen, E. D., Neilson, K., Ruan, G., Stammler, A., Voelker, D., Yan, B., Zhang, C., Klymkowsky, M. W., and Moody, S. A. (2008) Eya1 and Six1 promote neurogenesis in the cranial placodes in a SoxB1-dependent fashion. *Dev Biol* 320(1): 199-214.

Semenza, G. L. (2000) HIF-1 and human disease: one highly involved factor. *Genes Dev* 14(16): 1983-1991.

Seo, S., Richardson, G. A., and Kroll, K. L. (2005) The SWI/SNF chromatin remodeling protein Brg1 is required for vertebrate neurogenesis and mediates transactivation of Ngn and NeuroD. *Development* 132(1): 105-115.

Shenolikar, S., Voltz, J. W., Minkoff, C. M., Wade, J. B., and Weinman, E. J. (2002) Targeted disruption of the mouse NHERF-1 gene promotes internalization of proximal tubule sodium-phosphate cotransporter type IIa and renal phosphate wasting. *Proc Natl Acad Sci U S A* 99(17): 11470-11475.

Sive, H., Grainger, R., and Harland, R. (2000) *Early development of Xenopus laevis: A Laboratory Manual.* Cold Spring Harbor Laboratory Press, Cold Spring Harbor, NY.

Smale, S. T., and Baltimore, D. (1989) The "initiator" as a transcription control element. *Cell* 57(1): 103-113.

Smale, S. T. (1994) *Transcription: mechanisms and regulation.* Raven Press, New York.

Smith, J. C., Price, B. M., Green, J. B., Weigel, D., and Herrmann, B. G. (1991) Expression of a *Xenopus* homolog of Brachyury (T) is an immediate-early response to mesoderm induction. *Cell* 67(1): 79-87.

Soriano, P., Montgomery, C., Geske, R., and Bradley, A. (1991) Targeted disruption of the c-src proto-oncogene leads to osteopetrosis in mice. *Cell* 64(4): 693-702.

Srivastava, M., Begovic, E., Chapman, J., Putnam, N. H., Hellsten, U., Kawashima, T., Kuo, A., Mitros, T., Salamov, A., Carpenter, M. L., Signorovitch, A. Y., Moreno, M. A., Kamm, K., Grimwood, J., Schmutz, J., Shapiro, H., Grigoriev, I. V., Buss, L. W., Schierwater, B., Dellaporta, S. L., and Rokhsar, D. S. (2008) The Trichoplax genome and the nature of placozoans. *Nature* 454(7207): 955-960.

Srivastava, M., Simakov, O., Chapman, J., Fahey, B., Gauthier, M. E., Mitros, T., Richards, G. S., Conaco, C., Dacre, M., Hellsten, U., Larroux, C., Putnam, N. H., Stanke, M., Adamska, M., Darling, A., Degnan, S. M., Oakley, T. H., Plachetzki, D. C., Zhai, Y., Adamski, M., Calcino, A., Cummins, S. F., Goodstein, D. M., Harris, C., Jackson, D. J., Leys, S. P., Shu, S., Woodcroft, B. J., Vervoort, M., Kosik, K. S., Manning, G., Degnan, B. M., and Rokhsar, D. S. (2010) The Amphimedon queenslandica genome and the evolution of animal complexity. *Nature* 466(7307): 720-726.

Stein, P. L., Lee, H. M., Rich, S., and Soriano, P. (1992) pp59fyn mutant mice display differential signaling in thymocytes and peripheral T cells. *Cell* 70(5): 741-750.

Stein, P. L., Vogel, H., and Soriano, P. (1994) Combined deficiencies of Src, Fyn, and Yes tyrosine kinases in mutant mice. *Genes Dev* 8(17): 1999-2007.

Stoos, B. A., Naray-Fejes-Toth, A., Carretero, O. A., Ito, S., and Fejes-Toth, G. (1991) Characterization of a mouse cortical collecting duct cell line. *Kidney Int* 39(6): 1168-1175.

Strano, S., Munarriz, E., Rossi, M., Castagnoli, L., Shaul, Y., Sacchi, A., Oren, M., Sudol, M., Cesareni, G., and Blandino, G. (2001) Physical interaction with Yes-associated protein enhances p73 transcriptional activity. *J Biol Chem* 276(18): 15164-15173.

Sudol, M. (1994) Yes-associated protein (YAP65) is a proline-rich phosphoprotein that binds to the SH3 domain of the Yes proto-oncogene product. *Oncogene* 9(8): 2145-2152.

Sudol, M., Bork, P., Einbond, A., Kastury, K., Druck, T., Negrini, M., Huebner, K., and Lehman, D. (1995) Characterization of the mammalian YAP (Yes-associated protein) gene and its role in defining a novel protein module, the WW domain. *J Biol Chem* 270(24): 14733-14741.

Takeda, S., Bonnamy, J. P., Owen, M. J., Ducy, P., and Karsenty, G. (2001) Continuous expression of Cbfa1 in nonhypertrophic chondrocytes uncovers its ability to induce hypertrophic chondrocyte differentiation and partially rescues Cbfa1-deficient mice. *Genes Dev* 15(4): 467-481.

Taranova, O. V., Magness, S. T., Fagan, B. M., Wu, Y., Surzenko, N., Hutton, S. R., and Pevny, L. H. (2006) SOX2 is a dose-dependent regulator of retinal neural progenitor competence. *Genes Dev* 20(9): 1187-1202.

Tian, Y., Kolb, R., Hong, J. H., Carroll, J., Li, D., You, J., Bronson, R., Yaffe, M. B., Zhou, J., and Benjamin, T. (2007) TAZ promotes PC2 degradation through a SCFbeta-Trcp E3 ligase complex. *Mol Cell Biol* 27(18): 6383-6395.

Varelas, X., Sakuma, R., Samavarchi-Tehrani, P., Peerani, R., Rao, B. M., Dembowy, J., Yaffe, M. B., Zandstra, P. W., and Wrana, J. L. (2008) TAZ controls Smad nucleocytoplasmic shuttling and regulates human embryonic stem-cell self-renewal. *Nat Cell Biol* 10(7): 837-848.

Vassilev, A., Kaneko, K. J., Shu, H., Zhao, Y., and DePamphilis, M. L. (2001) TEAD/TEF transcription factors utilize the activation domain of YAP65, a Src/Yes-associated protein localized in the cytoplasm. *Genes Dev* 15(10): 1229-1241.

Vives, V., Su, J., Zhong, S., Ratnayaka, I., Slee, E., Goldin, R., and Lu, X. (2006) ASPP2 is a haploinsufficient tumor suppressor that cooperates with p53 to suppress tumor growth. *Genes Dev* 20(10): 1262-1267.

von Dassow, G., Schmidt, J. E., and Kimelman, D. (1993) Induction of the *Xenopus* organizer: expression and regulation of Xnot, a novel FGF and activin-regulated homeo box gene. *Genes Dev* 7(3): 355-366.

Wallingford, J. B., and Harland, R. M. (2001) *Xenopus* Dishevelled signaling regulates both neural and mesodermal convergent extension: parallel forces elongating the body axis. *Development* 128(13): 2581-2592.

Xia, Y., and Schneyer, A. L. (2009) The biology of activin: recent advances in structure, regulation and function. *J Endocrinol* 202(1): 1-12.

Yagi, R., Chen, L. F., Shigesada, K., Murakami, Y., and Ito, Y. (1999) A WW domain-containing yes-associated protein (YAP) is a novel transcriptional co-activator. *EMBO J* 18(9): 2551-2562.

Yagi, R., Kohn, M. J., Karavanova, I., Kaneko, K. J., Vullhorst, D., DePamphilis, M. L., and Buonanno, A. (2007) Transcription factor TEAD4 specifies the trophectoderm lineage at the beginning of mammalian development. *Development* 134(21): 3827-3836.

Yang, A., Schweitzer, R., Sun, D., Kaghad, M., Walker, N., Bronson, R. T., Tabin, C., Sharpe, A., Caput, D., Crum, C., and McKeon, F. (1999) p63 is essential for regenerative proliferation in limb, craniofacial and epithelial development. *Nature* 398(6729): 714-718.

Yang, A., Walker, N., Bronson, R., Kaghad, M., Oosterwegel, M., Bonnin, J., Vagner, C., Bonnet, H., Dikkes, P., Sharpe, A., McKeon, F., and Caput, D. (2000) p73-deficient mice have neurological, pheromonal and inflammatory defects but lack spontaneous tumours. *Nature* 404(6773): 99-103.

Ye, X., Hama, K., Contos, J. J., Anliker, B., Inoue, A., Skinner, M. K., Suzuki, H., Amano, T., Kennedy, G., Arai, H., Aoki, J., and Chun, J. (2005) LPA3-mediated lysophosphatidic acid signalling in embryo implantation and spacing. *Nature* 435(7038): 104-108.

Zaidi, S. K., Sullivan, A. J., Medina, R., Ito, Y., van Wijnen, A. J., Stein, J. L., Lian, J. B., and Stein, G. S. (2004) Tyrosine phosphorylation controls Runx2-mediated subnuclear targeting of YAP to repress transcription. *EMBO J* 23(4): 790-799.

Zhao, B., Wei, X., Li, W., Udan, R. S., Yang, Q., Kim, J., Xie, J., Ikenoue, T., Yu, J., Li, L., Zheng, P., Ye, K., Chinnaiyan, A., Halder, G., Lai, Z. C., and Guan, K. L. (2007) Inactivation of YAP oncoprotein by the Hippo pathway is involved in cell contact inhibition and tissue growth control. *Genes Dev* 21(21): 2747-2761.

Zimmers, T. A., Davies, M. V., Koniaris, L. G., Haynes, P., Esquela, A. F., Tomkinson, K. N., McPherron, A. C., Wolfman, N. M., and Lee, S. J. (2002) Induction of cachexia in mice by systemically administered myostatin. *Science* 296(5572): 1486-1488.

Zurita, M., Reynaud, E., and Aguilar-Fuentes, J. (2008) From the beginning: the basal transcription machinery and onset of transcription in the early animal embryo. *Cell Mol Life Sci* 65(2): 212-227.